Winter 12-17-2016

# Impacts of long-term precipitation manipulation on hydraulic architecture, xylem function, and canopy status in a piñon-juniper woodland

Patrick J. Hudson
*University of New Mexico*

Patrick J. Hudson
*Candidate*

Biology
*Department*

This dissertation is approved, and it is acceptable in quality and form for publication:

*Approved by the Dissertation Committee:*

William Pockman , Chairperson

Nate McDowell

Marcy Litvak

Chris Lippitt

# IMPACTS OF LONG-TERM PRECIPITATION MANIPULATION ON HYDRAULIC ARCHITECTURE XYLEM FUNCTION, AND CANOPY STATUS IN A PIÑON-JUNIPER WOODLAND

**by**

**PATRICK J. HUDSON**

B.A., B.S. Biology, Truman State University, 2004
M.Sc. Biology, University of Nebraska, 2006
M.Sc. Ecology and Evolutionary Biology, University of Tennessee, 2010

DISSERTATION

Submitted in Partial Fulfillment of the
Requirements for the Degree of

**Doctor of Philosophy**
**Biology**

The University of New Mexico
Albuquerque, New Mexico

**May, 2017**

## Acknowledgments

The research presented in this dissertation was supported by the Department of Energy's Office of Science (BER) awards to NGM and WTP. Additional support from the Sevilleta LTER (NSF DEB-0620482), the Sevilleta LTER summer graduate fellowship, and scholarships from the Department of Biology and the University of New Mexico was provided to PJH.

I would like to recognize the efforts of Judson Hill, Enrico Yepez, Jen Plaut, Clif Meyer, Renee Brown, James Elliot and many undergraduate assistants, as they were essential in establishing the PJ precipitation manipulation experiment. Ali Fretz, Ben Specter, Katie Sauer, Laura Pickrell, and Kelsey Flathers provided excellent field assistance. Caitlin Lippitt and William Brewer provided essential instruction in spectrometer, the Hanson Research Team assisted with laboratory procedures, and Dave Van Horn permitted access to laboratory space.

I wish to thank the Pockman Lab research group for experimental design, data collection, and data management assistance. I wish to thank my friends and family for their support in this endeavor. And finally, I wish to thank my lovely and extremely patient wife, who made it possible for me to see this through to the end.

# Impacts of long-term precipitation manipulation on hydraulic architecture, xylem function, and canopy status in a piñon-juniper woodland

by

Patrick J. Hudson

B.A., B.S. Biology, Truman State University, 2004
M.Sc. Biology, University of Nebraska, 2006
M.Sc. Ecology & Evolutionary Biology, University of Tennessee, 2010
Ph.D. Biology, University of New Mexico, 2017

## Abstract

The Southwestern US is predicted to become hotter and drier, as global climate change forces increasing temperatures and variability in timing and size of precipitation inputs. Drought stress has become more frequent in recent decades, and resulted in massive forest mortality in piñon-juniper woodlands. During recent severe droughts (2000-2003, 2009-2012), piñon pine (*Pinus edulis* Englem.) suffered disproportionately high mortality compared to co-occurring one-seed juniper (*Juniperus monosperma* [Engelm.] Sarg.). A large-scale precipitation manipulation experiment was established in a piñon-juniper woodland in central New Mexico to test hypotheses regarding tree survival and mortality with respect to altered water regimes. Our treatments consisted of water addition (+20% ambient precipitation), partial precipitation-exclusion (-45% ambient precipitation), and an exclusion-structure control. The research presented in this dissertation seeks to identify differences in hydraulic architecture between piñon and juniper to provide new insight into how these species survive extreme climate events. Hydraulic architecture is a fundamental control on water transport, which underpins plant productivity and survival. The extent to which mature trees can adjust hydraulic

architecture as a response to drought is unknown. In Chapter 1, we measured seasonal stem hydraulic performance for multiple years to assess the acclimation of hydraulic architecture in mature piñon and juniper after 3+ years of precipitation manipulation. In Chapter 2, we focused on defining the relative roles of abiotic and biotic stressors in piñon mortality. We established two additional treatment plots (an ambient control and the same drought treatment) in the same experiment to test the impact of drought while bark beetle attack was prevented by insecticide treatment. We measured piñon hydraulic architecture for five years following the start of experimental drought. In Chapter 3, we used the continuum of foliar health furnished by the precipitation manipulation experiment to investigate the links between foliar spectral reflectance signals and direct measurements of water stress and hydraulic function. Our findings suggest that 1) mature trees are unlikely to adjust hydraulic transport safety or efficiency in response to climate change, 2) bark beetles are critical mediators of piñon mortality during drought, and 3) spectral signals from foliage accurately predict water status and hydraulic function.

# Table of Contents

## List of Figures

## List of Tables

# Chapter 1

## Introduction

Semi-arid ecosystems cover ~40% of the earth surface, and by virtue of spatial extent, significantly contribute to the global cycling of water and carbon (Poulter *et al*. 2014). Tree species that comprise semi-arid woodlands and savannas typically demonstrate low productivity, as a consequence of extreme seasonal variability in temperature and precipitation. Yet these same species can possess lifespans on the order of centuries, even while situated at an ecologically critical threshold of precipitation (Romme *et al*. 2009). This precarious position, where precipitation first permits tree stature and a woody overstory canopy, is predicted to be highly sensitive to climate change. Recent patterns of drought-induced tree mortality in the Southwestern US confirm the proposed sensitivity semi-arid landcapes to climate change (Breshears *et al*. 2005, Williams *et al*. 2013). The mechanisms that cause mortality in trees are currently poorly understood, and thus future responses of forests to climate change are far from certain. Modeling efforts to predict global patterns of vegetation (dynamic global vegetation models, DGVMs) have traditionally treated plant function as static (Fisher *et al.* 2010, McDowell 2011). DVGMs also tend to lump species together based on broad physiognomic characters (evergreen vs. deciduous, broadleaf vs. needle-leaf) that fail to capture variation in species function and ecological impact, which is exacerbated in low-diversity ecosystems (Quillet *et al.* 2010, Reich *et al*. 2014). Thus, there is a clear need for information concerning the long-term species-specific responses of ecologically relevant traits to climate variation, because we lack an understanding of how long-lived

species can and will cope with climate change. Thus, models that can account for species-specific patterns of acclimation will provide the most accurate predictions of forest responses to climate change (Scheiter *et al*. 2013). My dissertation seeks to address this knowledge gap in species-specific function by investigating the acclimative potential of mature trees to climate forcing, from the prospective of branch level hydraulic structure and performance.

Piñon-juniper (PJ) woodland, the most common woody ecosystem in the Southwestern US, provides a model system in which to test hypotheses concerning acclimation of xylem function. PJ is co-dominated by two species, which lie at opposite ends of a plant functional continuum (McDowell *et al.* 2008). Piñon pine (*Pinus edulis* Englem.) is relatively isohydric, consistently maintaining stable leaf internal water status as moisture fluctuates. Isohydric behavior rapidly limits transpiration when soil moisture availability decreases during drought, thereby restricting photosynthetic carbon uptake. In contrast, one-seed juniper (*Juniperus monosperma* [Engelm.] Sarg.) is relatively anisohydric, and permits leaf water status to decline as soil dries. Anisohydric behavior maintains transpiration and carbon uptake over a larger range of soil moisture conditions, allow photosynthesis to continue (albeit at a reduced rate) as drought conditions persist (Martinéz-Vilalta *et al.* 2014, Klein 2014, Skelton *et al.* 2015). These two stomatal regulation behaviors carry associated physiological risks. In a drought of sufficient duration, isohydric species cannot replenish metabolic carbon, and risk depleting carbon reserves to the extent that metabolic demands cannot be met. In a drought of sufficient intensity, anisohydric species must generate large water potential gradients to extract water from dry soils, and in doing so, increase the probability of embolism and loss of

functional xylem. The fundamental differences in stomatal regulation strategy provide a starting point from which to develop mechanistic hypotheses regarding plant functional responses to climate change (McDowell *et al*. 2008).

In Chapter 1 (Hudson *et al*. in review), we investigated the acclimative potential of piñon and juniper hydraulic architecture within the context of a long-term precipitation manipulation experiment (Pangle *et al*. 2012). The precipitation manipulations consisted of water addition (+20% ambient precipitation), partial precipitation-exclusion (-45% ambient precipitation), and an exclusion-structure control. Supplemental watering elevated leaf water potential ($\Psi_W$), sapwood-area specific hydraulic conductivity ($K_S$) and leaf-area specific hydraulic conductivity ($K_L$) relative to the decreased precipitation treatment. Shifts in allocation of leaf area to sapwood area enhanced the difference between irrigated and droughted $K_L$ in piñon, but not juniper. Piñon and juniper achieved similar $K_L$ under ambient conditions, but juniper matched or outperformed piñon in all physiological measurements under both increased and decreased precipitation treatments. Vulnerability to embolism and xylem anatomy were unaffected by treatments in either species. We determined that neither piñon, nor juniper, demonstrated significant acclimation responses to either supplemental watering or experimental drought, and thus, mature trees in PJ are not likely to cope with climate change through acclimation of hydraulic architecture.

Data collection for Chapter 2 occurred simultaneously with Chapter 1. Chapter 2 focused on the initial drought responses in piñon, and was motivated by the rapid decline and mortality of piñon in the original experimental drought treatments in 2008-2009. Mass piñon mortality limited the original experimental investigation of hydraulic

responses to drought, and disentangling relative roles of carbon starvation and hydraulic failure as mechanisms of mortality. We installed two additional pesticide treatment plots to the long-term PJ precipitation manipulation experiment in Fall 2010. One plot functioned as an abiotic control, while the other was subject to experimental drought. This design allowed us to closely monitor the shifts stem, shoot, and leaf-level hydraulic activity associated with onset and perpetuation of chronic water shortage, while restricting the influence of confounding biotic mortality factors on drought stress responses in trees. As in Chapter 1, we observed minimal acclimation in hydraulic architecture, or leaf gas exchange, under experimental drought. We discovered that chronic experimental drought reduced quantity of water transported, but did not adversely impact water transport capacity. We also observed that our pesticide–treated piñon survived 6+ years of severe abiotic forcing and periodically intense local bark beetle activity that lead to untreated piñon mortality, while demonstrating physiological status identical to trees that succumbed to lethal beetle attack in the original experiment. This finding highlights the importance of insect pathogens as mechanisms of mortality in PJ woodlands.

In Chapter 3, we leveraged the continuum of apparent foliar water stress provided by the PJ precipitation manipulation experiment to investigate into the links between remotely sensed spectral reflectance, foliar water stress and subtending xylem hydraulic function. Water content is directly linked to foliar hydration, which is in turn maintained by xylem hydraulic supply (Tyree and Ewers 1991, Brodribb 2009). We hypothesized that there should be correlations between leaf spectral reflectance signals, and leaf water status and subtending xylem hydraulic function. While remote sensing has shown

promise for estimating foliar water content and water stress, no study has investigated the potential for harnessing spectral signals to predict shoot hydraulic function. Remote sensing also allows for the rapid assessment of broad spatial scales, which challenge standard field ecophysiological procedures. We used a suite of spectral vegetation indices related to canopy water content (CWC) and chlorophyll content (NBG), and standard xylem hydraulic function metrics, to assess three *a priori* established foliar stress categories based on visual signs of water stress. Even though *a priori* stress categories were not universally supported by either spectral or ecophysiological metrics, we were able to investigate plant function over a broad continuum foliar health and xylem integrity. By exploring spectral signatures with multiple regression and principal components analysis, we found strong correlations between spectral signals and direct measurements of plant water status, foliar hydration and structure, and stem hydraulic transport and xylem functional status. Species-specific SVI models always out-performed models based on pooled data, which echoes the issue of functional variation within plant function types, and argues for the necessity of species-specific data to enhance model accuracy. We also identified SVIs that best diagnosed piñon exhibiting physiological function and foliar status indicative of trees with high insect-related mortality risk.

Climate forecasts for the Southwestern US have converged on a future scenario that is expected to be both hotter and drier (Seager *et al*. 2007, Sheffield and Wood 2008). Drought stress is projected to increase in extent, duration, and severity, exacerbated by increased variability in smaller precipitation pulses and increased temperatures (Seager *et al*. 2010, Williams *et al*. 2010). Widespread mortality linked to persistent drought from 2000-2003 and 2009-2014 triggered differential mortality in PJ,

with site-specific piñon mortality rates ranging from 40-95%, compared to 2-25% for juniper (Breashears *et al*. 2005, Williams *et al*. 2010, USDA 2015). Thus, the future of PJ woodland is in question, and model projections of mortality are dire (McDowell *et al*. 2015). This dissertation seeks to provide 1) high-resolution data concerning species-specific responses to climate change to further our understanding of mature tree function under strong abiotic forcing, as well as 2) a novel approach for rapid landscape scale assessment of water status, hydraulic function and mortality risk.

Chapters 2 and 3 represent manuscripts currently in preparation for publication. The chapters are included as constitutive elements of my dissertation, but the manuscripts, when published, will represent the culmination of collaborations with multiple co-authors and advisors.

# Chapter 2

# Impacts of long-term precipitation manipulation on hydraulic architecture and xylem anatomy of piñon and juniper in Southwest USA

## 2.1 Introduction

Plant hydraulic architecture describes key aspects of xylem structure that predict plant function (Zimmerman 1983 Tyree and Ewers 1991). Comparative research has quantified the variation in hydraulic architecture among diverse taxa, revealing the correlation between vulnerability to embolism and local soil water potential (e.g. Pockman and Sperry 2000, Maherali *et al*. 2004, Choat *et al*. 2012). Parallel measurements have revealed the variation in other traits such as intrinsic xylem conductivity, stomatal regulation, and allocation of leaf area per unit sapwood area determine plant function over the operational range of xylem water potential (e.g. Tyree and Ewers 1991, Oren *et al*. 1999, Martinéz-Vilalta *et al*. 2009). Despite our knowledge of inter-specific variation in hydraulic architecture and intra-specific differences among populations, the ability of individuals to modify hydraulic architecture in response to directional change or long-term fluctuation in climate drivers is poorly understood (Mencuccini *et al*. 2003).

Shifts in hydraulic architecture in response to environmental changes are potentially important because the expected response of long-lived species depends on

whether hydraulic architecture is static or dynamically responsive to climate. In aridlands, altered precipitation regime and increased vapor pressure deficit as temperature increases are expected to increase the frequency and severity of drought in the next 50-100 years (Seager *et al*. 2007, Sheffield and Wood 2008, Williams *et al*. 2013). Whether or not the hydraulic architecture and function of trees can change in response to fluctuating climate is difficult to investigate experimentally, but of great importance for forecasting vegetation responses to climate change because current vegetation models treat hydraulic traits as static (Fisher *et al.* 2010, McDowell 2011, McDowell *et al*. 2015, McMahon *et al*. 2011).

Intra-specific variation in hydraulic architecture, performance, and associated anatomy, is well-established as growth conditions vary. Shoot level structural changes, such as decreases in leaf area that effectively increase leaf specific hydraulic conductance, coincide with reduced moisture availablity (Grier and Running 1977, Mencuccini and Grace 1996, Martinéz-Vilalta and Piñol 2002, Mencuccini 2003, McDowell *et al.* 2006, Martinéz-Vilalta *et al.* 2009, Martin-StPaul *et al*. 2013). Embolism vulnerability decreases along moisture gradients or in contrasting environments, with relatively dry sites or drought treatments promoting increased resistance to loss of conductivity in both observational studies (Alder *et al.* 1996, Beikircher and Mayer 2009, Herbette *et al.* 2010, Corcuera *et al.* 2011, Wortemann *et al.* 2011, Barnard *et al.* 2011) and greenhouse experiments (Stiller 2009, Awad *et al.* 2010, Placova and Hacke 2012). Moreover, hydraulic transport capacity has been shown to decrease with reduced water availability or experimental drought (Maherali and DeLucia 2000, Ladjal *et al.* 2005, Medeiros and Pockman 2011, Fonti *et al.* 2012), consistent with

the proposed trade-off between hydraulic safety and efficiency (Tyree, Davis and Cochard 1994, Pockman and Sperry 2000, Manzoni *et al.* 2013; but see Gleason *et al.*, 2016). In response to drought, plants produce conducting elements with reduced lumen diameters, leading to reduction in hydraulically weighted lumen diameter ($D_H$ as described in Pockman and Sperry 2000, Sperry and Hacke 2004, Beikircher and Mayer 2009, Bryukhanova and Fonti 2012, Fonti *et al.* 2012), and conducting efficiency, as described by the Hagen-Poiseuille law (Zimmerman 1983, Tyree and Ewers 1991). Secondary cell wall thickness typically increases, resulting in enhanced conduit thickness to span ratio, an anatomical trait observed to closely correlate with embolism resistance ($(t/b)^2$, Hacke *et al.* 2001, Pitterman *et al.* 2006).

Do individuals of long-lived species modify hydraulic architecture in response to changing or fluctuating climate? Tree ring analyses suggest that aspects of secondary xylem anatomy reflect the climate of the growth year, with drier years producing smaller conduits (Zweifel *et al.* 2006, Sterck *et al.* 2008, Fonti *et al.* 2012), as cell expansion depends on suitable turgor pressure, and is impaired by drought (Hisao and Acevedo 1974, Sheriff and Whitehead 1984). Accordingly, hydraulic transport capacity should be reduced when the hydroactive xylem reflects the accumulation of wood growth from multiple years of suboptimal climate (Fonti *et al.* 2010, Bryukhanova and Fonti 2012). Ring-porous angiosperms exhibit a high degree of inter-annual plasticity in hydraulic performance and embolism vulnerability, with early-wood vessel diameter in *Quercus* species significantly correlated to spring temperature and precipitation, and current-year xylem dominating water transport (Zweifel *et al.* 2006, Fonti and García-González 2008, Fonti *et al.* 2012, Voelker *et al.* 2012). In contrast, effects of inter-annual plasticity may

be muted in gymnosperms that maintain several years' worth of functional xylem because older xylem produced under more favorable conditions remains active (Sterck *et al.* 2008, Eilmann *et al.* 2009).

Despite demonstrated intraspecific differences in hydraulic architecture between microsites, we lack empirical evidence of *in situ* adjustment of hydraulic architecture under altered water availability. In this study, our goal was to determine whether long-term precipitation manipulation promoted acclimation of xylem function in mature piñon-juniper woodland where the two dominant species lie at opposite ends of a plant functional continuum (McDowell *et al.* 2008). Piñon is relatively isohydric, maintaining leaf water potentials of approximately -2.5 MPa as soil moisture fluctuates, rapidly limiting transpiration, and thus carbon uptake, during drought. In contrast, juniper is relatively anisohydric, permitting leaf water potential to decline as soil dries, maintaining transpiration and carbon uptake over a larger range of soil moisture conditions (McDowell *et al*. 2008, Plaut *et al.* 2012, Limousin *et al.* 2013, Martinéz-Vilalta *et al.* 2014, Klein 2014, Skelton *et al.* 2015). We defined xylem hydraulic function in terms of intrinsic transport capability (sapwood-specific conductivity, $K_S$, $kg \bullet m^{-1} \bullet s^{-1} \bullet MPa^{-1}$), shoot-level hydraulic supply (leaf-specific conductivity, $K_L$, $g \bullet m^{-1} \bullet s^{-1} \bullet MPa^{-1}$), and vulnerability to embolism. We hypothesized that 1) $K_S$ and $K_L$ should vary in proportion to water availability, with higher $K_S$ and $K_L$ in irrigated individuals than those subjected to drought, 2) the consistent water potentials in isohydric piñon should promote little or no acclimation of embolism vulnerability across treatments, while the wide variation of water potential among treatments in anisohydric juniper should promote acclimation of hydraulic architecture relative to untreated controls such that embolism resistance

increases with drought, and 3) changes in hydraulic transport efficiency and safety should correlate with shifts in anatomical structure.

## 2.2 Materials and Methods

### *2.2.1 Study site*

Our research used a rainfall manipulation experiment established in 2007 in a piñon-juniper woodland at the Sevilleta National Wildlife Refuge in central New Mexico, USA (34º23'11" N, 106º31'46" W, 1911 m; for details see Pangle *et al.* 2012, Plaut *et al*. 2012). Mean annual precipitation is 367.6 mm•yr$^{-1}$, with mean annual temperature of 12.7ºC, mean July maximum of 31.0ºC and mean December minimum of -3.3ºC (Moore 2014). We established three replicate blocks of four treatments: ambient control (100% precipitation), irrigation (~130% precipitation) drought (~55% of ambient rainfall) and cover control (100% precipitation same coverage of inverted water troughs). Although shoot water potential measurements began in August 2007 (Pockman and McDowell 2015), here we use only data with concurrent hydraulic conductivity measurements (2010-2014). Due to complete piñon mortality in drought treatments of two replicate blocks in 2008, this study focused on the remaining block where target piñon trees persisted in the drought treatment. Branch samples collected for hydraulic conductivity measurements were harvested in June (pre-monsoon) and August (post-monsoon onset) of 2010, 2012, 2013 and 2014. Branch samples used for vulnerability curves were collected between August and November 2014.

### *2.2.2 Shoot $\Psi_W$*

We cut samples for predawn and midday water potential (hereafter $\Psi_{PD}$ and $\Psi_{MD}$,) from each target tree between 0430-0545h and between 1200-1400h. Samples were stored in plastic bags with a scrap of moist paper towel to prevent desiccation, stored in shaded, insulated boxes before processing (between 15-60 minutes). Water potential ($\Psi_W$, MPa) was measured using a pressure chamber (PMS, Corvallis, OR).

*2.2.3 Hydraulic conductivity*

Branches (~16 cm in length and 2-5 mm in diameter) cut from trees were sealed in humid plastic bags and transported to the laboratory where they were refrigerated until they were measured (within 24 h). Before measurement, samples were submerged in 20 mM KCl solution, and trimmed to ~4 cm in length, to remove distal embolized conduits. Samples were then inserted into a steady state flow meter (SSFM) to measure hydraulic conductance, $K$, $kg \bullet s^{-1} \bullet MPa^{-1}$ (see Hudson *et al.* 2010 and Feild *et al*. 2011 for full description of methods). The hydraulic head pressure was supplied by gas tank, and maintained at 0.08 MPa, and we used degassed 20mM KCl as a sap surrogate to control for ion-dependent effects on stem hydraulic function (Zwienecki *et al*. 2001). We calculated stem hydraulic conductivity ($K_h$, $kg \bullet m \bullet s^{-1} \bullet MPa^{-1}$) by multiplying $K$ by sample length. Sapwood cross-sections were measured for each sample to normalize $K_h$ at tissue level ($K_S$, sapwood -specific hydraulic conductivity, $kg \bullet m^{-1} \bullet s^{-1} \bullet MPa^{-1}$). Sapwood area was measured from cross sections taken at the sample distal end. Sections were stained with safaranin-O (0.01%), and photographed at 10x using a dissecting microscope (Carl Zeiss MicroImaging, Gottingen, Germany). We used ImageJ software (NIH Image, Bethesda, MD) to determine sapwood area ($A_S$) from images by subtracting pith area from cross section area. Distal leaf area for each sample was used to normalize $K_h$ at

shoot level ($K_L$, leaf-specific hydraulic conductivity, g•m$^{-1}$•s$^{-1}$•MPa$^{-1}$). Leaf area was measured using a scanner and ImageJ software. To calculate $A_S$:$A_L$, sapwood area was divided by leaf area and multiplied by $10^4$.

*2.2.4 Estimating transpiration supply*

We derived branch-estimated transpiration ($E_b$, mmol m$^{-2}$ s$^{-1}$) from a modified form of Darcy's Law (Tyree and Ewers 1991, Manzoni *et al.* 2013):

$$E_b = \left(\frac{K}{A_L}\right)\Delta\Psi$$

where $K$ is branch conductance (mmol•s$^{-1}$•MPa$^{-1}$, derived by dividing $K$ by molar mass of water), $A_L$ is branch leaf area (m$^2$), and $\Delta\Psi$ is the driving gradient for water transport ($\Psi_{PD}$-$\Psi_{MD}$, MPa). $E_b$ is in the same units as transpiration measured by portable leaf level gas exchange equipment (i.e., LiCor 6400 infrared gas analyzer, LiCor Inc., Lincoln, NE, USA), and represents a point measurement similar to that described by Wullschleger, Meinzer and Vertessy (1998). $E_b$ will over estimate actual transpiration, because it cannot account for resistances imposed by extraxylary transport, mesophyll conductance, stomatal conductance, or boundary layer conductance, all of which will reduce water transport relative to shoot xylem.

*2.2.5 Vulnerability to embolism*

We measured embolism vulnerability of branches (~30 cm in length and 5-8 mm in diameter) cut from trees under water, transferred to water-filled containers and allowed to rehydrate in a refrigerator or under vacuum infiltration over night, or until measurement within 48 hours of collection. Rehydrated branches had indistinguishable

$K_S$ compared to vacuum infiltrated branches ($p = 0.5$ for piñon, $p = 0.61$ for juniper), so we switched to rehydration refilling as it allowed for more rapid sample processing. Prior to measurement, we trimmed samples while submerged in 20 mM KCl solution. Hydraulic conductivity was measured as above, with the initial $K_h$ value designated $K_{max}$. After $K_{max}$ was established, the sample was placed in a double-ended pressure sleeve, and the air injection technique (Sperry and Saliendra 1994) was used to generate embolism-propagating stress. Pressurization lasted two minutes, and samples were depressurized slowly (~ 2 MPa per minute). We established that pressurization for two minutes resulted in similar loss of conductivity observed with longer (5 or 10 min) treatment (data not shown). Samples were allowed to equilibrate following depressurization, and then reconnected to the SSFM to measure $K$. Percent loss of conductivity was calculated as:

$$PLC = 100 \bullet \left(1 - \frac{K_i}{K_{max}}\right)$$

where $K_i$ is the measurement of $K$ after the $i^{th}$ pressurization. A total of five or six pressurizations were carried out on each sample, depending on species. Juniper samples were pressurized over a span of 1.5 - 14 MPa, while piñon samples were pressurized over a span of 1.5 – 6 MPa.

We used a Weibull function to generate vulnerability curves using PLC data points (Neufeld *et al.* 1992). A Weibull function was preferred over a sigmoid function because a Weibull forces the vulnerability curve to start at the origin (i.e., 0 stress results in 0 PLC). The structure of the Weibull function is:

$$PLC = 100 - 100 \bullet e^{\left[-\left(\frac{\Psi_w}{a}\right)^b\right]}$$

where $a$ and $b$ are curve fitting parameters (Hubbard *et al.* 2001). Parameters $a$ and $b$

were subsequently used to calculate $P_{50}$ from the Weibull fit, according to the equation:

$$P_{50} = a \bullet \sqrt[b]{-\ln(0.5)}$$

The derivative of the Weibull function at $P_{50}$ was then used to find the slope of the line tangent to $P_{50}$. The x-intercept of this line is $P_e$, the air entry threshold (Domec and Gartner 2001), and the x-value when y = 100 is $P_{max}$, the hydraulic failure threshold. The difference between $P_e$ and $P_{max}$ is the drought stress interval (DSI, MPa), and represents the span of water potentials over which a plant experiences drought stress but maintains some degree of hydraulic function.

*2.2.6 Wood anatomy*

Hand sections were obtained from vulnerability curve samples, stained with Safranin-O, and photographed at 400x on a compound microscope (Zeiss AxioImager M1, Zeiss). Only early-wood tracheids from recent growth were measured, as these tracheids are responsible for the majority of water transport (Domec and Gartner 2002, Bouche *et al.* 2014). Lumen area and adjacent anticlinal walls ($T_W$) were traced using ImageJ. Lumen diameters ($D$) were calculated as the square root of lumen area, which is more appropriate for rectilinear tracheids (Sperry and Hacke 2004, Hacke *et al.* 2004). A minimum of 20 tracheids from each sample were measured, for $N$ = 300 tracheids per species, per treatment. We confirmed that cross section lumen diameter distributions were similar to those measured in macerated samples. The hydraulically weighted lumen diameter ($D_H$) was calculated as:

$$D_H = 2\left(\frac{\Sigma r^5}{\Sigma r^4}\right)$$

where *r* is the lumen radius, in microns (Sperry and Hacke 2004). Conduit thickness to span ratio $(T_W/D)^2$ was calculated as the square of the ratio of adjacent double wall thickness to lumen diameter (Hacke *et al*. 2001).

*2.2.7 Wood density*

Wood density ($\rho_W$, $g \cdot cm^{-3}$) was measured by volumetric displacement. A small piece of branch, immediately adjacent to the $K_h$ sample, was stripped of bark, split along the long axis, and stripped of pith. One of the halves was shortened, to aid in sub-sample identification. Each sub-sample submerged in a beaker of water on a scale. The resulting mass change caused by the subsample is equal to volume of water displaced; mass was converted to volume by dividing by the density of water at standard temperature and pressure ($1\ g \cdot cm^{-3}$). The mass of paired sub-samples was determined after drying in a coin envelope for 48 hours at 60ºC. $\rho_W$ is calculated as dry mass divided by fresh volume (McCulloh *et al.* 2014).

*2.2.8 Data analysis*

We used R (R Core Team 2012) and the packages lme4 (Bates, Maechler & Bolker, 2012) and nlme (Pinheiro *et al.*, 2016) to perform a linear mixed effects analysis of the relationship between our physiological response variables and drought imposition both before and after monsoon precipitation input. We set treatment, period (before or after monsoon onset), and the interaction term as fixed effects. As random effects, we structured the model to allow for random intercepts for individual trees and sampling dates. Separate models for pre- and post-monsoon data were generated if the full model indicated a significant period effect. When visual inspection of residual plots revealed

obvious deviations from homoscedasticity or normality (Winter 2013), square root or natural log transformations were employed to meet necessary model assumptions. *P*-values were obtained by likelihood ratio tests of the full model with the effect in question against the model without the effect in question. We also composed models that used the interaction of experimental day and treatment as a fixed effect, with target tree as a random effect. This model structure allowed us to identify sampling dates where water status or hydraulic function differed significantly across treatments within species. Reported values of water potential and hydraulic conductivity are least squares mean estimates ± modeled standard error.

Covariation of water stress, hydraulic function, treatment, and period were also assessed using linear mixed effects models. We examined the relationships of $K_S$, $K_L$, and $E_b$ to $\Psi_{PD}$, which we used as a proxy for water stress intensity. For response variables where $\Psi_{PD}$ was determined to be a significant fixed effect, but treatment was not, data were pooled and a post-hoc linear regression was used to determine the significance and strength of the relationship between water stress and hydraulic function. Reported coefficients (intercepts and slopes) are least squares mean estimates ± modeled standard error.

We used a MANOVA framework to detect significant differences in vulnerability to embolism and tracheid anatomy due to treatment and species. Subsequent comparisons of means (univariate ANOVA with Tukey HSD comparisons of means) were conducted if significant treatment effects were discovered. Data were analyzed in R, and all values presented are mean ± standard error.

## 2.3 Results

### *2.3.1 Climate and treatment effects on plant water status*

Precipitation inputs to the various treatments over the three years preceding our measurements totaled 1110.9 mm, 982.4 mm, and 637.6 mm for irrigation, control, and drought respectively. During the measurement years, ambient annual precipitation ranged from a minimum of 252 mm in 2011 to a maximum of 385.8 mm in 2013 (Fig. 2.1a) and averaged 304.2 (± 1 SE = 23.1) mm $yr^{-1}$, which was less than the 20-year mean reported from a nearby LTER meteorological station (362.7 mm $yr^{-1}$, 1989-2009, Cerro Montosa #42; http://sev.lternet.edu/). We estimated precipitation for drought and irrigation plots using the known percentage rainout coverage of each drought plot and the volume of water added to irrigation plots (Pangle *et al.* 2012). Supplemental water addition elevated irrigation precipitation inputs to 411.7 ± 27.7 mm $yr^{-1}$, from 2010-2014, which was 21.1% greater than ambient (average irrigation was 81.8 ± 4.3 mm $yr^{-1}$, Fig. 2.1a & b). Based on projected 45% precipitation reduction, drought treatment annual precipitation was calculated to be 162.7 ± 12.7 mm $yr^{-1}$ for years 2010 to 2014 (Fig. 2.1b).

Plant water status of piñon and juniper, as measured by predawn water potential was strongly affected by our treatments (Fig. 2.2a & b). As expected, irrigation had a stronger effect on plant water status during the spring dry period, while drought structures had a stronger effect during summer monsoon. Piñon water status responded more strongly to water addition, while juniper water status responded more strongly to water withholding. Before the monsoon, our irrigation treatments raised $\Psi_{PD}$ by 0.59 MPa

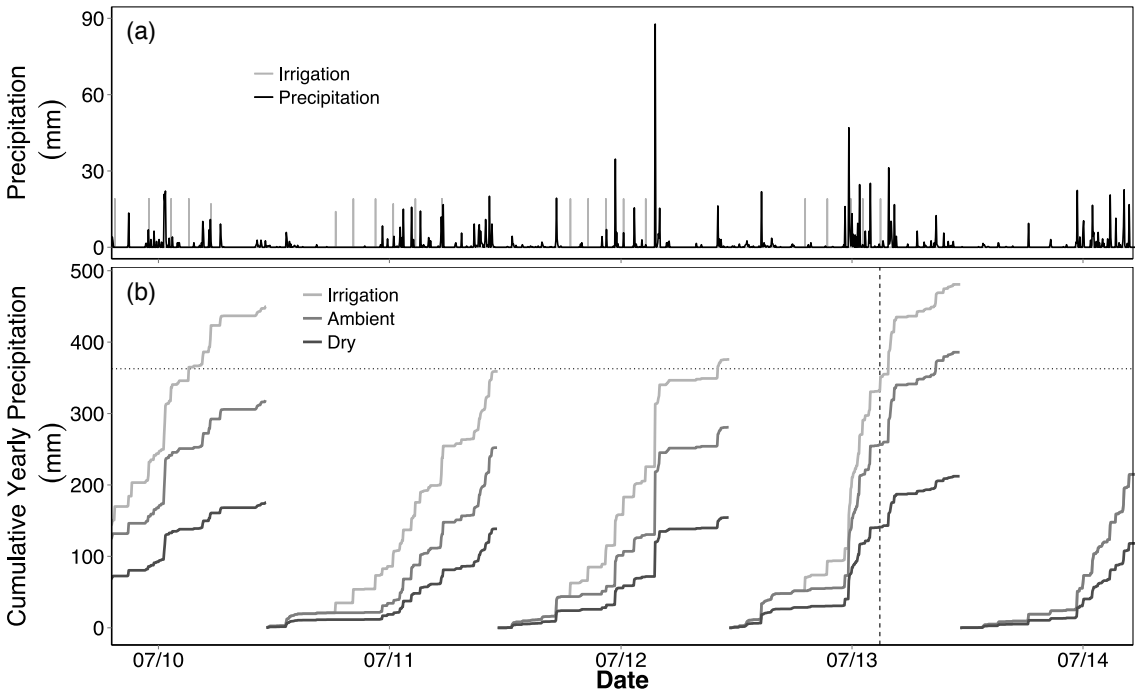


Figure 2.1: Absolute (a) and cumulative yearly (b) precipitation and irrigation inputs on experimental plots from May 1st 2010 to October 1st 2014. In (a), black vertical lines indicate precipitation events, gray vertical lines represent irrigation treatment supplemental watering. Pre- monsoon sampling dates are denoted by - , post-monsoon onset sampling dates are denoted by +. Solid lines in (b) represent treatment cumulative yearly water inputs, the horizontal dotted line represents the 20 year average (362.7 mm $yr^{-1}$, 1989-2009) from nearest site meteorological station, and the vertical dashed line denotes the last supplemental watering; after this date, ambient and irrigation treatments received identical precipitation inputs.

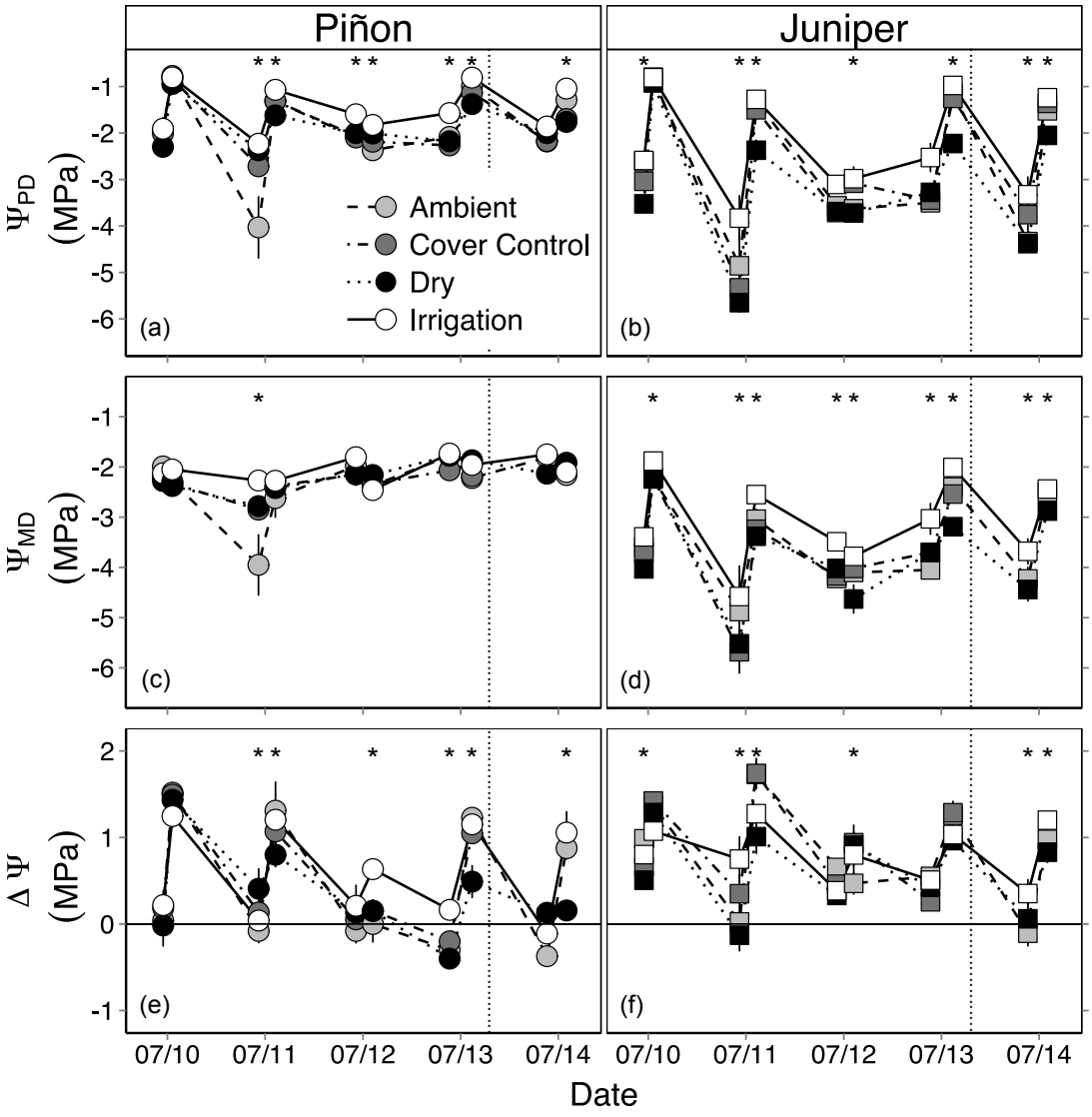


Figure 2.2: Mean predawn water potential ($\Psi_{PD}$), midday water potential ($\Psi_{MD}$), and driving gradient ($\Delta\Psi$) of pre- and post-monsoon onset sampling of piñon (a,c,e) and juniper (b,d,f) from June 2010 through August 2014. Circles represent piñon means, squares represent juniper means. Error bars are ± 1 SE. Asterisks indicate significant treatment effects for a given sampling date ($p < 0.05$). Supplemental water addition ended in 2013, as did midday Cover Control measurements, and is indicated by the vertical dotted line.

(24.5%) and 0.58 MPa (16.2%) for piñon and juniper, respectively, relative to ambient conditions. Following the monsoon, drought structures decreased $\Psi_{PD}$ by 0.2 MPa (15.5%) and 0.59 MPa (37.6%) for piñon and juniper, respectively, relative to ambient conditions. For both species, irrigation elevated $\Psi_{PD}$ relative to all other treatments before monsoon onset, while ambient $\Psi_{PD}$ did not differ from drought treatment (Fig. 2.3a). In all treatments, we observed higher $\Psi_{PD}$ for piñon compared to juniper. After monsoon onset, irrigated piñon continued to have higher $\Psi_{PD}$ than all other treatments, but $\Psi_{PD}$ in irrigated juniper was no longer distinct from cover control juniper. Drought $\Psi_{PD}$ was lowered relative to ambient treatment for both species. After the start of the monsoon, piñon $\Psi_{PD}$ was only higher than juniper in the water addition and water withholding treatments (Fig. 2.3a).

Piñon $\Psi_{MD}$ converged on -2.2 MPa (Fig. 2.2c), both pre- and post-monsoon, although irrigated individuals had higher $\Psi_{MD}$ compared to all other treatments before the monsoon (Fig. 2.3b). Though broadly consistent with isohydric $\Psi_{W}$ regulation, during the particularly dry 2011 premonsoon sampling period, ambient treatment piñon $\Psi_{PD}$ (-4.03 ± 0.67) and $\Psi_{MD}$ (-3.95 ± 0.61 MPa) fell below the isohydric threshold reported at this site and in the literature (e.g. West *et al*. 2007, McDowell *et al*. 2008, Breshears *et al*. 2009, Plaut *et al*. 2012, Limousin *et al*. 2013, Pangle *et al*. 2015). Before the monsoon, non-irrigated juniper also converged on a common $\Psi_{MD}$ (~ -4.2 MPa, Fig. 2.2d), though irrigated trees had higher water status. After the monsoon began, irrigated juniper $\Psi_{MD}$ was higher than ambient and cover control, which was in turn higher than drought $\Psi_{MD}$

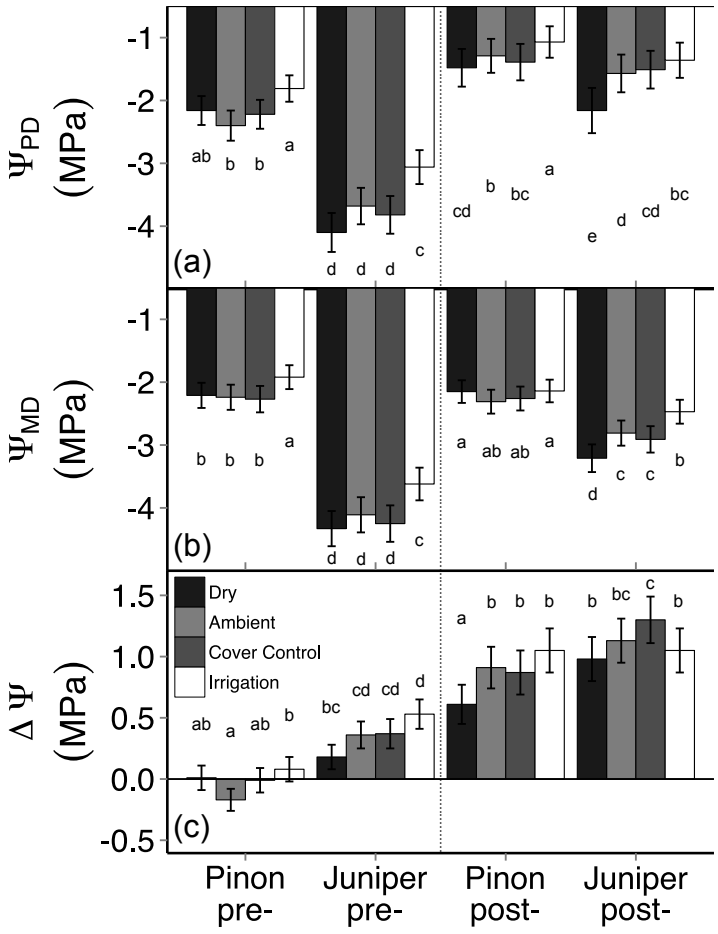


Figure 2.3: Overall experimental means of (a) predawn water potential ($\Psi_{PD}$), (b) midday water potential ($\Psi_{MD}$), and (c) driving gradient for transpiration ($\Delta\Psi$) for pre- and post-monsoon onset sampling of piñon and juniper. Letters indicate differences significant at $p < 0.05$, and comparisons are restricted to within sampling period, between species and across treatments. Error bars are ± 1 SE.

(Fig. 2.3b). Minimum juniper $\Psi_{PD}$ (-5.65 ± 0.17) and $\Psi_{MD}$ (-5.68 ± 0.44 MPa) occurred in drought and cover control during the hot dry pre-monsoon period of 2011.

Driving gradient for transpiration ($\Delta\Psi$, MPa) was impacted by treatment for both species (Figs. 2.2e & f). Prior to monsoon activity, irrigation increased $\Delta\Psi$ above all other treatments for piñon, whereas only irrigation and drought treatments differed for juniper (Fig. 2.3c). After the monsoon, drought treatment had reduced $\Delta\Psi$ compared to all other treatments for piñon, while cover control treatment had elevated $\Delta\Psi$ compared to both drought and irrigation treatments for juniper. Interestingly, $\Delta\Psi$ was not different between species in either the ambient or irrigation treatments, but was lower for piñon in the drought and cover control treatments.

$\Psi_{PD}$ strongly predicted $\Psi_{MD}$ for both species ($p < 0.0001$) before the monsoon, but the relationship was stronger in anisohydric juniper ($R^2 = 0.89$) than isohydric piñon ($R^2 = 0.67$, Fig. 2.4a). After the monsoon, $\Psi_{PD}$ continued to be a strong predictor of $\Psi_{MD}$ ($R^2 = 0.81$) in juniper, but ceased to have a significant relationship in piñon ($R^2 = 0.02$, Fig. 4c). Consequently, the power of $\Psi_{PD}$ to predict $\Delta\Psi$ shifted from weak ($R^2 = 0.07$) to strong ($R^2 = 0.67$) with monsoon onset in piñon, while this linear relationship remained consistent and moderate in juniper ($R^2 = 0.39$ pre-, $R^2 = 0.31$ post-monsoon, Fig. 2.4b & d). No treatment effects were found for these relationships in either species.

*2.3.2 Shoot level hydraulic architecture*

Variation in long-term moisture availability yielded differences in allocation ratios of sapwood area to leaf area (Fig. 2.5a). Irrigated piñon reduced $A_S$:$A_L$ relative to ambient ($p = 0.0003$) and droughted ($p = 0.02$) piñon, but droughted piñon did not increase $A_S$:$A_L$ relative to ambient ($p = 0.2$, Fig. 2.6a). Patterns of tissue allocation in

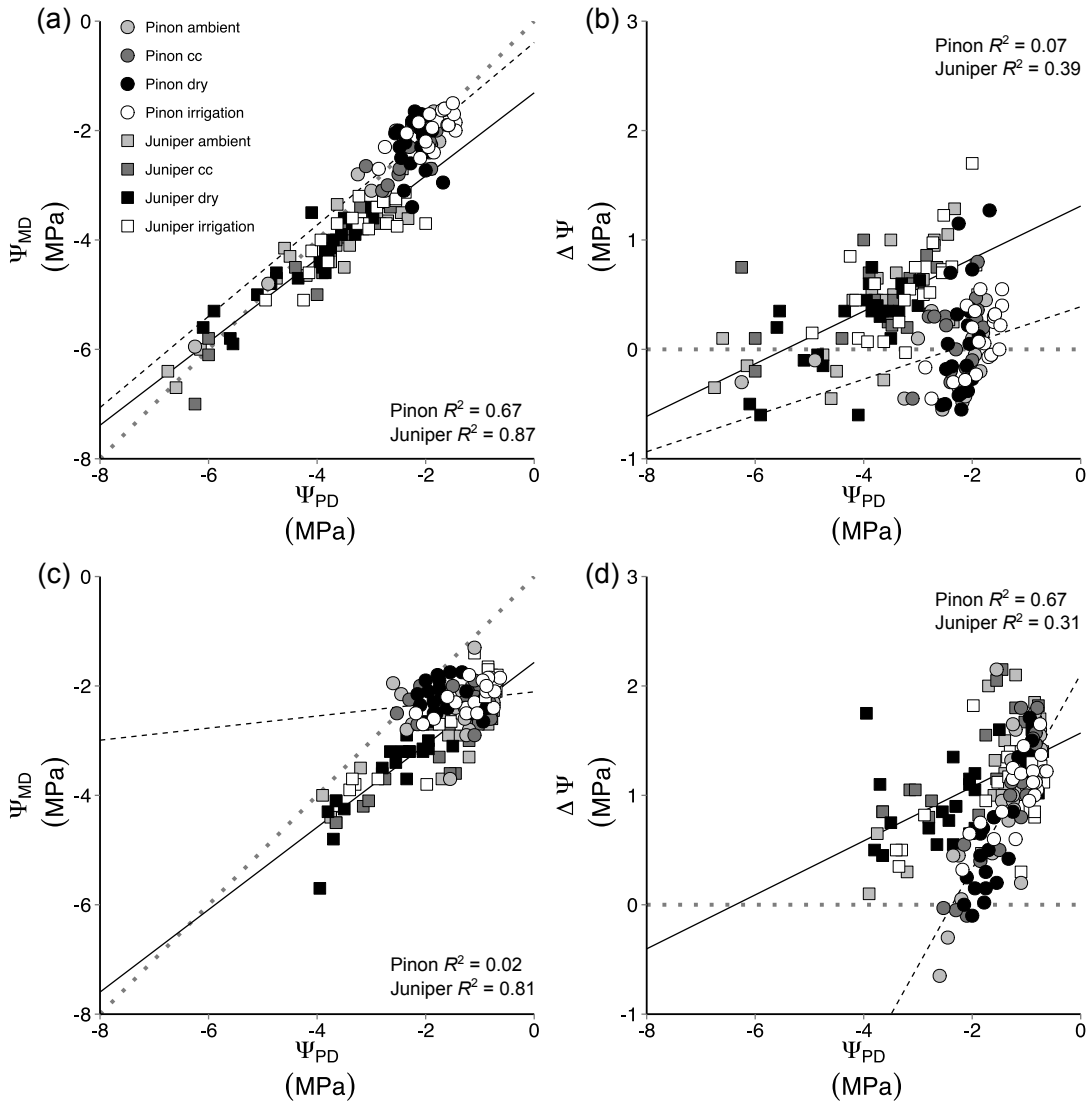


Figure 2.4: Relationships between predawn water potential ($\Psi_{PD}$) and midday water potential ($\Psi_{MD}$) for piñon (circles, dashed linear fit line) and juniper (squares, solid linear fit line) before and after monsoon onset (a,c). Dotted gray line indicates 1:1 scaling. Relationships between and driving gradient for piñon (circles, dashed linear fit line) and juniper (squares, solid linear fit line) before and after monsoon onset (b,d). Dotted gray line at $\Delta\Psi = 0$ indicates the point at which no driving gradient for transpiration exists.

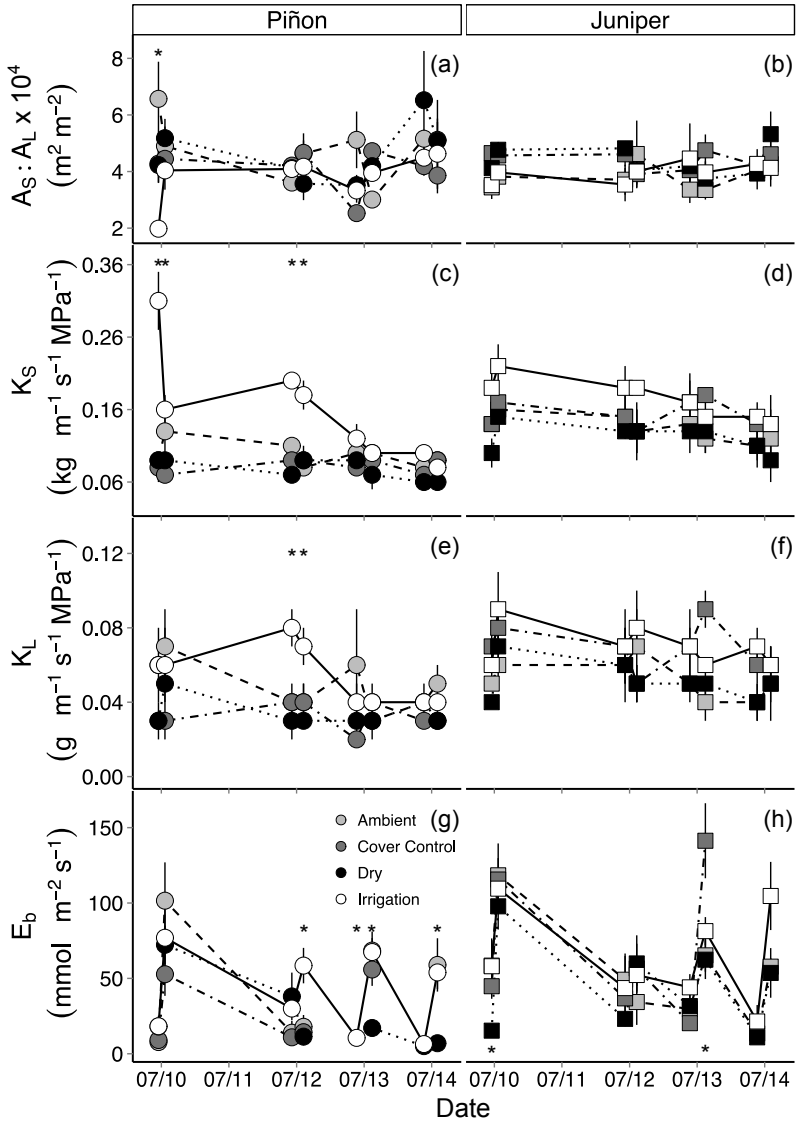


Figure 2.5: Mean (a,b) sapwood area to leaf area ratio ($A_S$:$A_L$); (c,d) sapwood-specific hydraulic conductivity ($K_S$); (e,f) leaf-specific hydraulic conductivity ($K_L$); and (g,h) branch estimated transpiration ($E_b$) for piñon (a,c,e,g) and juniper (b,d,f,h) from each sampling date. Error bars are ± 1 SE. Asterisks indicate significant treatment effects for a given sampling date ($p < 0.05$).

response to precipitation manipulation were less clear for juniper (Fig. 2.5b). Drought and cover control treatments had increased $A_S$:$A_L$ relative to ambient ($p$ = 0.023 and 0.007, respectively), while irrigated trees only reduced $A_S$:$A_L$ compared to cover control ($p$ = 0.018, Fig. 2.6a). Between species, piñon and juniper maintained similar $A_S$:$A_L$ values in all treatments, except ambient, wherein piñon had higher $A_S$:$A_L$ than juniper ($p$ = 0.009, Fig. 2.6a).

Sapwood-specific hydraulic conductivity was significantly impacted by precipitation manipulation (Fig. 2.5c & d). $K_S$ did not vary between pre-/post-monsoon sampling dates, yet we found $K_S$ increased with increasing moisture availability in both species, and dynamics of treatment effects varied by species (Fig. 2.6b). Irrigated piñon displayed a higher $K_S$ than all other treatments ($p < 0.0001$ for all comparisons), which did not differ from one another. In contrast, irrigated juniper deviated from droughted and ambient juniper ($p$ = 0.007 and $p$ = 0.04, respectively) but not cover control. Juniper $K_S$ was greater than piñon in all treatments, but only significantly different in the drought and cover control treatments ($p$ = 0.04, $p$ = 0.0003, respectively).

Experimental treatments influenced shoot level hydraulic supply (Fig. 2.5e & f). As with $K_S$, $K_L$ was not affected pre-/post-monsoon changes in precipitation, but did scale with treatment water availability. Ambient and irrigated piñon had higher $K_L$ than cover control and drought piñon ($p < 0.03$, Fig. 2.6c). Irrigated juniper had higher $K_L$ than drought juniper ($p$ = 0.04), though neither treatment deviated significantly from ambient. Between species, $K_S$ and $A_S$:$A_L$ varied such that in ambient conditions, piñon and juniper achieved similar rates of $K_L$ ($p$ = 0.8, Table 2.2). However, in both water addition and water withholding treatments, juniper achieved higher $K_L$ than piñon ($p < 0.02$, Fig. 2.6c).

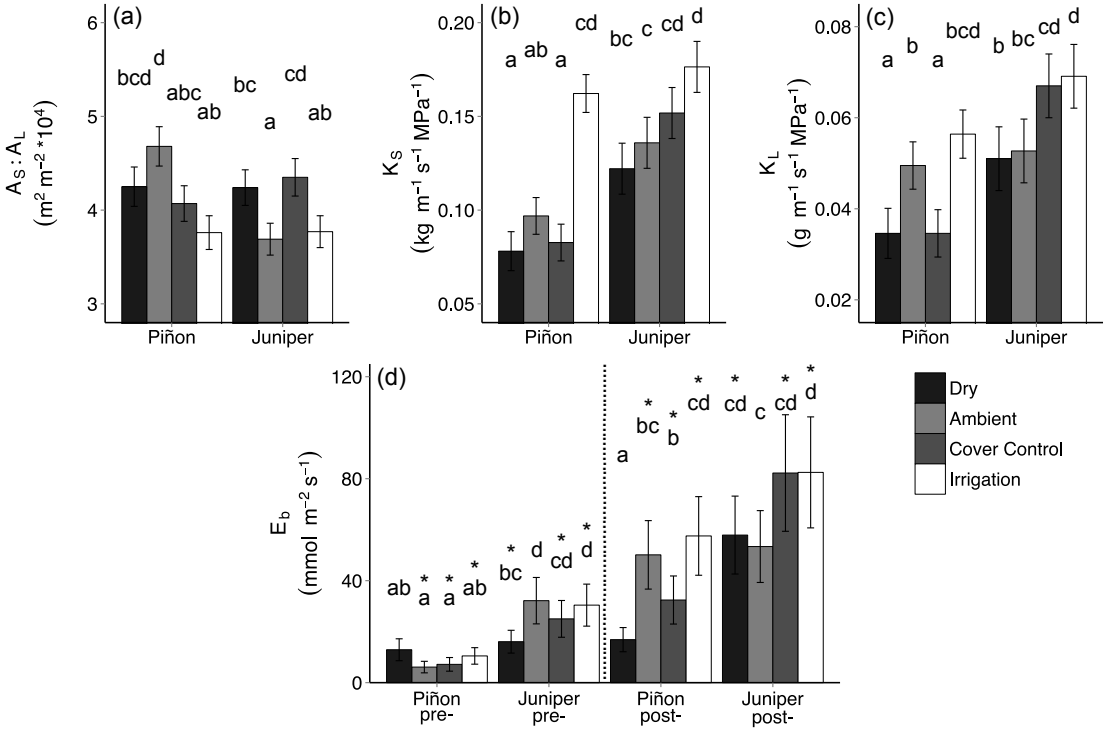


Figure 2.6: Overall experimental means of (a) sapwood area to leaf area ratio ($A_S$:$A_L$), (b) sapwood-specific hydraulic conductivity ($K_S$), (c) leaf-specific hydraulic conductivity ($K_L$), and (d) branch estimated transpiration ($E_b$) by species and treatment over study duration. Error bars ± 1 SE, and different letters indicate significant differences at $p \leq 0.05$. In (d), comparisons between treatments and species are displayed by season (pre-/post- monsoon onset, separated by vertical dotted line), and asterisks indicate significant season effects within treatment and species.

Branch estimated transpiration responded to monsoon precipitation, and we observed season by treatment interaction effects (Fig. 2.5g & h, Fig. 2.6d). $E_b$ did not vary in piñon across treatments pre-monsoon ($p > 0.05$). Experimental drought suppressed $E_b$ in piñon relative to all other treatments after monsoon onset ($p > 0.05$), while water addition elevated $E_b$ compared to cover control ($p = 0.047$), but not ambient piñon ($p = 0.470$). Droughted juniper had lower $E_b$ than ambient and irrigation treatments before monsoon onset ($p < 0.01$). Monsoon precipitation raised $E_b$ in all experimental treatments ($p \geq 0.05$), but not ambient ($p = 0.16$), and only ambient and irrigation treatments deviated from each other ($p = 0.03$). Prior to the monsoon, piñon had lower $E_b$ than juniper in all treatments except drought ($p < 0.004$), but after monsoon onset, piñon and juniper achieved equivalent $E_b$ in irrigation and ambient treatments ($p > 0.2$).

*2.3.3 Relationships between water stress and hydraulic performance*

We found no relationship between $\Psi_{PD}$ and $K_S$ ($p = 0.43$ and $p = 0.21$ for piñon and juniper, respectively, Table 2.1, Fig. 2.7a, Table 2.2) or $K_L$ ($p = 0.21$ and $p = 0.07$ for piñon and juniper, respectively, Table 2.1, Fig. 2.7b, Table 2.3). $\Psi_{PD}$ co-varied with $E_b$ (Table 2.1, Fig. 2.7c, Table 2.4), and after linear mixed effects models failed to reveal significant differences in the relationship across treatments within piñon ($p = 0.47$) or juniper ($p = 0.17$), we pooled the treatment data for both species. $\Psi_{PD}$ explained similar proportions of variation in $E_b$ for both species (piñon $R^2 = 0.41$, juniper $R^2 = 0.45$). Model slopes and intercepts were used to estimate $\Psi_{PD}$ at zero $E_b$ (referred to hereafter as $\Psi_{E=0}$), the point at which stomata remain closed and transpiration is zero. Our estimates of $\Psi_{E=0}$ in piñon(-2.34 ± 0.09 MPa) and juniper (-4.86 ± 0.19 MPa) were consistent with their isohydric and anisohydric stomatal regulation, respectively.

Table 2.1: Coefficients ± standard error of the linear mixed effects model regressions between $\Psi_{PD}$ (MPa) and $K_S$ (kg $m^{-1}$ $s^{-1}$ $MPa^{-1}$), $K_L$ (g $m^{-1}$ $s^{-1}$ $MPa^{-1}$), and $E_b$ (mmol $m^{-2}$ $s^{-1}$). Response variable data were log transformed as necessary to meet assumptions of normality. *P*-values for ambient treatments indicate significance of relationship between response variable and $\Psi_{PD}$; all other *p*-values indicate significance of difference between treatment slopes and ambient control slope.

| **$K_S$** | | | | | |
|---|---|---|---|---|---|
| **Species** | **Treatment** | **Intercept** | **Slope** | **$R^2$** | ***p*-value** |
| Piñon | | | | | |
| | Ambient | 0.12 ± 0.02 | 0.014 ± 0.013 | - | 0.26[a] |
| | Cover Control | 0.08 ± 0.03 | -0.002 ± 0.018 | - | 0.38[a] |
| | Dry | 0.08 ± 0.04 | -0.003 ± 0.021 | - | 0.43[a] |
| | Irrigation | 0.07 ± 0.03 | -0.067 ± 0.020 | - | 0.0001[b] |
| | Model: lme($K_S$ ~ $\Psi_{PD}$ * Treatment, na.action = na.omit, method = "ML") | | | | |
| Juniper | | | | | |
| | Ambient | 0.14 ± 0.02 | 0.003 ± 0.006 | - | 0.56[a] |
| | Cover Control | 0.17 ± 0.03 | 0.009 ± 0.008 | - | 0.51[a] |
| | Dry | 0.14 ± 0.03 | 0.004 ± 0.009 | - | 0.90[a] |
| | Irrigation | 0.17 ± 0.03 | -0.002 ± 0.009 | - | 0.57[a] |
| | Model: lme($K_S$ ~ $\Psi_{PD}$ * Treatment, na.action = na.omit, method = "ML") | | | | |
| **$K_L$** | | | | | |
| Piñon | | | | | |
| | Ambient | 0.061 ± 0.010 | 0.007 ± 0.005 | - | 0.20[a] |
| | Cover Control | 0.038 ± 0.015 | 0.002 ± 0.008 | - | 0.54[a] |
| | Dry | 0.049 ± 0.017 | 0.008 ± 0.009 | - | 0.92[a] |
| | Irrigation | 0.041 ± 0.014 | -0.011 ± 0.008 | - | 0.03[b] |
| | Model: lme($K_L$ ~ $\Psi_{PD}$ * Treatment, na.action = na.omit, method = "ML") | | | | |
| Juniper | | | | | |
| | Ambient | 0.053 ± 0.010 | -0.00006 ± 0.005 | - | 0.99[a] |
| | Cover Control | 0.080 ± 0.015 | 0.0052 ± 0.008 | - | 0.27[a] |
| | Dry | 0.067 ± 0.016 | 0.0054 ± 0.009 | - | 0.27[a] |
| | Irrigation | 0.069 ± 0.015 | 0.00001 ± 0.008 | - | 0.99[a] |
| | Model: lme($K_L$ ~ $\Psi_{PD}$ * Treatment, na.action = na.omit, method = "ML") | | | | |
| **$E_B$** | | | | | |
| Piñon | | | | | |
| | Ambient | 130.76 ± 16.02 | 56.78 ± 10.29 | - | <0.0001[a] |
| | Cover Control | 91.23 ± 25.31 | 40.06 ± 16.79 | - | 0.32[a] |
| | Dry | 115.81 ± 27.37 | 53.59 ± 16.62 | - | 0.85[a] |
| | Irrigation | 98.81 ± 22.65 | 38.03 ± 15.04 | - | 0.22[a] |
| | All Treatments | **109.68 ± 9.02** | **47.46 ± 6.02** | **0.41** | **<0.0001** |
| | Model: lme($E_b$ ~ $\Psi_{PD}$ * Period, na.action = na.omit, method = "ML") | | | | |
| Juniper | | | | | |
| | Ambient | 108.98 ± 12.33 | 20.71 ± 4.63 | - | <0.0001[a] |
| | Cover Control | 161.06 ± 18.81 | 35.48 ± 6.94 | - | 0.036[b] |
| | Dry | 107.60 ± 19.64 | 21.16 ± 6.87 | - | 0.95[a] |
| | Irrigation | 124.71 ± 17.29 | 27.46 ± 6.82 | - | 0.32[a] |
| | All Treatments | **124.42 ± 6.71** | **25.83 ± 2.47** | **0.45** | **<0.0001** |
| | Model: lme($E_B$ ~ $\Psi_{PD}$ * Period, na.action = na.omit, method = "ML") | | | | |

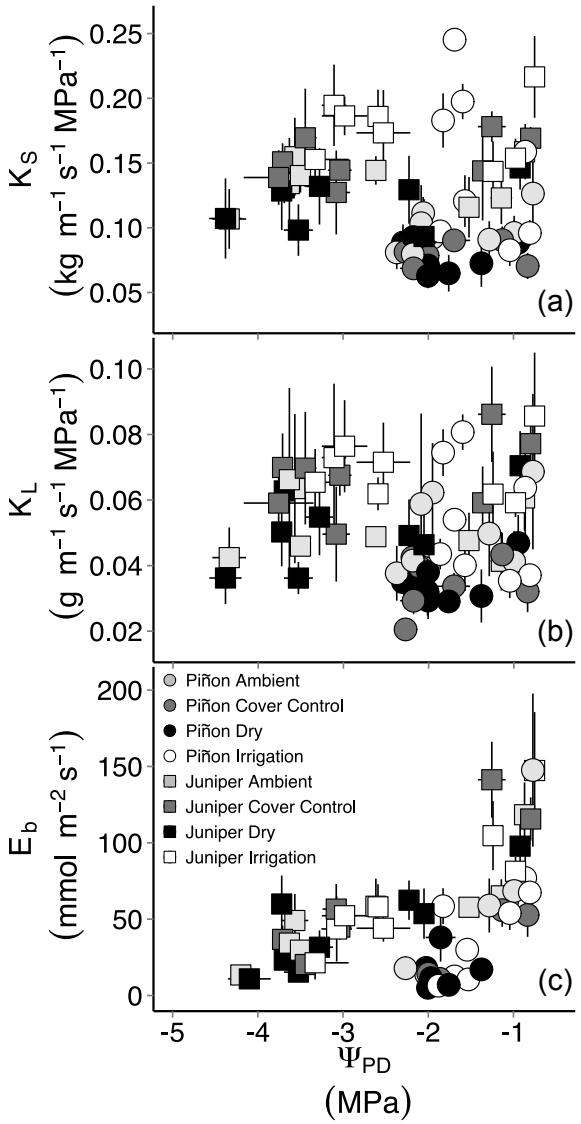


Figure 2.7. Relationships between pre-dawn water potential ($\Psi_{PD}$) and (a) sapwood-specific hydraulic conductivity ($K_S$), (b) leaf-specific hydraulic conductivity ($K_L$), and (c) branch estimated transpiration ($E_b$). Error bars are ± 1 SE; data from all years are pooled.

Table 2.2: Summary of the linear mixed models of the relationship between $K_S$ and $\Psi_{PD}$ for both species. $K_S$ and $\Psi_{PD}$ were used as response and explanatory variables in both the piñon and juniper models.

| Species | Fixed Effects | numDF | denDF | F-value | p-value |
|---|---|---|---|---|---|
| Piñon | Intercept | 1 | 119 | 758.9537 | **<0.0001** |
| | $\Psi_{PD}$ | 1 | 119 | 0.6241 | 0.4311 |
| | Treatment | 3 | 16 | 25.1419 | **<0.0001** |
| | $\Psi_{PD}$:Treatment | 3 | 119 | 5.9201 | **0.0008** |
| Juniper | Intercept | 1 | 128 | 529.6056 | **<0.0001** |
| | $\Psi_{PD}$ | 1 | 128 | 3.0161 | 0.0848 |
| | Treatment | 3 | 16 | 2.9705 | 0.0632 |
| | $\Psi_{PD}$:Treatment | 3 | 128 | 0.5008 | 0.6824 |

*Note:* Full model: lme($K_S$ ~ $\Psi_{PD}$*Treatment, random=~1| tree, na.action=na.omit, method="ML")

Table 2.3: Summary of the linear mixed models of the relationship between $K_L$ and $\Psi_{PD}$ for both species. $K_L$ and $\Psi_{PD}$ were used as response and explanatory variables for both juniper model and piñon models.

| Species | Fixed Effects | numDF | denDF | F-value | p-value |
|---|---|---|---|---|---|
| Piñon | Intercept | 1 | 119 | 350.2519 | **<0.0001** |
| | $\Psi_{PD}$ | 1 | 119 | 1.5801 | 0.2112 |
| | Treatment | 3 | 16 | 4.9275 | **0.0130** |
| | $\Psi_{PD}$:Treatment | 3 | 119 | 1.8522 | 0.1414 |
| Juniper | Intercept | 1 | 128 | 397.3040 | **<0.0001** |
| | $\Psi_{PD}$ | 1 | 128 | 3.3139 | **0.071** |
| | Treatment | 3 | 16 | 2.0639 | 0.1454 |
| | $\Psi_{PD}$:Treatment | 3 | 128 | 0.7426 | 0.5285 |

*Note:* Full model: lme($K_L$ ~ $\Psi_{PD}$*Treatment, random=~1| tree, na.action=na.omit, method="ML")

Table 2.4: Summary of the linear mixed models of the relationship between $E_b$ and $\Psi_{PD}$ for both species. $E_b$ and $\Psi_{PD}$ were used as response and explanatory variables for both piñon and juniper models.

| Species | Fixed Effects | numDF | denDF | F-value | p-value |
|---|---|---|---|---|---|
| Piñon | Intercept | 1 | 64 | 133.62688 | **<0.0001** |
| | $\Psi_{PD}$ | 1 | 64 | 69.10819 | **<0.0001** |
| | Treatment | 3 | 16 | 0.88108 | 0.4717 |
| | $\Psi_{PD}$:Treatment | 3 | 64 | 0.69693 | 0.5573 |
| Juniper | Intercept | 1 | 109 | 492.2495 | **<0.0001** |
| | $\Psi_{PD}$ | 1 | 109 | 113.4729 | **<0.0001** |
| | Treatment | 3 | 16 | 1.8953 | 0.1711 |
| | $\Psi_{PD}$:Treatment | 3 | 109 | 1.8808 | 0.1371 |

*Note:* Full model: lme($E_b$ ~ $\Psi_{PD}$*Treatment, random=~1| tree, na.action=na.omit, method="ML")

*2.3.4 Vulnerability to embolism and hydraulic decline*

Embolism vulnerability did not vary among treatments in either species ($p = 0.45$ for piñon, $p = 0.83$ for juniper, Fig. 2.8a), so we pooled species data to generate composite curves. Piñon was significantly more vulnerable to embolism than juniper. For the four curve parameters calculated ($P_e$, $P_{50}$, $P_{max}$, and DSI), piñon values were roughly half as large as juniper (Table 2.5). Plotting the decline of $K_S$ with increasing simulated drought stress (Fig. 2.8b) showed that juniper possessed greater rehydrated maximum $K_S$ compared to piñon ($p = 0.0009$). Maximum $K_S$ was nearly twice as large as native $K_S$ for all treatments in juniper (one sample t-test, $p < 0.03$), but did not differ in piñon ($p > 0.4$).

*2.3.5 Anatomical structure and wood density*

Early wood tracheids were structurally similar in both species across all treatments (Fig. 2.9). Compared to juniper in the same treatment, piñon tracheids tended to have larger lumens and slightly, though not significantly, higher $D_H$, with the exception that droughted piñon had a significantly higher $D_H$ than droughted juniper (Fig. 9a). We detected no differences in double wall thickness ($T_W$) across treatments or between species (Fig. 2.9b). The combination of similar $T_W$ and reduced $D_H$ in juniper led to a significantly greater thickness to span ratio ($(T_W/D)^2$) compared to piñon in all treatments (Fig. 2.9c), which is consistent with the reported relationship between embolism resistance and $(T_W/D)^2$ (Hacke *et al.* 2001, Bouche *et al.* 2014). MANOVA did not detect significant differences in tracheid anatomy across treatments in piñon ($p = 0.91$) or juniper ($p = 0.44$). Wood density did not differ significantly between species or across treatments (Fig. 2.9d).

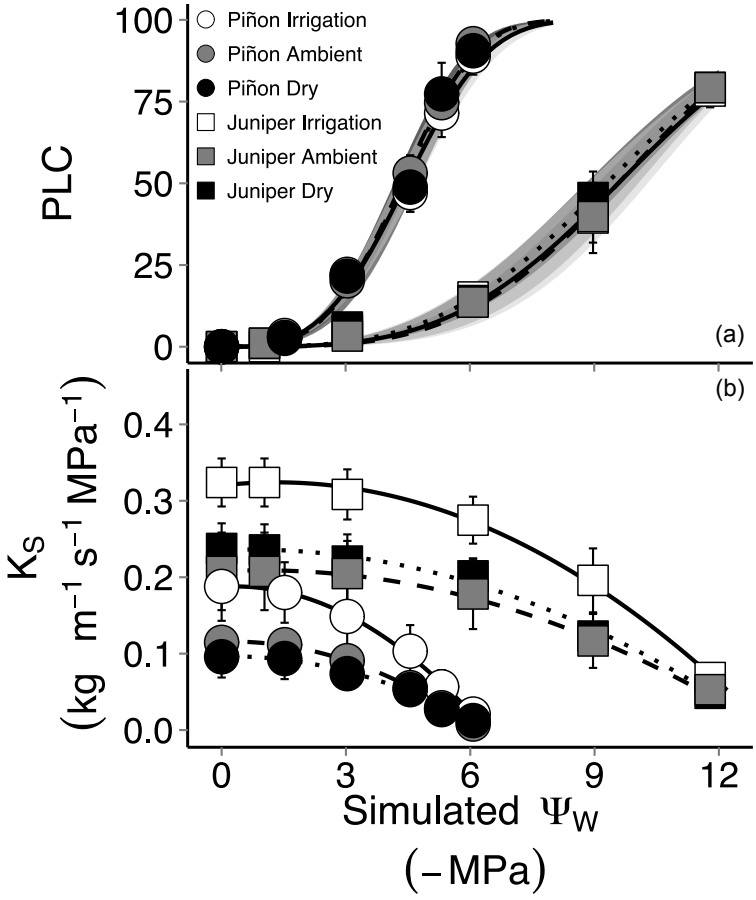


Figure 2.8: Treatment specific relationships between air-injection simulated water potential and (a) percent loss conductivity, and (b) absolute decline in sapwood-specific hydraulic conductivity ($K_S$), for piñon (circles) and juniper (squares). Solid lines denote irrigation fits, dashed lines denote ambient control fits, and dotted lines denote drought treatment fits. Shaded regions about the vulnerability curves in (a) are minimum/maximum vulnerability curves based on mean PLC ± 1 SE for each treatment, within each species.

Table 2.5: Parameters extracted from vulnerability curves. Letters denote significant differences within species across treatments; asterisks denote significant differences between species within treatment ($p \leq 0.05$).

| **Species** | **Treatment** | $P_e$ **(-MPa)** | $P_{50}$ **(-MPa)** | $P_{max}$ **(-MPa)** | **DSI (MPa)** |
|---|---|---|---|---|---|
| Piñon | | | | | |
| | Ambient | 2.59 ± 0.07* | 4.36 ± 0.1* | 6.13 ± 0.22* | 3.53 ± 0.26* |
| | Dry | 2.60 ± 0.28* | 4.43 ± 0.19* | 6.24 ± 0.54* | 3.64 ± 0.78* |
| | Irrigation | 2.56 ± 0.27* | 4.48 ± 0.22* | 6.41 ± 0.39* | 3.84 ± 0.5* |
| Juniper | | | | | |
| | Ambient | 5.34 ± 0.14* | 9.39 ± 0.43* | 13.44 ± 0.73* | 8.09 ± 0.61* |
| | Dry | 5.65 ± 0.73* | 9.29 ± 0.44* | 12.93 ± 0.52* | 7.28 ± 0.93* |
| | Irrigation | 6.13 ± 1.05* | 9.53 ± 0.67* | 12.92 ± 0.63* | 6.79 ± 1.09* |

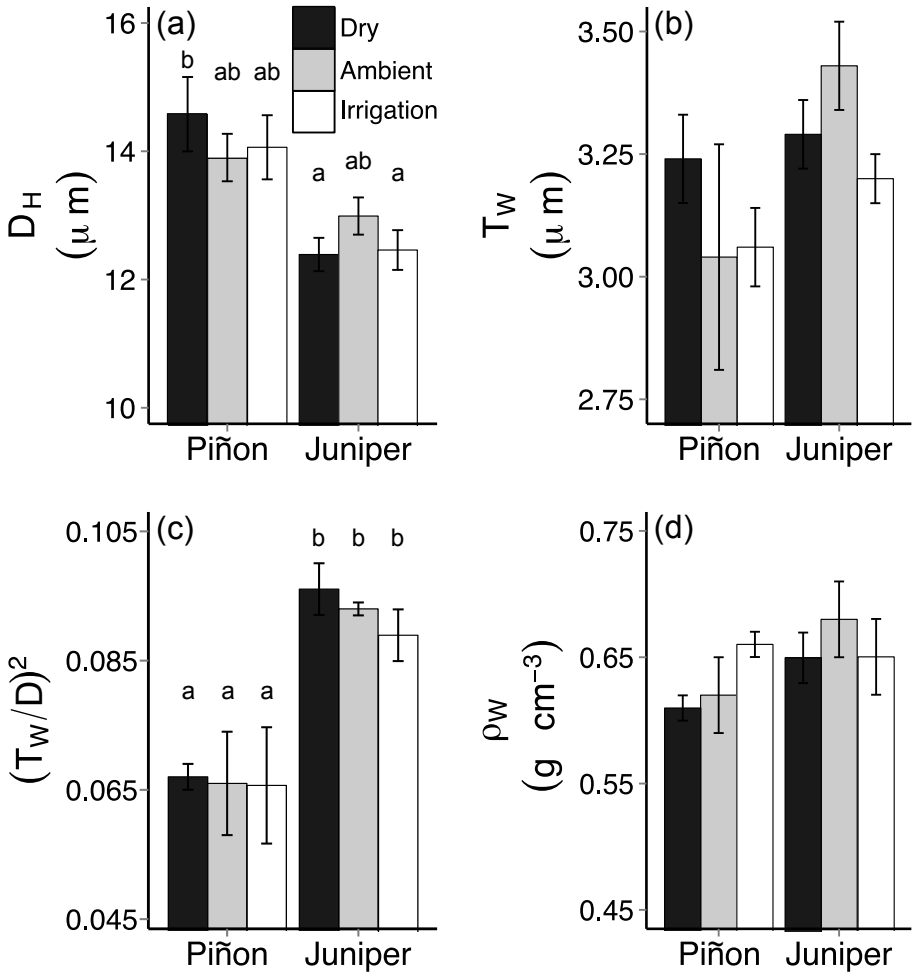


Figure 2.9: Barplots for tracheid anatomy and wood density measurements from piñon ($N$ = 3 per treatment) and juniper ($N$ = 3 or 5 per treatment) vulnerability curve samples collected in 2014. Parameters shown are (a) tracheid hydraulically-weighted lumen diameter ($D_H$), (b) tracheid double wall thickness ($T_W$), (c) tracheid thickness to span ratio ($(T_W/D)^2$), and (d) wood density ($\rho_W$). Bars labeled with different letters are significantly different as determined by *post hoc* Tukey HSD tests at 95% confidence level.

## 2.4 Discussion

### *2.4.1 Acclimation responses to altered precipitation regimes*

Despite the sustained and significant effects of our treatments on plant water status (Figs. 2.1 & 2.2), we observed only limited evidence of species-specific acclimation in hydraulic architecture. Although irrigated piñon increased investment in leaf area (decreased $A_S$:$A_L$), the concomitant increase in $K_S$ yielded similar $K_L$ to ambient trees (Fig. 2.5, Fig. 2.6). The combination of similar tracheid $D_H$ (Fig. 2.9), increased $\Psi_{PD}$ (Fig. 2.3), and reduced PLC (Fig. 2.10) suggests that increased $K_S$ in irrigated trees was due to decreased embolism formation rather than altered xylem structure. Ultimately, the irrigation response in piñon was to add leaves in proportion to shoot hydraulic conductivity, rather than enhance shoot hydraulic conductivity.

The increased $K_S$ in irrigated vs. ambient juniper, in the absence of adjustment of $A_S$:$A_L$ across treatments, suggests increased water availability induced a modest increase in xylem conducting efficiency. Embolism formation, predicted to be minimal in both treatments (maximum PLC < 12%, Fig. 2.10), is unlikely to have contributed to this result. Yet earlywood $D_H$ was also consistent across treatments (Fig. 2.9), implying that changes in conducting efficiency occurred via changes at the level of pit structure.

Although irrigation led to shoot-level responses, after more than six years of decreased moisture availability the only significant response observed was a reduction of leaf area in juniper (Fig. 2.6a). The similarity in maximum pre-monsoon water stress in ambient and drought treatments for both species (Fig. 2.3), coupled with unchanged embolism vulnerability (Fig. 2.7), suggests similar drought impacts for these two treatments (Fig. 2.10). Droughted piñon had reduced $K_L$ compared to ambient piñon (Fig.

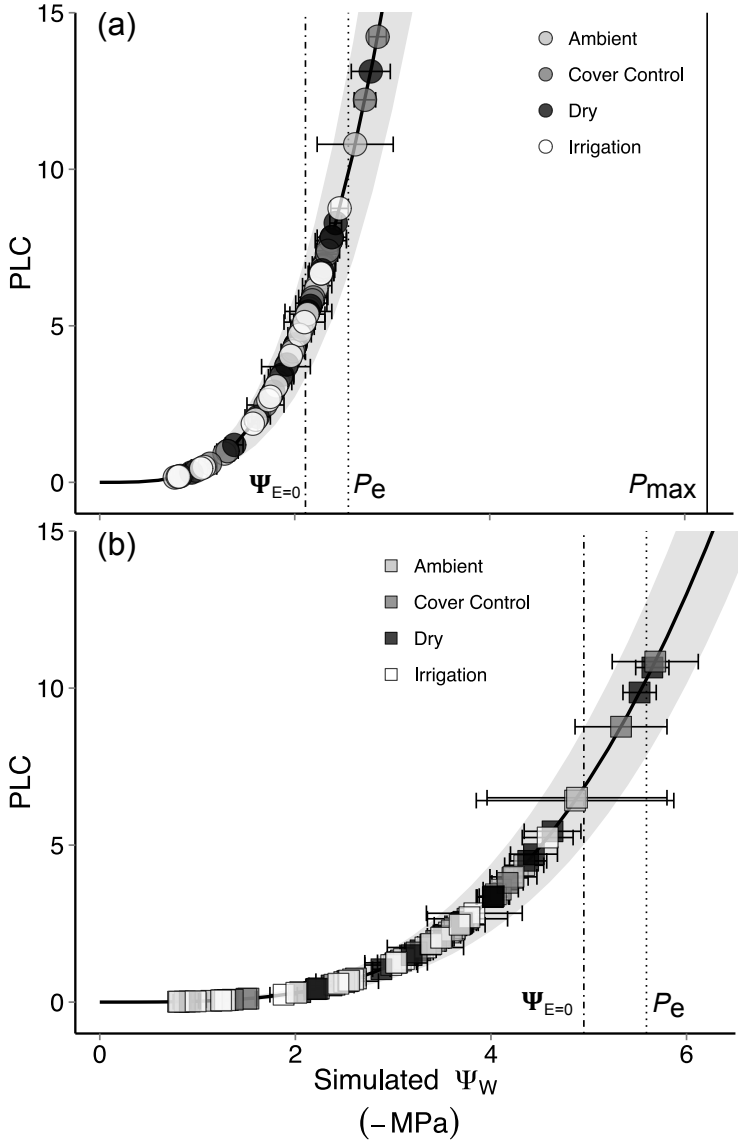


Figure 2.10: Predicted percent loss of conductivity based on mean water status for piñon (circles, a) and juniper (squares, b). Horizontal error bars are ±1 SE. Vulnerability curves are composites based on pooled species data, and the shaded areas about the curves represent min/max curves based on ± 1 SE from mean PLC. Dot-dash vertical lines indicate $\Psi_{PD}$ of zero transpiration ($\Psi_{E=0}$), dotted vertical lines indicate $P_e$ (drought stress onset), and the solid vertical line in (a) represents $P_{max}$ (hydraulic failure threshold). Two extremely dry points (2011 premonsoon piñon ambient $\Psi_{PD}$ and $\Psi_{MD}$) have been omitted.

2.6c), but similar embolism resistance (Fig. 2.8, Table 2.5), which indicates piñon have minimal ability to compensate for chronic water shortage. The drought treatment reduction in $K_L$ may be attributable to reduced ability to repair embolism via impaired phloem function due to insufficient hydration (Nardini *et al*. 2011, Sevanto 2014), or reduced proportion of viable cross-sectional area (Hudson *et al*. unpublished results). In contrast, droughted juniper maintained similar $K_L$ as in ambient juniper by reducing leaf area (Fig. 2.6c), demonstrating a homeostatic mechanism for maintaining hydraulic supply to photosynthetic tissue when challenged by chronic water shortage (Mencuccini and Grace 1994, McDowell *et al.* 2006, Martínez-Vilalta *et al*. 2009, Martin-StPaul *et al.* 2013). The low predicted PLC values in both drought and ambient treatments (Fig. 2.10) suggest that mechanisms responsible for leaf area reduction observed in juniper must operate at relatively low predicted loss of shoot xylem hydraulic conductivity.

The absence of significant shifts in embolism vulnerability (Fig. 2.7) and earlywood tracheid anatomy ($T_W$, $D_H$, and $(T_W/D)^2$, Fig. 2.9) in either species supports the hypothesis that mature trees have little ability to modify embolism vulnerability. Limited adjustment in hydraulic architecture has been observed in other conifers (Mencuccini & Comstock 1997, Martínez-Vilalta & Piñol 2002, Martínez-Vilalta *et al*. 2009, Corcuera *et al*. 2011, Lamy *et al*. 2011, Klein *et al*. 2013, Lamy *et al*. 2013). Importantly, this finding suggests that, unlike developmental differences between individuals in different microsites, acclimation of established individuals will not contribute to the climate change responses of widespread coniferous biomes such as piñon-juniper woodland.

*2.4.2 Relative performance of piñon and juniper*

Our observations that juniper, the more drought-tolerant species (Linton and Sperry 1998, West *et al*. 2007, McDowell *et al.* 2008, Plaut *et al*. 2012, Limousin *et al*. 2013, Pangle *et al*. 2015), matched or exceeded piñon performance in all measured hydraulic metrics does not support the proposed hydraulic efficiency versus safety trade-off (as discussed in Tyree, Davis and Cochard 1994). The comparable $K_S$ and superior embolism resistance of juniper to piñon was also surprising because wood density did not vary between species (Fig. 2.9d). Wood density, which is expected to reflect the carbon cost associated with secondary cell wall lignification (Pittermann *et al*. 2006), is often negatively correlated with $K_S$ and $K_L$ (Bucci 2004, Meinzer *et al*. 2008), and positively correlated with embolism resistance (Hacke *et al*. 2001, Hacke and Jansen 2009, Meinzer *et al*. 2009). Because juniper routinely exhibits more negative water potentials than piñon (Fig. 2.2, Fig. 2.3) and is much more resistant to embolism formation and spread (Fig. 2.10), we predicted that juniper xylem would have increased wood density due to enhanced lignification of tracheid secondary walls. The similarity between piñon and juniper earlywood tracheids (Fig. 2.9) defied this prediction. Earlywood tracheids in piñon and juniper are small compared to other conifers (Pitterman *et al*. 2006, Sperry *et al*. 2006). The constraints of opposing design optima for hydraulic transport and safety may limit plasticity in earlywood tracheid anatomy, especially if the tracheids may be close to a minimum critical lumen size necessary for hydraulic function (Bouche *et al*. 2014).

Investigation of pit structure and function is the logical next step to understand the dramatic differences in transport and safety between piñon and juniper xylem. Pit

membrane size (i.e., margo size if torus size remains constant) has been shown to respond to drought stress in piñon (Gaylord *et al*. 2015), with drought stressed trees producing tracheids with smaller pit membranes. Reduced margo area diminishes flow between adjacent tracheids, and may account for the reduced $K_S$ values measured in droughted trees. Though margo porosity is not linked to embolism vulnerability (Bouche *et al*. 2014), emboli propagate via pit connections, so pit structure and function may directly inform embolism vulnerability (Bouche *et al*. 2014, Zelinka *et al*. 2015). The degree to which the torus overlaps the pit aperture determines the magnitude of pressure difference necessary to promote embolism spread (Bouche *et al*. 2014). Members of the genus *Pinus* have thin, flat, disc-shaped tori, while *Juniperus* species have thick, convex, lens- shaped tori (Bauch 1972). The more robust juniper torus may be more resistant to air-seeding (Zelinka *et al*. 2015, and the combination of a more robust torus in a margo of equivalent porosity may explain the seemingly paradoxical result that juniper matches or exceeds piñon in both hydraulic efficiency and safety. Further investigation of the pit structure of these two species is necessary to test this hypothesis.

*2.4.3 Comparison of hydraulic function in current climate context,*

Although piñon and juniper did not exhibit the expected differences in hydraulic architecture, their patterns of function were consistent with the well-established functional differences between the study species (Linton and Sperry 1998, West *et al*. 2007, McDowell *et al*. 2008, Plaut *et al*. 2012, Limousin *et al*. 2013, Pangle *et al*. 2015). Under ambient conditions, higher $A_S$:$A_L$ allowed piñon to compensate for lower $K_S$ and to maintain an equivalent $K_L$ and $E_b$ to juniper (Fig. 2.6). Post-monsoon $\Delta\Psi$ was similar in both species such that differences in leaf level processes (i.e., stomatal or mesophyll

conductance) should be responsible for differences in gas exchange and carbon capture between piñon and juniper when water is available. As soil moisture decreased, the characteristic differences in embolism vulnerability and stomatal regulation between piñon and juniper produced very different functional responses. The relationship between $E_b$ and $\Psi_{PD}$ predicted anisohydric juniper to continue transpiration to drier soil conditions, and isohydric piñon to cease transpiration at relatively modest values of water stress (Fig. 2.7c). The values of $\Psi_{E=0}$ we calculated (-2.34 MPa for piñon, and -4.89 MPa for juniper) correspond with observations of $\Psi_{PD}$ of zero assimilation from studies on piñon/juniper leaf-level gas exchange: Williams and Ehleringer (2000) reported -2.0 MPa for piñon sampled across a latitudinal gradient spanning central Arizona to northern Utah; Lajtha and Barnes (1991) reported -2.2 MPa for piñon and -4.6 MPa for juniper from northern New Mexico; and Limousin *et al*. (2013) reported -2.55 MPa for piñon and -4.94 to -6.90 MPa for juniper from the same population of target trees measured in this study. Our shoot hydraulic estimates of $E_b$ were consistent with reported values of leaf-level gas exchange (stomatal conductance) for piñon and juniper in the literature (Limousin *et al*. 2013, Garcia-Forner *et al*. 2015). Direct measurement of gas exchange at the leaf level has the advantage of integrating the various conductances along the soil-plant-atmosphere hydraulic path, and incorporates the complex dynamics of water transport in both roots and leaves. We do not suggest that our calculations of $E_b$ supplant leaf-level gas exchange measurements, but that our data are complimentary to these direct measurements. Our methods provide insight to performance in a low resistance portion of the plant hydraulic path length, and differences between branch hydraulics

calculated transpiration rates and measured transpiration rates might elucidate the magnitude of leaf-specific hydraulic resistances on gas exchange.

*2.4.4 Functional consequences of isoshydry vs anisohydry*

Our estimates of $\Psi_{E=0}$ support the hypothesis that plants sacrifice transpiration and carbon capture to preserve xylem hydraulic integrity (Tyree and Sperry 1989, Sperry 2000, Cochard and Delzon 2013). In both species, $\Psi_W$ rarely exceeded $P_e$, and then only by small margins (Fig. 2.10, though in the extremely dry premonsoon sampling of 2011, water potentials from ambient piñon predicted ~40% PLC). This indicates that both species generally employ an embolism avoidance strategy by closing stomata and limiting gas exchange as plant water status approaches $P_e$ (Domec *et al*. 2008, Meinzer *et al*. 2009, Martinéz-Vilalta *et al.* 2014). Juniper had a larger absolute difference between $\Psi_{E=0}$ and $P_e$ than piñon (0.77 MPa vs. 0.24 MPa), but the relative magnitudes of the differences for both species were similar ($P_e$ was 14.9% greater than $\Psi_{E=0}$ in juniper, and 9.9% greater in piñon).

While our results do not challenge the isohydric/anisohydric labels of piñon and juniper, both species appear to have similar relative risks for embolism (Fig. 2.10), despite their disparate positions on the continuum from isohydric to anisohydric stomatal regulation (Klein 2014). However, because piñon operated within a more restricted range of water potentials, we observed piñon exhibiting $\Psi_W$ values in excess of $P_e$ more frequently than juniper. Our predictions of PLC are thus consistent with other studies (Plaut *et al*. 2012, McDowell *et al*. 2013, Garcia-Forner *et al*. 2015) that found piñon was more likely to experience significantly greater PLC compared to juniper, with surviving piñon enduring *c*.45% PLC, while juniper PLC stayed below 15%. Slight differences in

reported values of Weibull fit parameters from vulnerability curves and measured $\Psi_{MD}$ produced different estimates of PLC across studies, but do not negate the conclusion that isohydric piñon suffers greater loss of hydraulic function than anisohydric juniper. This refutes the hypothesis that isohydric species should be less prone to embolism and hydraulic failure (per McDowell *et al*. 2008 and Skelton *et al*. 2015). It is noteworthy that our study, as well as that of Garcia-Forner *et al.* (2015), studied trees that survived drought; PLC was observed to be significantly higher in these same species (and at the same site as this study) for trees that died (McDowell *et al*. 2013), in line with strong evidence that prolonged, elevated PLC promotes mortality (cf. Anderegg *et al*. 2015).

*2.4.5 Implications for predicted future climate scenarios*

Our results suggest piñon will be more susceptible to local extirpation than juniper in projected climate scenarios for the semi-arid SWUS (Seager 2007, Williams *et al*. 2013, McDowell *et al*. 2015), as juniper matched or out-performed piñon in every hydraulic metric we measured. Though juniper did not demonstrate major adjustments in xylem structure or function, more negative $\Psi_{E=0}$ and $P_e$ should confer an enhanced likelihood of survival in the novel climate space generated if temperatures rise and precipitation inputs become smaller and/or less frequent across the semi-arid SWUS, as predicted by future climate models (Seager *et al*. 2007, Williams *et al*. 2013). Increased aridity, as a function of enhanced atmospheric demand combined with reduced soil moisture pools, will impose more strict limits on carbon capture by both species (McDowell *et al*. 2015). Both piñon-juniper woodlands and juniper savannas currently function as net carbon sinks, but sink strength in both of these systems is predicted to diminish with increasing temperature and/or reduced precipitation (Anderson-Teixeira *et*

*al*. 2011, Biederman *et al*. 2016). Piñon mortality will exacerbate loss of ecosystem sink strength (Bonan 2008, Reichstein *et al.* 2014), especially if mass mortality occurs over the entire piñon-juniper range, and have serious implications for terrestrial-atmosphere carbon balance over a significant portion of southwestern US vegetated landscapes (Krofcheck *et al*. 2016). Thus mass piñon mortality will contribute to an increasingly challenging climate for surviving piñon. Absent the ability to produce more drought-resistant xylem needed to extract water from drier soils, or maintain positive $\Delta\Psi$ over more negative $\Psi_{soil}$ conditions, piñon are unlikely to maintain gas exchange and the positive carbon balance necessary to meet growth, maintenance, and defense demands in a hotter, drier SWUS.

# Chapter 3

# Drought responses of piñon pine protected from bark beetle attack: quantifying hydraulic adjustments driven by chronic abiotic stress

## 3.1 Introduction

Accelerated loss of forests attributed to drought and warming have become evident in recent decades (van Mantegem *et al.* 2009, Allen *et al.* 2010, Weed *et al.* 2013). Drought, a function of critically low soil moisture content driven by limited precipitation, may be exacerbated by high atmospheric demand for water vapor (Williams *et al*. 2013, Trenberth *et al*. 2014, Allen *et al*. 2015). Climate models predict increases in temperature and greater variability in precipitation, particularly in arid lands; both scenarios are likely to increase the frequency and severity of drought in these regions (Seager *et al.* 2007, Sheffield and Wood 2008, Williams *et al*. 2013). Observations of drought-related tree mortality have revealed differential impacts and species-specific patterns of mortality (McDowell *et al*. 2008, Peng *et al*. 2011). Mortality for some species appears to be wholly driven by abiotic factors (Anderegg *et al*. 2012), while mortality in other species arises from the interactions of abiotic and biotic stressors (Breshears *et al*. 2005, Raffa *et al*. 2008, Gaylord *et al*. 2013). Insects, particularly bark beetles (Curculionidae: Scolytinae), have been directly implicated in recent (circa 1990) massive forest mortality events in North America, affecting more that 60 million ha and killing billions of trees between 1997-2006 (Raffa *et al.* 2008, Bentz *et al.* 2010, Hicke *et*

*al.* 2016). Bark beetles function as natural disturbance agents that regulate population dynamics of host tree species through selective colonization and elimination of stressed, or less competitive, individuals (Bentz *et al*. 2013). However, increasing temperatures, especially in winter months, accelerate bark beetle reproduction and generational turn over, so a warmer climate is predicted to permit an increased number of bark beetle generations per year, which could increase the likelihood of population eruptions (Raffa 2008, Bentz *et al*. 2010, Bentz *et al*. 2013). Population eruptions in concert with drought have resulted in mortality events that have restructured landscapes and altered ecosystem dynamics of carbon and water cycling (Bonan 2008), and may become more frequent if increasing temperatures drive drought severity (Kurz *et al*. 2008, Bentz *et al*. 2010).

Piñon-juniper woodland represents a model system for investigating the relative roles of drought stress and insect pathogen pressure on tree mortality. Recent severe drought episodes (1999-2003, 2009-2013) were punctuated by widespread mass mortality of piñon (Breshears *et al*. 2005, USDA 2015) across the semi-arid southwestern US. Defining the proximal cause of death in piñon is complicated by the complex interactions of abiotic and biotic factors that contribute to mortality (Shaw *et al*. 2005; McDowell 2011; McDowell *et al*. 2011). Piñon typically demonstrate strict stomatal control at relatively mild soil water potentials; in droughts of sufficient duration, mortality may occur as a consequence of metabolic demand exceeding metabolic reserves (carbon starvation; McDowell *et al*. 2008, Plaut *et al*. 2013, Sevanto *et al*. 2014, Dickman *et al*. 2015). Recent field studies, however, found evidence that predicted piñon to incur extensive embolism (~40% loss of conductivity), particularly under severe drought conditions (Plaut *et al*. 2012, Garcia-Fourner *et al*. 2015). This suggests that, for piñon,

carbon starvation and hydraulic failure may be intertwined processes, rather than independent mortality factors (McDowell 2011, Plaut *et al*. 2013, Garcia-Fourner *et al.* 2015, Hudson *et al*. in review). Piñon mortality is almost invariably linked to bark beetle activity (Breshears *et al*. 2005, Shaw *et al*. 2005, Clifford *et al*. 2009, Breshears *et al*., 2009, Floyd *et al*. 2009, Clifford *et al*. 2013). Drought stress predisposes piñon to piñon bark beetle (*Ips confusus* (LeConte)) attack, as reduced carbon assimilation restricts carbon resources available for resin production, the primary mechanism by which piñon repel insect invasion (Raffa *et al*. 2008, Gaylord *et al*. 2013).

A precipitation manipulation experiment designed to test hypotheses regarding mechanisms of mortality in PJ was implemented at the Sevilleta Long Term Ecological Research (LTER) site in 2007 (Pangle *et al*. 2012). Within one year, piñon subjected to experimental drought conditions began to die. Regional bark beetle activity was not particularly intense (2008-2009), especially compared to prior outbreaks (2002-2003) and subsequent outbreaks (2013-2014; USDA 2004, 2015). Yet in this timeframe, bark beetles infested and killed all mature piñon subjected to experimental drought (-45% annual precipitation). These trees had lower predawn water status and transported less water relative to control trees for seven months preceding beetle attack (Plaut *et al*. 2012, Gaylord *et al*. 2013).

In order to assess the relative contributions of potential abiotic and biotic mechanisms of piñon mortality, an additional study was established in 2010 at the same site to characterize piñon hydraulic responses to prolonged water stress, when piñon were protected from lethal biotic pathogens To this end, we installed two additional treatment plots to the long-term PJ precipitation manipulation experiment (Pangle *et al*. 2012). Both

plots were treated with an insecticide to deter beetle infestation. One plot functioned as an abiotic control, while the other was subject to experimental drought. This design allowed us to closely monitor the shifts in stem, shoot, and leaf-level hydraulic activity associated with onset and perpetuation of chronic water shortage, while restricting the influence of confounding biotic mortality factors on drought stress responses in trees. We hypothesized that 1) hydraulic transport would scale with water availability, 2) isohydric regulation would prevent acclimation in xylem hydraulic safety and efficiency by maintaining consistent water status and water potential gradients, and 3) water restriction and strict stomatal regulation would severely limit gas exchange and photosynthetic carbon uptake in experimental drought, potentially predisposing piñon to mortality by abiotic forcing.

## 3.2 Materials and Methods

### *3.2.1 Study site*

Our research was an extension of a rainfall manipulation experiment established in 2007 in a piñon-juniper woodland at the Sevilleta National Wildlife Refuge in central New Mexico, USA (34º23'11" N, 106º31'46" W, 1911 m; for details see Pangle *et al.* 2012, Plaut *et al*. 2012). Mean annual precipitation is 367.6 mm•yr$^{-1}$, and is strongly influenced by the North American monsoon, which delivers the majority of annual precipitation in July, August and September. Mean annual temperature is 12.7ºC, with a mean July maximum of 31.0ºC and mean December minimum of -3.3ºC (Moore 2014). For detailed site descriptions of vegetation and edaphic factors, see Pangle *et al*. 2012 and Plaut *et al*. 2012.

We established two beetle control treatments in November of 2010: ambient control with insecticide application (100% precipitation), and experimental drought with insecticide application (~55% precipitation). The insecticide (Tengard SFR Oneshot, 36.8% Permethrin, United Phosphorus, Inc., King of Prussia, PA) was professionally applied to target tree trunks three times a year, from 2011 to 2015. Care was taken to avoid exposing canopy foliage to the insecticide, to prevent interference with photosynthetic activity. Experimental drought was imposed on target trees by installing troughs that collected ~ 45% of incoming precipitation and shunted the water off-plot (Pangle *et al*. 2012). Data collection of shoot water potential and shoot hydraulic conductivity on target trees began in June 2010, five months prior to drought infrastructure installation. Leaf level gas exchange measurements commenced in April 2011, and sap-flow sensors were installed in May 2011.

### *3.2.2 Shoot $\Psi_W$*

Samples for predawn and midday water potential (hereafter $\Psi_{PD}$ and $\Psi_{MD}$,) were cut from each target tree between 0430-0545h and between 1200-1400h. Samples were stored in plastic bags with a scrap of moist paper towel to prevent desiccation, in shaded, insulated boxes before processing (between 15-60 minutes). Water potential ($\Psi_W$, MPa) was measured using a Scholander-type pressure chamber (PMS, Corvallis, OR).

### *3.2.3 Stem sap-flow*

We measured stem sap-flow using Granier heat dissipation sap-flow sensors installed in target trees (n = 10 per treatment, Pangle *et al*. 2015, and references therein). Two sensor arrays were installed in each target tree in May 2011. Sap-flow ($J_S$, $g \bullet m^{-2} \bullet s^{-1}$) was calculated according to methods describe by Granier (1987) and Goulden and Field

(1994), and used to model plant hydraulic conductance (modeled $k_S$, g•m$^{-2}$•s$^{-1}$•MPa$^{-1}$) based on Darcy's Law (Sperry et al. 2002) as:

$$modeled\ k_S = \left(\frac{E}{\Delta\Psi}\right)$$

with $E$ equal to midday $J_S$ (measured between 1100-1400h), and $\Delta\Psi$ representing the driving gradient for transpiration defined as $\Psi_{PD} - \Psi_{MD}$ (Pangle *et al*. 2015). Although sensors recorded measurements every 15 seconds, we have restricted the dataset to midday $J_S$, and dates when water potentials were measured. We further refined our data by limiting $J_S$ values to positive values of $\Delta\Psi$, and modeled $k_s$ values to values of $\Delta\Psi \geq$ 0.5 MPa (Pangle *et al*. 2015).

*3.2.4 Shoot hydraulic conductivity*

Branches (~16 cm in length and 5-8 mm in diameter) cut from trees were sealed in humid plastic bags and transported to the laboratory where they were refrigerated until they were measured (within 24 h). Before measurement, samples were submerged in 20 mM KCl solution, and trimmed to ~4 cm in length, to remove distal embolized conduits. Hydraulic conductance ($K$, kg•s$^{-1}$•MPa$^{-1}$) was measured by steady state flow meter, and normalized to sample length, sample xylem cross sectional area, and distal leaf area to calculate hydraulic conductivity ($K_h$, kg•m•s$^{-1}$•MPa$^{-1}$), sapwood-specific conductivity ($K_S$, kg•m$^{-1}$•s$^{-1}$•MPa$^{-1}$), and leaf- specific conductivity ($K_L$, g•m$^{-1}$•s$^{-1}$•MPa$^{-1}$), respectively (see Hudson et al. 2010, Feild et al. 2011 for full method description). Sapwood area was divided by distal leaf area to produce $A_S$:$A_L$. $K$ was normalized to leaf area and multiplied by $\Delta\Psi$ to calculate branch estimated transpiration ($E_b$, mmol m$^{-2}$ s$^{-1}$; Manzoni *et al*. 2013, Hudson *et al*. in review)

*3.2.5 Vulnerability to embolism*

Embolism vulnerability of branches was measured as described in Hudson *et al*. (in review). We used the air-injection method (Sperry and Salindra 1994) to propagate embolism in branch samples at 0.5, 1.5, 3, 4.5, and 6 MPa. Percent loss of conductivity was calculated as:

$$PLC = 100 \bullet \left(1 - \frac{K_i}{K_{max}}\right)$$

where $K_i$ is the measurement of $K$ after the $i^{th}$ pressurization. A total of five pressurizations were carried out on each sample. Weibull functions were fit to PLC data to generate vulnerability curves (Neufeld *et al.* 1992):

$$PLC = 100 - 100 \bullet e^{\left[-\left(\frac{\Psi_w}{a}\right)^b\right]}$$

where $a$ and $b$ are curve fitting parameters (Hubbard *et al.* 2001). Parameters $a$ and $b$ were subsequently used to calculate $P_e$ (air entry threshold), $P_{50}$, $P_{max}$ (hydraulic failure threshold), and drought stress interval (DSI, $P_{max}$-$P_e$) (Hudson *et al*. in review, Chapter 2).

*3.2.6 Wood density and anatomy*

Wood density ($\rho_W$, g•cm$^{-3}$) of vulnerability curve samples was measured by volumetric displacement (McCulloh *et al.* 2014, Hudson *et al.* in review). Tracheid anatomy was assessed on hand sections obtained from vulnerability curve samples (Hudson *et al*. in review). Only early-wood tracheids from recent growth were measured, as these tracheids are responsible for the majority of water transport (Domec and Gartner 2002, Bouche *et al.* 2014). Lumen area and adjacent anticlinal walls ($T_W$) were traced

using ImageJ. Lumen diameters ($D$) were calculated as the square root of lumen area, which is more appropriate for rectilinear tracheids (Sperry and Hacke 2004, Hacke *et al.* 2004). Fifty tracheids from each sample were measured, for $N = 250$, per treatment. We confirmed that cross section lumen diameter distributions were similar to those measured in macerated samples. The hydraulically weighted lumen diameter, $D_H$, was calculated as:

$$D_H = 2\left(\frac{\Sigma r^5}{\Sigma r^4}\right)$$

where $r$ is the lumen radius, in microns (Sperry and Hacke 2004). Conduit thickness to span ratio $(T_W/D)^2$ was calculated as the square of the ratio of adjacent double wall thickness to lumen diameter (Hacke *et al*. 2001).

*3.2.7 Leaf gas exchange*

Leaf gas exchange was measured using portable infrared gas exchange systems (LI-6400 infrared gas analyzer, LiCor Inc., Lincoln, NE, USA) outfitted with 2 x 3 cm red/blue LED light-source chambers (6400-02B LED, LiCor Inc.). We used the methods and instrument settings described in Limousin et al. 2013, with the exception that we used $CO_2$ cartridges with the LiCor 6400 $CO_2$ mixer to set chamber [$CO_2$] at 400 ppm, as opposed to relying on ambient air [$CO_2$]. Measurements were made on five target trees per treatment, and coincided with dates of water potential sampling. Before the monsoon, previous year foliage was measured, as current year foliage had yet to reach maturity. Current year foliage was measured once needle expansion was complete, typically in July or August. One south-facing shoot from each target tree was flagged at the beginning of each sampling campaign, and measured repeatedly, starting before sunrise (dark

respiration, $R_d$) and continuing at 1.5 hour intervals until gas exchange (light saturated net assimilation rate, $A_n$, stomatal conductance, $g_S$, and transpiration, $E$) decreased for three successive intervals (between 1130-1430h depending on sampling date). Measurements were taken at ambient temperature (11-43ºC depending on sampling date and time of day) and relative humidity (7-74%).

Photosynthetic response to varying sub-stomatal [$CO_2$] ($A$:$C_i$ curves) were made in October 2012, under well-watered conditions, as in Limousin *et al*. 2013. Curves consisted of ten steps, starting from 400 ppm (~ambient [$CO_2$]) and decreasing by half to 200, 100, and 50 ppm before increasing to 300, 500, 700, 1000, 1500 and 2000 ppm. Leaves were given 10 minutes to equilibrate at each step before measurements were made.

*3.2.8 Data analysis*

We used R (R Core Team 2012) and the packages lme4 (Bates and Maechler, 2010) and nlme (Pinheiro *et al.*, 2016) to perform a linear mixed effects analysis of the relationship between our hydraulic response variables and drought imposition both before and after monsoon precipitation input. We set treatment, period (before or after monsoon onset), and the interaction term as fixed effects. As random effects, we structured the model to allow for random intercepts for individual trees and sampling dates. Separate models for pre- and post-monsoon data were generated if the full model indicated a significant period effect. When visual inspection of residual plots revealed obvious deviations from homoscedasticity or normality (Winter 2013), square root or natural log transformations were employed to meet necessary model assumptions. *P*-values were obtained by likelihood ratio tests of the full model with the effect in question against the

model without the effect in question. We also composed models that used the interaction of experimental day and treatment as a fixed effect, with target tree as a random effect. This model structure allowed us to identify sampling dates where hydraulic response variables differed significantly across treatments. Reported values of water potential and hydraulic conductivity are least squares mean estimates ± modeled standard error.

Covariation of water stress, sap-flow, shoot conductivity, gas exchange, treatment, and period were also assessed using linear mixed effects models. We examined the relationships of $J_S$, $k_S$, $K_S$, $K_L$, $E_b$, $A_n$, $g_S$, and $E$ to $\Psi_{PD}$, which we used as a proxy for water stress intensity. When the correlation between $\Psi_{PD}$ and response variable was not influenced by treatment, or period, data were pooled and a *post-hoc* linear regression was used to determine the significance and strength of the relationship. Reported coefficients (intercepts and slopes) are least squares mean estimates ± modeled standard error.

Maximum carboxylation rates of Rubisco, $V_{c\ max}$, were extracted from $A$:$C_i$ data using the R package plantecophys (Duursma 2016). We used an ANOVA framework to test for significant differences in $V_{c\ max}$ and vulnerability to embolism due to treatment. Data were analyzed in R, and all values presented are mean ± standard error.

## 3.3 Results

### *3.3.1 Effectiveness of beetle exclusion*

Against a background of lethal bark beetle presence, all target piñon in this experiment survived 6+ years of experimental drought, and demonstrated no signs of bark beetle attack. Bark beetle activity in the region was consistent with statewide surveys of beetle activity, which was low from 2010-2012, spiked in 2013 and 2014, and

finally declined in 2015 (USDA 2015). Local beetle presence was nonexistent in 2011 and low in 2012, likely due to the effect of extreme cold temperatures in February 2011 that exceeded bark beetle cold tolerance (Chansler 1966). Regional beetle activity surged in 2013, with aerial surveys reporting over 96 $km^2$ of impacted PJ on Chupadera Mesa, within 25 km of our site (USDA 2015). On-site beetle traps reflected regional beetle population trends, with over 9000 bark beetles captured between April-October 2013. Piñon mortality in non-sprayed plots rose to four trees in 2013, and then spiked in 2014, when nine target trees were infested with bark and twig beetles. These mortality events were distributed across the blocks and treatments of the original precipitation manipulation experiment. By the end of 2014, non-sprayed plots lost 49% of target piñon trees, and every instance of piñon mortality was associated with beetle attack.

*3.3.2 Climate and treatment effects on plant water status*

During measurement years, ambient annual precipitation varied from a minimum in 2015 (245.4 mm by last sampling date) to a maximum in 2013 (385.8 mm), for an average of 289.5 ± 20.6 $mm \bullet yr^{-1}$ (Fig. 3.1a). This was ~80% of the 20-year mean reported from a nearby LTER meteorological station (362.7 $mm \bullet yr^{-1}$, 1989-2009, Cerro Montosa #42; http://sev.lternet.edu/). We estimated precipitation inputs to the drought treatment using the known percentage rainout coverage (Pangle *et al.* 2012), and based on projected 45% precipitation reduction, drought treatment annual precipitation was calculated to be 159.2 ± mm $yr^{-1}$ for years 2011 to end August 2015 (Fig. 3.1b). With the exception of 2013, the entire experiment was conducted under below-average annual precipitation inputs. Predawn water potential was strongly affected by experimental drought treatment ($p < 0.0001$) and monsoon precipitation ($p = 0.002$) (Fig. 3.1c). Before

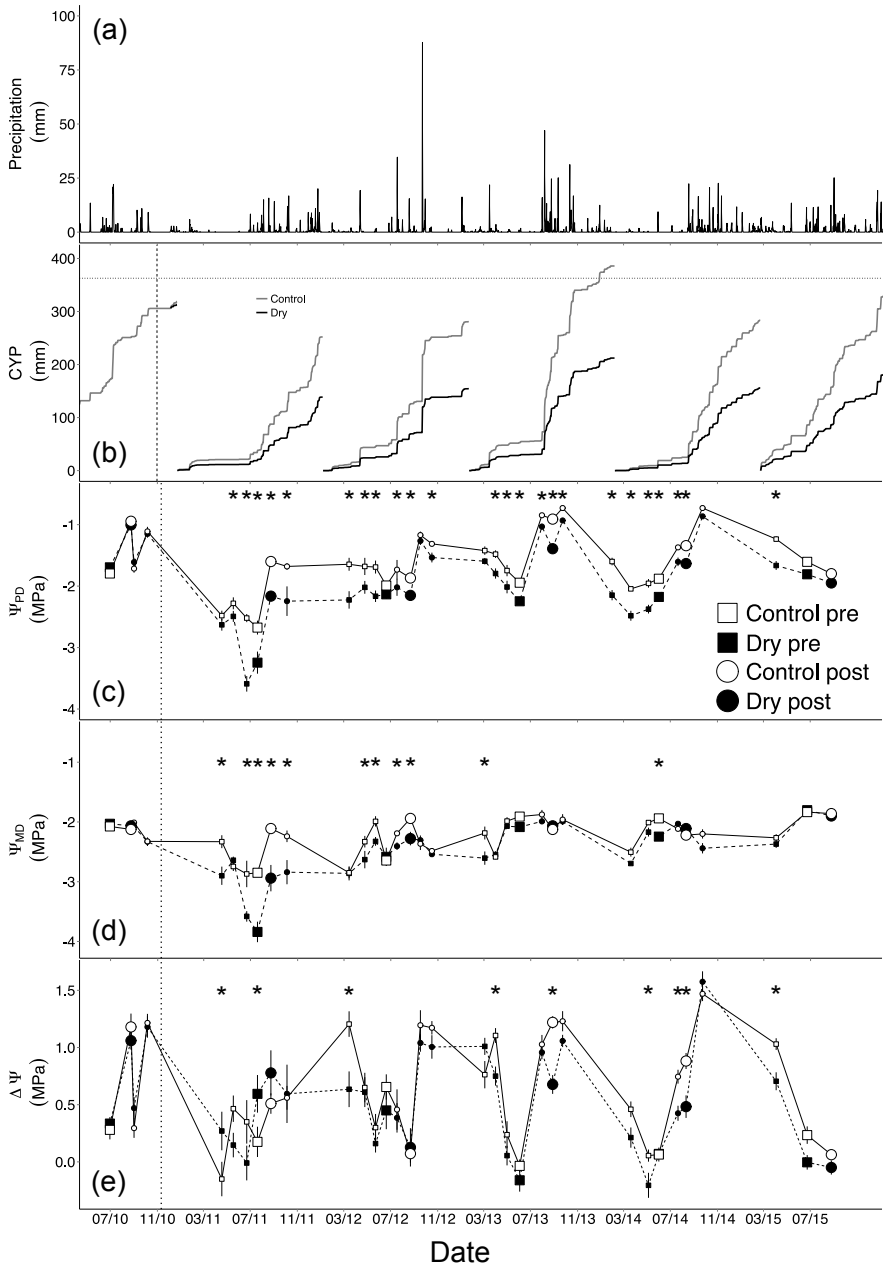


Figure 3.1: Precipitation inputs and plant water status for 5+ year period starting in 2010. Daily precipitation (a), cumulative yearly precipitation (b), predawn (c) and midday (d) water potential, and driving gradient for transpiration (e). In (b), horizontal dotted line represents 20 year average precipitation (362.7 mm $yr^{-1}$) from nearest meteorological station, and vertical dashed line represents installation of drought structures and beginning of experimental manipulation. Values in panels (c), (d), and (e) are mean ± 1 SE. Large symbols signify sampling efforts when all hydraulic measurements were collected.

the monsoon, experimental drought lowered $\Psi_{PD}$ by 0.38 MPa (-2.23 ± 0.12 MPa compared to -1.85 ± 0.11 MPa for control). $\Psi_{PD}$ increased in both groups following the monsoon, but drought structures continued to decrease $\Psi_{PD}$, by 0.27 MPa compared to control (-1.55 ± 0.12 MPa and -1.28 ± 0.11 MPa, respectively). $\Psi_{PD}$ dropped to minimum values in both treatments in the extremely dry late pre-monsoon sampling of 2011 (Fig. 3.1c).

Both control and drought treatment piñon converged on treatment-specific values of $\Psi_{MD}$ (-2.2 ± 0.06 MPa for control, -2.42 ± 0.07 for drought, $p < 0.0001$), which is broadly consistent with isohydric $\Psi_W$ regulation (Fig. 3.1d). However, during the particularly dry 2011 pre-monsoon sampling period, $\Psi_{MD}$ (-3.95 ± 0.61 MPa) dropped below the isohydric threshold typically observed at this site (Plaut *et al*. 2012, Limousin *et al*. 2013, Pangle *et al*. 2015) and in the literature for this species (e.g. West *et al*. 2007, McDowell *et al*. 2008, Breshears *et al*. 2009).

The driving gradient for transpiration, calculated as the difference between $\Psi_{PD}$ and $\Psi_{MD}$ ($\Delta\Psi$, MPa), was impacted by both treatment ($p = 0.004$) and period ($p = 0.01$) (Fig. 3.1e). Drought structures decreased $\Delta\Psi$ by the same amount (0.13 MPa) before and after monsoon onset. Monsoon precipitation nearly doubled $\Delta\Psi$ in control (0.39 ± 0.09 MPa to 0.77 ± 0.12 MPa, $p = 0.02$), and more than doubled $\Delta\Psi$ in drought treatment (0.26 ± 0.09 MPa to 0.64 ± 0.12 MPa, $p = 0.01$).

*3.3.3 Climate and treatment effects on stem sap-flow*

For most of the experimental period, mean midday $J_S$ was low in both treatments, and similar to midday $J_S$ observed in droughted piñon during the original experiment in

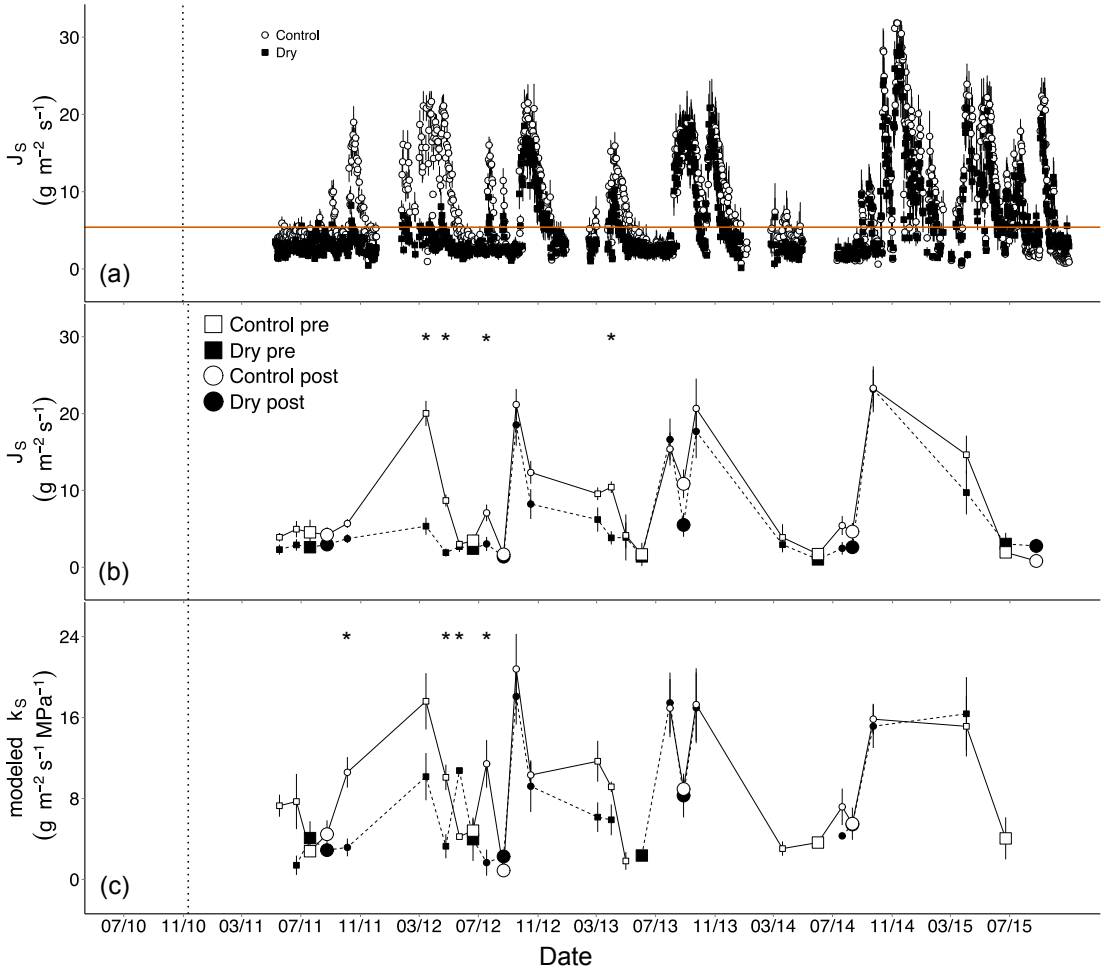


Figure 3.2: Mean midday sap-flow over the entire experimental duration (a), water potential sampling date mean midday sap-flow (b) and modeled hydraulic conductance (c). Vertical dotted line indicates experimental drought structure installation. In (a), red line indicates critical low sap-flow threshold identified by Plaut *et al*. 2012. In (b) and (c), large symbols represent sampling dates when all hydraulic measurements were collected. Asterisks indicate sampling dates when treatment differences were significant at $p \leq 0.05$.

2008 (~ 5 g•m$^{-2}$•s$^{-1}$, Plaut *et al*. 2012, Fig. 3.2a). The largest treatment effects were observed in early spring (March-April) 2012. Treatment values became more similar as spring progressed, prior to monsoon onset. Overall midday mean $J_S$ did not differ between treatments (Control $J_S$ = 8.50 ± 1.48 g•m$^{-2}$•s$^{-1}$, Drought $J_S$ = 6.32 ± 1.54 g•m$^{-2}$•s$^{-1}$, $p$ = 0.25). For direct sampling dates, we observed no treatment effects on $J_S$ (p = 0.08) or modeled $k_S$ ($p$ = 0.27), most likely because treatment differences in $J_S$ where balanced by treatment differences in $\Delta\Psi$; control trees had slightly higher $J_S$ (Fig. 3.2b) but lower $\Delta\Psi$ compared to droughted trees, which lead to consistent modeled $k_S$ between treatments (Fig. 3.2c).

*3.3.4 Climate and treatment effects on hydraulic architecture*

Allocation of sapwood area to leaf area demonstrated a marked increase from 2011 to 2012, during the driest portion of the experiment. $A_S$:$A_L$ proceeded to drift back to pre-experiment values over the remainder of the experiment (Fig. 3.3a). Neither treatment ($p$ = 0.47), nor period ($p$ = 0.41), effects were detected on $A_S$:$A_L$.

Sapwood-specific conductivity ($K_S$) demonstrated a decline from pre-experiment 2010 sampling to dry 2011 conditions (Fig. 3.3b). Neither treatment ($p$ = 0.67), nor period ($p$ = 0.33) effects were detected on $K_S$. As with $K_S$, leaf-specific conductivity ($K_L$) declined from pre-experiment conditions as water became scarce in 2011 (Fig. 3.3c). Drought treatment reached minimum $K_L$ in August 2011, but recovered to control $K_L$ values by the end of 2011. From this point, both species displayed similar dynamics in $K_L$ until the end of the experiment. Neither treatment ($p$ = 0.35), nor period ($p$ = 0.39) influenced $K_L$ over the entire span of the experiment. Branch estimated transpiration ($E_b$) was diminished from pre-experiment values by prevailing drought conditions in 2011

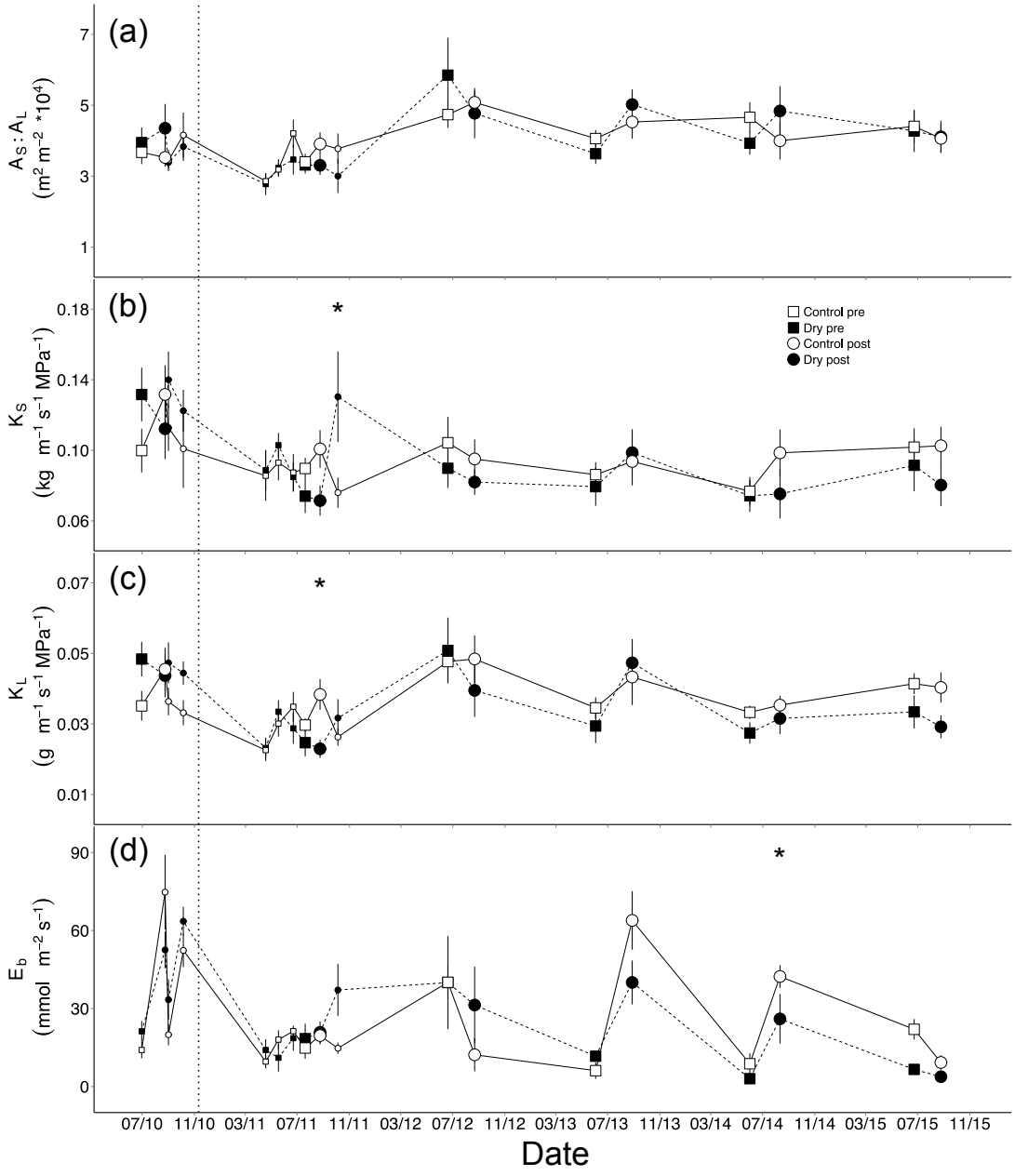


Figure 3.3: Mean ± SE values of shoot hydraulic measurements made from 2011-2015. Large symbols represent sampling dates when all hydraulic measurements, including water potential, were collected. The vertical dotted line indicates the installation of drought structures and the beginning of experimental manipulation. Large symbols represent sampling dates when all hydraulic measurements were collected. Asterisks indicate sampling dates when treatment differences were significant at $p \leq 0.05$.

(Fig. 3.3d). Drought treatment $E_b$ rebounded more quickly than control $E_b$, and reached post-monsoon values in 2011 similar to post-monsoon values through 2014. In contrast, control $E_b$ did not rebound until pre-monsoon 2012, and then fell again in post-monsoon 2012. $E_b$ responded to seasonal water availability in 2013 and 2014, i.e., during and following a year with slightly above average precipitation input. Neither treatment ($p$ = 0.07), nor period ($p$ = 0.21), effects were detected for $E_b$ over the entire span of the experiment.

*3.3.5 Climate and treatment effects on leaf gas exchange*

Leaf level gas exchange responded more strongly to seasonal variation in water availability than to experimental drought. Maximum net assimilation ($A_n$) and stomatal conductance ($g_S$) tracked precipitation, leading to elevated gas exchange post-monsoon onset (max $A_n$ $p$ = 0.04, max $g_S$ $p$ = 0.02, Fig. 3.4 a & b). The uncharacteristically high rates of gas exchange recorded in March 2012 (Fig. 3.4a, b, & c) coincided with similarly high values of $J_S$ and $\Delta\Psi$ (Fig. 3.3b, Fig. 3.1e), which may be explained by significant winter precipitation inputs between December 2011-March 2012 (97.53 mm, Fig. 3.1a). Conversely, low August 2015 gas exchange rates coincided with low values of $J_S$ and $\Delta\Psi$, as less than 5 mm of precipitation fell between August 1$^{st}$ and the post- monsoon sampling date of August 25$^{th}$, compared to the ~76 mm July precipitation total. Though neither treatment ($p$ = 0.57), nor period ($p$ = 0.09), effects were detected for transpiration ($E$), we did observe a treatment*period interaction ($p$ = 0.007). Monsoon precipitation elevated $E$ from pre-monsoon conditions in drought treatment trees (pre- 0.14 ± 0.05, post- 0.37 ± 0.09 mmol $m^{-2}$ $s^{-1}$, $p$ = 0.02), but not in control trees (pre- 0.24 ± 0.07,

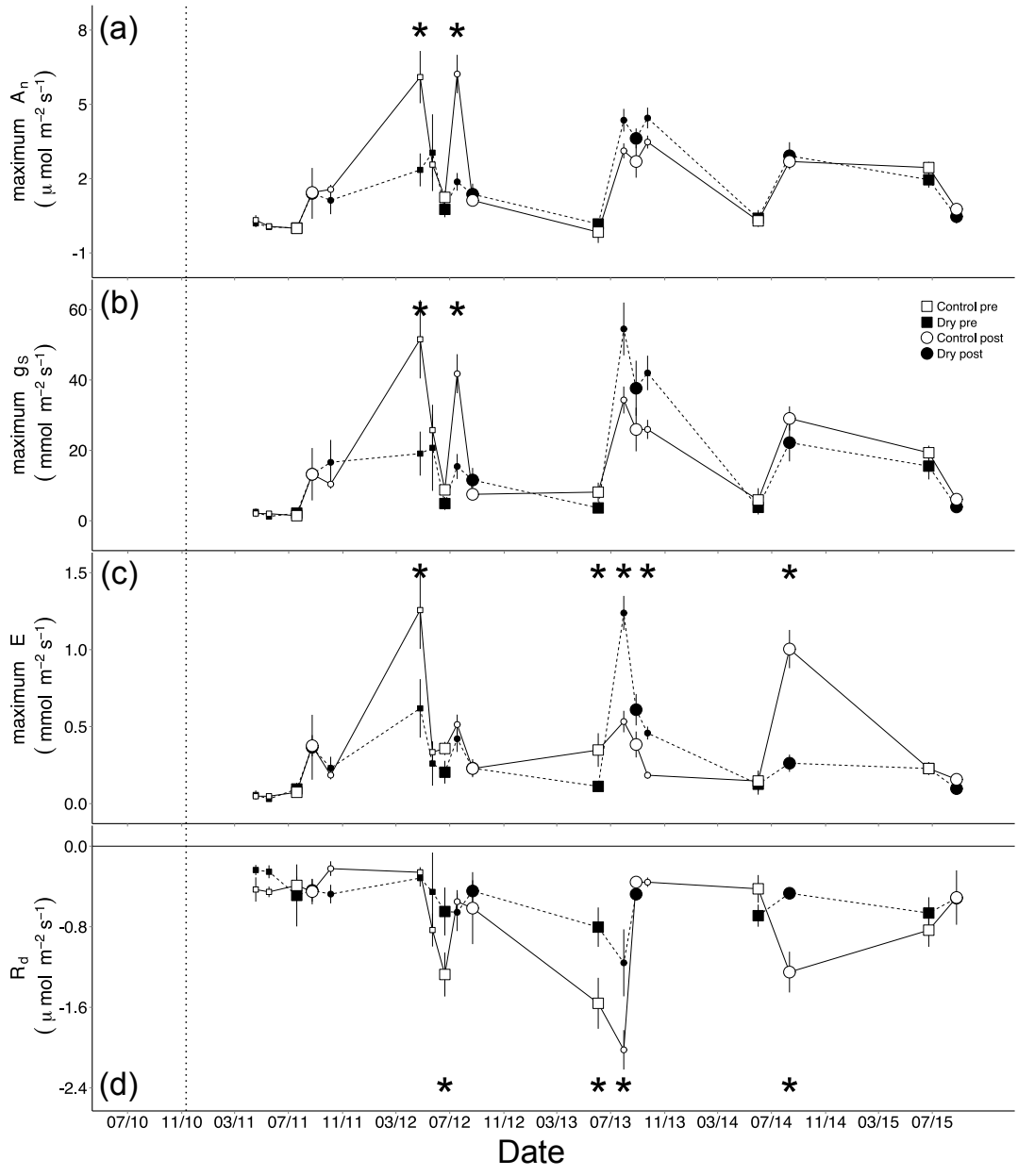


Figure 3.4: Mean ± SE values of leaf gas exchange measurements made from 2011-2015. Large symbols represent sampling dates when all hydraulic measurements, including water potential, were collected. The vertical dotted line indicates the installation of drought structures and the beginning of experimental manipulation. Large symbols represent sampling dates when all hydraulic measurements were collected. Asterisks indicate sampling dates when treatment differences were significant at $p \leq 0.05$.

post- 0.36 ± 0.09 mmol $m^{-2}$ $s^{-1}$, $p = 0.24$) (Fig. 3.4c). Finally, we found that trees in the drought treatment had reduced respiration rates relative to control trees ($p = 0.05$), though no period effect was detected ($p = 0.83$) (Fig. 3.4d).

*3.3.6 Impact of drought stress on hydraulic function*

$\Psi_{PD}$ predicted $\Psi_{MD}$ in both treatments prior to monsoon precipitation ($p < 0.0001$), but the relationship was stronger in droughted trees ($R^2 = 0.42$) than control trees ($R^2 = 0.13$) (Fig. 3.5a, Table 3.1). After the monsoon, $\Psi_{PD}$ was more weakly correlated with droughted tree $\Psi_{MD}$ ($p < 0.0001$, $R^2 = 0.13$), and did not correlate with control tree $\Psi_{MD}$ ($p = 0.8$). The power of $\Psi_{PD}$ to predict $\Delta\Psi$ shifted from moderate ($p < 0.0001$, $R^2 = 0.34$) to strong ($R^2 = 0.72$) with the onset of the monsoon in control trees, while this linear relationship shifted from weak to moderate in droughted trees ($R^2 = 0.17$ pre-, $R^2 = 0.46$ post-monsoon). We detected significant treatment, period and treatment*period interaction effects on the relationship between $\Psi_{PD}$ and $\Delta\Psi$ (Fig. 3.5b, Table 3.1, Table 3.2). Experimentally droughted trees had significantly shallower slopes than control trees ($p < 0.0001$). Monsoon precipitation increased slopes in both treatments ($p = 0.001$ pre- and post-monsoon), but the increase was proportionally greater in drought treatment trees.

All other hydraulic response variables, save $K_S$, correlated with $\Psi_{PD}$ such that as water stress intensified, hydraulic performance decreased (Fig. 3.5, Fig. 3.6, Table 3.1, Table 3.2). No treatment, period, or treatment*period interaction effects were detected for the relationships between $\Psi_{PD}$ and $K_L$ or $A_n$. $\Psi_{PD}$ was not strongly correlated with either max $A_n$ ($R^2 = 0.33$), or $K_L$ ($R^2 = 0.1$). Experimental drought had an impact on relationships between $\Psi_{PD}$ and $E_b$, $g_S$ and $E$ (Fig. 3.6d, b & c, Table 3.1, Table 3.2).

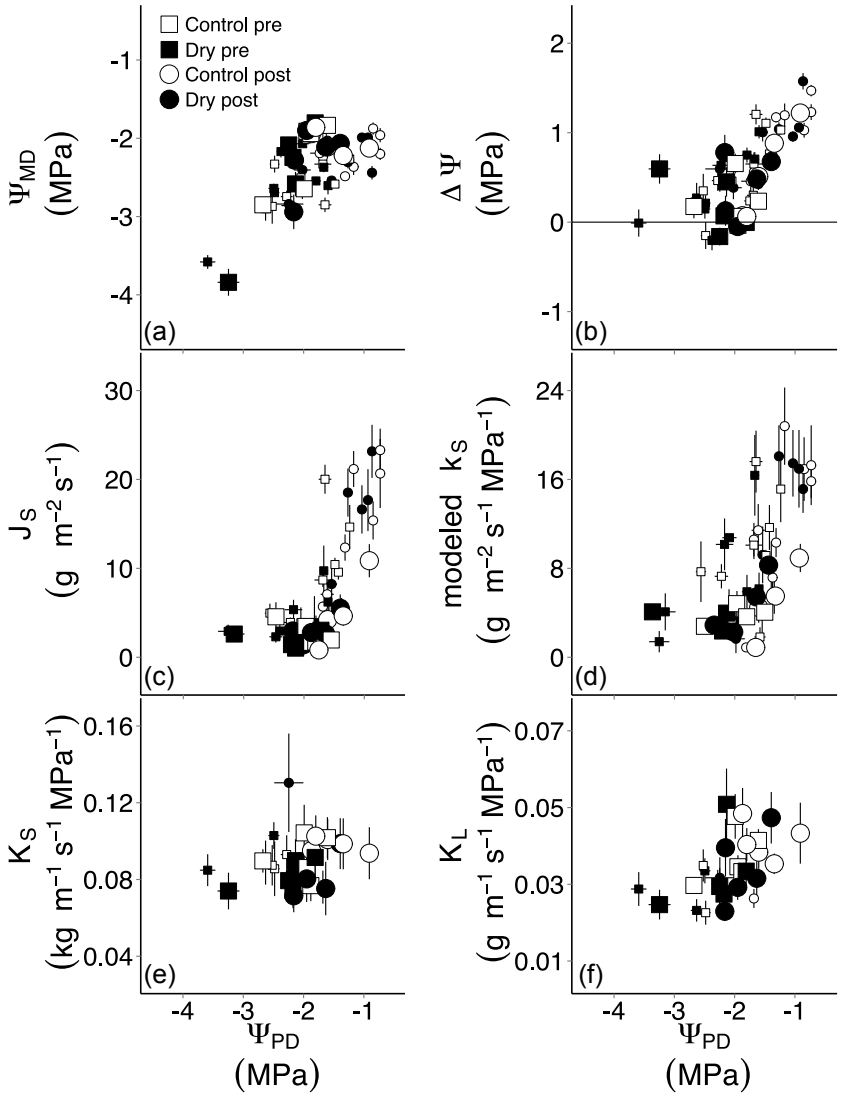


Figure 3.5: Relationships between mean values of predawn water potential and hydraulic transport parameters. Large symbols represent sampling efforts when all hydraulic measurements were collected. Error bars are ± 1 standard error. Data from 2011-2015 are pooled.

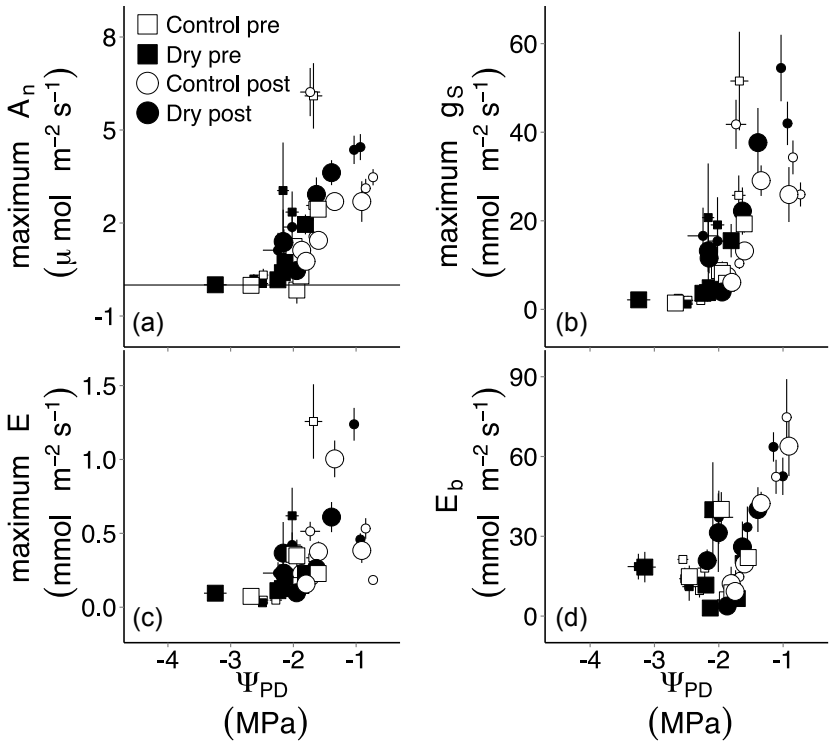


Figure 3.6: Relationships between mean values of predawn water potential and leaf gas exchange (a-c), and transpiration supply (d). Large symbols represent sampling efforts when all hydraulic measurements were collected. Error bars are ± 1 standard error. Data from 2011-2015 are pooled.

Table 3.1: Coefficients ± standard error of the linear mixed effects model regressions between predawn water potential ($\Psi_{PD}$) and hydraulic response variables for significant relationships determined by linear mixed effects modeling (see Table S1). Coefficients of determination are for *post-hoc* linear regressions, with associated *p*-values indicated as: * 0.05-0.01, ** 0.01-0.001, *** < 0.001. † indicate $\Psi_{PD}$[RV = 0] that exceed $P_e$ (-2.59 MPa), and therefore predict an increase in risk of embolism formation and spread.

| Parameter | Treatment | Period | Intercept | Slope | $R^2$ | $\Psi_{PD}$[RV = 0] |
|---|---|---|---|---|---|---|
| $\Psi_{MD}$ | | | | | | |
| | Control | Pre- | -1.67 ± 0.14 | 0.36 ± 0.07 | 0.13*** | – |
| | Control | Post- | -2.15 ± 0.1 | -0.01 ± 0.07 | NS | – |
| | Dry | Pre- | -1.1 ± 0.19 | 0.65 ± 0.09 | 0.42*** | – |
| | Dry | Post- | -1.82 ± 0.14 | 0.29 ± 0.09 | 0.13*** | – |
| $\Delta\Psi$ | | | | | | |
| | Control | Pre- | 1.67 ± 0.14 | 0.64 ± 0.07 | 0.34*** | -2.59 |
| | Control | Post- | 2.15 ± 0.1 | 1.01 ± 0.07 | 0.72*** | -2.12 |
| | Dry | Pre- | 1.10 ± 0.19 | 0.35 ± 0.09 | 0.17*** | -3.17† |
| | Dry | Post- | 1.82 ± 0.14 | 0.71 ± 0.09 | 0.46*** | -2.59 |
| $J_S$ | | | | | | |
| | Pooled | Pre- | 13.43 ± 1.96 | 3.77 ± 0.93 | 0.11*** | -3.56† |
| | Pooled | Post- | 27.98 ± 2.34 | 12.59 ± 1.33 | 0.38*** | -2.22 |
| Modeled $k_S$ | | | | | | |
| | Pooled | Pre- | 0.80 ± 0.16 | 0.16 ± 0.08 | NS | – |
| | Pooled | Post- | 1.20 ± 0.18 | 0.43 ± 0.11 | 0.13*** | -2.78† |
| $K_L$ | | | | | | |
| | Pooled | – | 0.05 ± 0.003 | 0.007 ± 0.001 | 0.009*** | -7.31† |
| $E_b$ | | | | | | |
| | Control | Post- | 117.4 ± 11.7 | 59.66 ± 7.61 | 0.55*** | -1.97 |
| | Dry | Post- | 80.54 ± 17.4 | 28.82 ± 10.2 | 0.29*** | -2.79† |
| Max $A_n$ | | | | | | |
| | Pooled | – | 5.11 ± 0.37 | 1.80 ± 0.19 | 0.36*** | -2.83† |
| Max $g_S$ | | | | | | |
| | Control | – | 41.84 ± 4.67 | 14.07 ± 2.62 | 0.21*** | -2.97† |
| | Dry | – | 59.75 ± 6.74 | 21.61 ± 3.49 | 0.56*** | -2.77† |
| Max $E$ | | | | | | |
| | Control | – | 0.61 ± 0.11 | 0.14 ± 0.06 | 0.04* | -4.11† |
| | Dry | – | 1.06 ± 0.15 | 0.37 ± 0.08 | 0.45*** | -2.89† |

Table 2. Summary of linear mixed effects models of the relationships between physiological response variables (RV) and predawn water potential ($\Psi_{PD}$).

| RV | Fixed Effects | numDF | denDF | F-value | *p*-value |
|---|---|---|---|---|---|
| $\Psi_{MD}$ | Intercept | 1 | 574 | 20923.02 | **< 0.0001** |
| | $\Psi_{PD}$ | 1 | 574 | 248.14 | **< 0.0001** |
| | $\Psi_{PD}$:Treatment | 1 | 574 | 18.17 | **< 0.0001** |
| | $\Psi_{PD}$:Period | 1 | 574 | 24.18 | **< 0.0001** |
| $\Delta\Psi$ | Intercept | 1 | 574 | 1108.61 | **< 0.0001** |
| | $\Psi_{PD}$ | 1 | 574 | 507.60 | **< 0.0001** |
| | $\Psi_{PD}$:Treatment | 1 | 574 | 18.2 | **< 0.0001** |
| | $\Psi_{PD}$:Period | 1 | 574 | 24.21 | **< 0.0001** |
| $J_S$ | Intercept | 1 | 323 | 203.35 | **< 0.0001** |
| | $\Psi_{PD}$ | 1 | 323 | 179.69 | **< 0.0001** |
| | $\Psi_{PD}$:Treatment | 1 | 323 | 0.69 | 0.41 |
| | $\Psi_{PD}$:Period | 1 | 323 | 43.54 | **< 0.0001** |
| Modeled $k_S$ | Intercept | 1 | 219 | 141.71 | **< 0.0001** |
| | $\Psi_{PD}$ | 1 | 219 | 34.38 | **< 0.0001** |
| | $\Psi_{PD}$:Treatment | 1 | 219 | 0.22 | 0.64 |
| | $\Psi_{PD}$:Period | 1 | 219 | 6.10 | **0.01** |
| $K_S$ | Intercept | 1 | 254 | 264.25 | **< 0.0001** |
| | $\Psi_{PD}$ | 1 | 254 | 2.84 | 0.09 |
| | $\Psi_{PD}$:Treatment | 1 | 254 | 0.24 | 0.62 |
| | $\Psi_{PD}$:Period | 1 | 254 | 0.98 | 0.32 |
| $K_L$ | Intercept | 1 | 254 | 314.19 | **< 0.0001** |
| | $\Psi_{PD}$ | 1 | 254 | 22.03 | **< 0.0001** |
| | $\Psi_{PD}$:Treatment | 1 | 254 | 0.03 | 0.87 |
| | $\Psi_{PD}$:Period | 1 | 254 | 0.54 | 0.46 |
| $E_b$ | Intercept | 1 | 168 | 137.96 | **< 0.0001** |
| | $\Psi_{PD}$ | 1 | 168 | 51.57 | **< 0.0001** |
| | $\Psi_{PD}$:Treatment | 1 | 168 | 3.93 | **0.05** |
| | $\Psi_{PD}$:Period | 1 | 168 | 21.04 | **< 0.0001** |
| Max $A_n$ | Intercept | 1 | 157 | 247.33 | **< 0.0001** |
| | $\Psi_{PD}$ | 1 | 157 | 95.3 | **< 0.0001** |
| | $\Psi_{PD}$:Treatment | 1 | 157 | 1.63 | 0.20 |
| | $\Psi_{PD}$:Period | 1 | 157 | 0.1 | 0.75 |
| Max $g_S$ | Intercept | 1 | 157 | 246.56 | **< 0.0001** |
| | $\Psi_{PD}$ | 1 | 157 | 111.83 | **< 0.0001** |
| | $\Psi_{PD}$:Treatment | 1 | 157 | 5.04 | **0.03** |
| | $\Psi_{PD}$:Period | 1 | 157 | 2.46 | 0.12 |
| Max $E$ | Intercept | 1 | 157 | 211.21 | **< 0.0001** |
| | $\Psi_{PD}$ | 1 | 157 | 46.89 | **< 0.0001** |
| | $\Psi_{PD}$:Treatment | 1 | 157 | 7.87 | **0.0057** |
| | $\Psi_{PD}$:Period | 1 | 157 | 0.18 | 0.67 |

Note: Full Model: lme(RV ~ YPD*Treatment*Period, random=~1|Tree, na.action=na.omit, method= "ML")

Drought treatment reduced the slope of the relationship, and the strength of the correlation, between $E_b$ and $\Psi_{PD}$ (drought treatment $R^2 = 0.29$, control $R^2 = 0.55$). The dynamics of the response of $E_b$ to $\Psi_{PD}$ is an outcome of the relationship between $\Delta\Psi$ and $\Psi_{PD}$ - drought treatment maintained positive $\Delta\Psi$ over a broader span of $\Psi_{PD}$, but droughted trees did not allow $\Psi_{PD}$ to fall below -2.5 MPa frequently. Experimental drought increased the slopes of the relationships between $\Psi_{PD}$ with $g_S$ and $E$. The treatment effects on the relationships of $\Psi_{PD}$ and leaf gas exchange indicate that drought treatment increased gas exchange sensitivity to water stress.

Monsoon precipitation changed relationships between $\Psi_{PD}$ and $J_S$, modeled $k_S$, and $E_b$ (Fig. 3.5c & d, 3.6d, Table 3.1, Table 3.2). In all cases, $R^2$ values increased and steeper slopes were found between the response variables and $\Psi_{PD}$ in the post-monsoon sampling period. $\Psi_{PD}$ had no relationship with pre-monsoon modeled $k_S$ or $E_b$, and was a weak predictor of $J_S$ ($R^2 = 0.11$). Increased water availability changed relationships such that $\Psi_{PD}$ became a weak predictor of drought treatment $E_b$ ($R^2 = 0.29$) and a moderate predictor of control $E_b$ ($R^2 = 0.55$), a modest predictor of $J_S$ ($R^2 = 0.38$), and a weak predictor of modeled $k_S$ ($R^2 = 0.13$).

Linear mixed models permitted the calculation of $\Psi_{PD}$ of zero function for water potential, sapflow, shoot conductivity, and leaf gas exchange response variables (RV) ($\Psi_{PD}[RV = 0]$, Fig. 3.5, Fig. 3.6, Table 3.1). Nearly all these values of $\Psi_{PD}[RV = 0]$ were close to $P_e$ (-2.59 MPa). $\Psi_{PD}[\Delta\Psi = 0]$ became less negative with monsoon onset (Fig. 3.5b). Drought treatment $\Psi_{PD}[\Delta\Psi = 0]$ exceeded $P_e$ pre-monsoon, and matched $P_e$ post-monsoon; control $\Psi_{PD}[\Delta\Psi = 0]$ matched $P_e$ pre-monsoon, and shifted to less negative

with monsoon precipitation. This pattern of stomatal regulation is predicted to allow embolism spread when water is scarce, but limit embolism spread when water is available. Thus, piñon abandons strict isohydry under some drought conditions. $\Psi_{PD}[J_S = 0]$ exceeded $P_e$ before the monsoon, but not after (Fig. 3.5c). No linear relationship was detected for modeled $k_S$ pre-monsoon, but post-monsoon $\Psi_{PD}[k_S = 0]$ exceeded $P_e$ (Fig. 3.5d). $\Psi_{PD}[K_L = 0]$ was more similar to $P_{max}$ (-7.59 MPa compared to -6.35 MPa) than $P_e$. (Fig. 3.5f). No relationship between $E_b$ and $\Psi_{PD}$ was detected pre-monsoon; post-monsoon, drought treatment reduced $\Psi_{PD}[E_b = 0]$ such that drought $\Psi_{PD}[E_b = 0]$ exceeded $P_e$ while control did not (Fig. 3.6d). All leaf gas exchange variables returned $\Psi_{PD}[0]$ values more negative than $P_e$. (Fig. 3.6a, b, c). Piñon is therefore predicted to incur some degree of embolism in the maintenance of hydraulic transport and gas exchange as soil moisture diminishes, and the degree of embolism is exacerbated by drought, whether seasonal or experimentally imposed.

*3.3.7 Xylem vulnerability and photosynthetic capacity*

Vulnerability to embolism was not affected by treatment, so we pooled the data to generate a composite vulnerability curve to predict PLC based on $\Psi_W$ (Fig. 3.7). Drought treatment did not trigger an adjustment in $P_e$, $P_{50}$, $P_{max}$ or span between $P_e$ and $P_{max}$, which is consistent with results reported elsewhere for piñon (Hudson *et al*. in review). Similarly, suboptimal water availability did not influence xylem construction, as we detected no differences in wood density, or earlywood tracheid anatomy (Fig. 3.8).

As with xylem vulnerability curves, $A$:$C_i$ curves did not respond to experimental drought (Fig. 3.9). Lack of treatment effects on $A_n$ were consistent with lack of treatment

effects on carboxylation efficiency ($V_{C\ max}$, Welch Two Sample t-test, $p = 0.67$, Fig. 3.9 insert).

## 3.4 Discussion

### *3.4.1 Importance of beetles for piñon mortality*

This study is unique in that we excluded bark beetles, which are consistently implicated in piñon pine mortality, allowing us to investigate physiological responses to drought in the absence of biotic influence. The 5-year survival of hill-slope piñon subjected to the same drought treatment as our original experiment (Plaut *et al*. 2012), which lacked pesticide treatments and exhibited rapid mortality with high bark beetle activity, reinforces the important role that bark beetles play in determining the rate of drought-induced mortality. The application of pesticides to control bark beetles revealed that the drought tolerance of piñon in the absence of these important pathogens is considerably greater than our original experiment would suggest.

The survival of all target trees in this experiment leads to the conclusion that prolonged restriction of $J_S$ (Fig. 3.2a) does not lead to lethal carbon starvation or hydraulic failure, at least within six years of severely restricted precipitation inputs. The mortality outcomes of this study contrast significantly with those of the original precipitation manipulation experiment, which witnessed complete drought treatment piñon mortality within two years of experimental drought imposition (Plaut *et al*. 2012). It is also worth noting that piñon in the original experiment received more precipitation in the time leading up to death. The precipitation inputs of the two years preceding mortality in the original experiment (340 and 331 mm, respectively) represent ~40% of the total

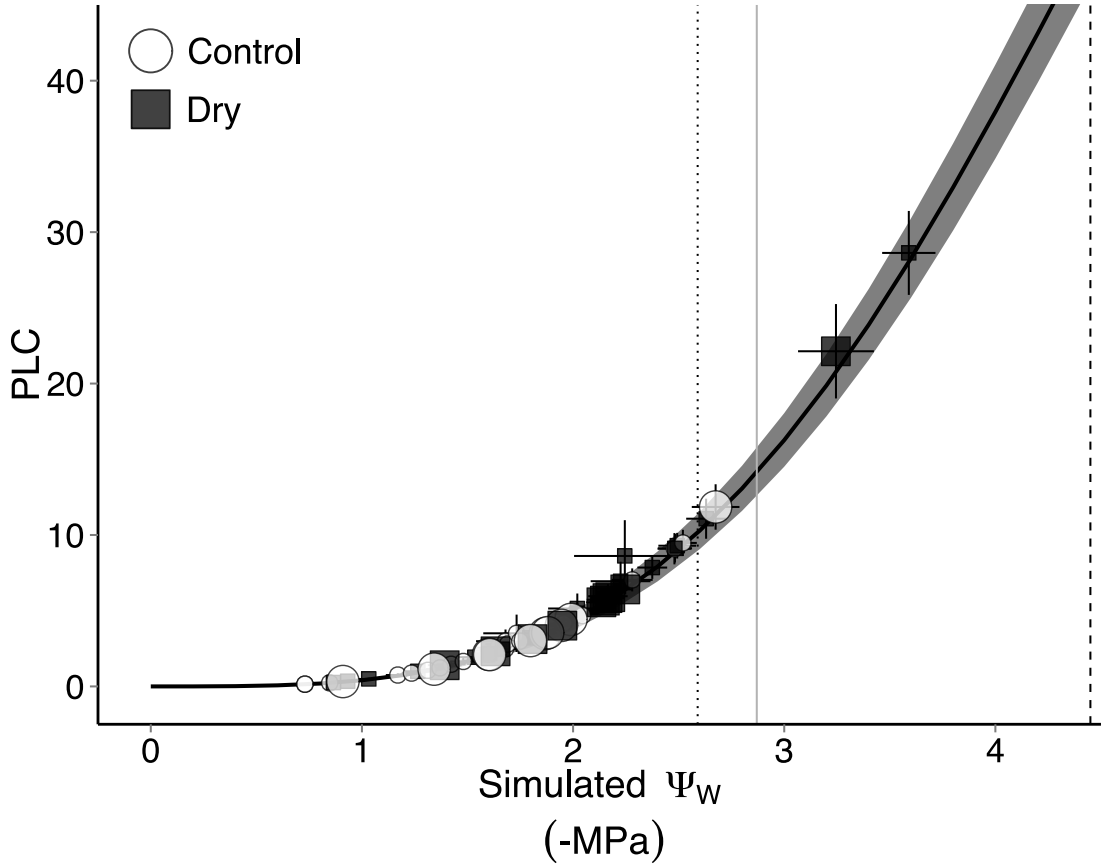


Figure 3.7: Predicted percent loss of conductivity (PLC) from measured shoot water potential ($\Psi_W$). Both predawn and midday data are displayed. Large symbols signify sampling efforts when all hydraulic measurements were collected. $\Psi_{PD}$ of zero assimilation ($A_n$) is indicated by the vertical light grey line (2.83 –MPa). The vertical dotted line is $P_e$ (2.59 –MPa) and the vertical dashed line is $P_{50}$ (4.46 –MPa). The curve was derived from pooling all PLC data, with grey shading representing PLC ± 1 standard error. Error bars associated with data points are ± 1 standard error.

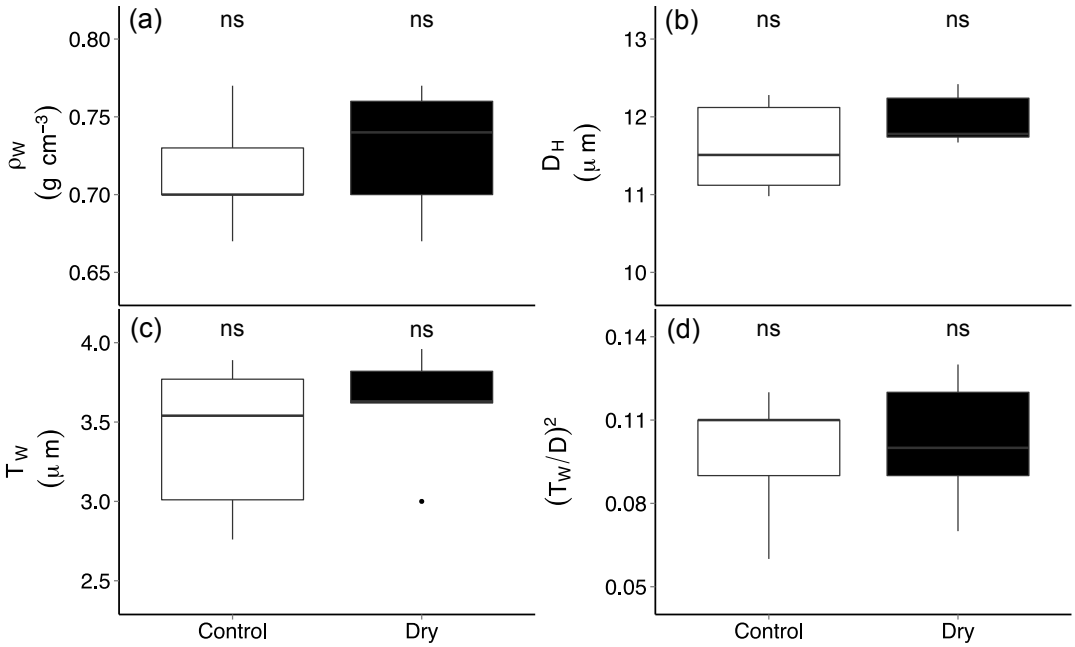


Figure 3.8: Boxplots for (a) wood density ($\rho_W$), (b) earlywood tracheid diameter ($D_H$), (c) double wall thickness ($T_W$), and (d) thickness to span ratio ($(T_W/D)^2$). Measurements were made on vulnerability curve samples collected in 2014 ($N = 5$ trees per treatment).

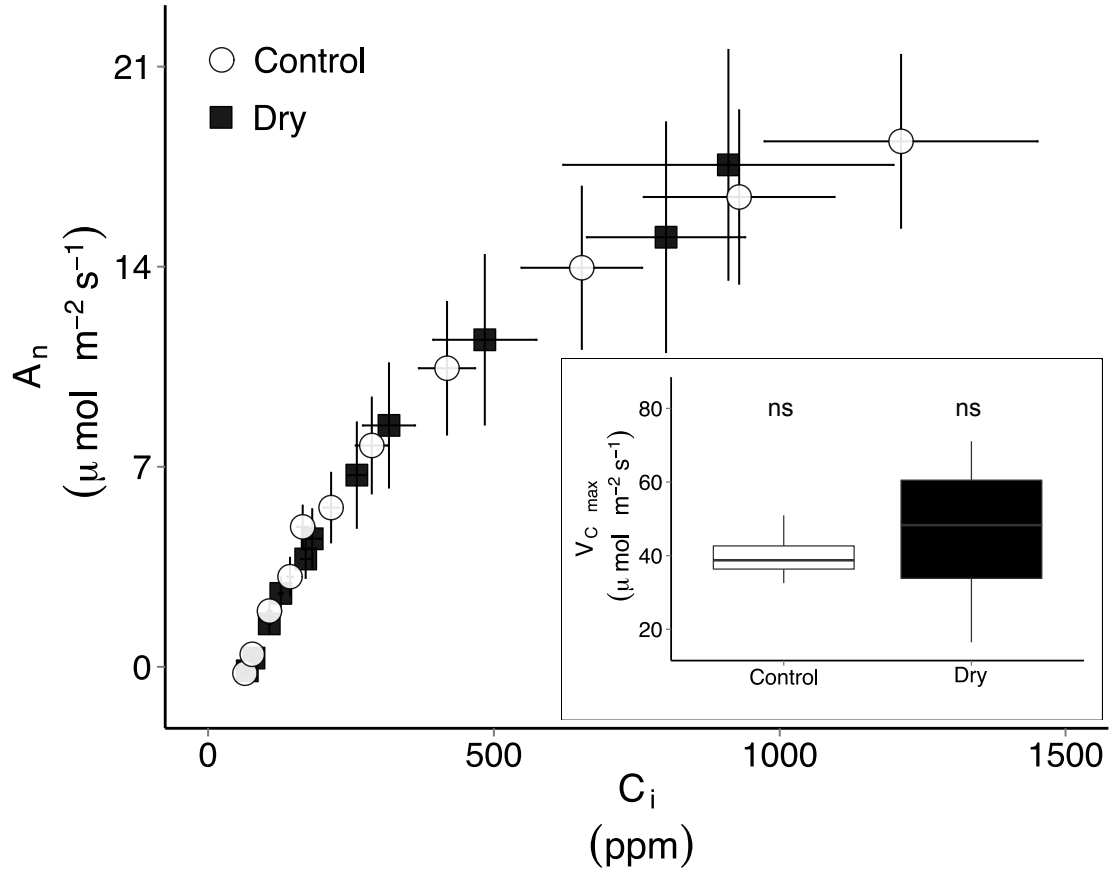


Figure 3.9: Relationship between internal $CO_2$ concentration and net assimilation rate ($A_n$). Data are pooled from five target trees in each treatment. Error bars are ± 1 standard error. Inset figure compares maximum carboxylation rates ($V_{C\ max}$) derived from individual $A$:$C_i$ curves.

precipitation inputs from January 2010 to August 2015 (Fig. 3.1b). In other words, the naturally occurring drought conditions were more severe over the course of this beetle exclusion experiment than the original experiment. Piñon that died in the original drought treatments in 2008 and 2009 exhibited low rates of $J_S$ (< 5.4 g $m^{-2}$ $s^{-1}$) for eight consecutive months (Plaut *et al*. 2012). Though sap-flow sensors were installed in early spring 2011, the absence of rain beginning in October 2010 (Fig. 3.1a) gives us confidence to suggest the insecticide-treated piñon survived an interval of at least 14 months at or below the critically low sap-flow threshold that characterized trees that died in the original experiment (Fig. 3.2a).

*3.4.2 Piñon hydraulic responses to chronic drought*

Hydraulic traits that responded most strongly to drought stress, whether natural or experimental, were either directly ($J_S$, $E_b$, $g_S$, $E$), or indirectly ($A_n$) related to the quantity of water transported (Fig. 3.5c, 3.6). Measurements of transport efficiency (modeled $k_S$, $K_S$, $K_L$), on the other hand, were not as substantially affected by drought stress (Fig. 3.5d, e, f). In other words, drought reduced the total amount of water transported by target piñon, but did not reduce their water transport capacity. Our observation that metrics of transport efficiency remained similar across treatments is consistent with the predicted consequences of an isohydric stomatal regulation (Martinez-Vilalta *et al*. 2014, Skelton *et al*. 2015). Reduced quantities of soil moisture resulted in less water available for transport. Water transport was in turn restricted by strict stomatal limitation, as piñon $\Psi_{PD}$ and $\Psi_{MD}$ indicated elevated water status relative to $\Psi_{soil}$, as inferred from co-occurring juniper $\Psi_W$ measurements (data not shown, Pangle *et al*. 2015). Strict stomatal limitation prevented pervasive shoot embolism to typically less than 15% PLC (Fig. 3.7,

though note two instances of high PLC as a result of extremely dry 2011), thereby preserving a viable hydraulic network. Thus, if piñon hydraulically disconnect from critically dry soils before significant embolism spread, sap-flow and gas exchange will cease, but conductivity will be maintained. Piñon has been shown to increase transpiration rapidly following rainfall (West *et al*. 2007, Pangle *et a*l. 2015), possibly due to rapid production or repair of fine roots. By preserving conductivity (Fig. 3.7), piñon can respond quickly to capitalize on precipitation inputs (Fig. 3.2), while minimizing costs associated with recovery of xylem hydraulic conductivity (Franks *et al*. 2007).

The lack of acclimation in hydraulic architecture and transport efficiency (Fig. 3.3), transport safety (Fig. 3.7), or earlywood tracheid anatomy (Fig. 3.8), is consistent with the literature regarding limited acclimation of hydraulic architecture in mature conifers (Mencucucci and Grace 1996, Martinez-Vilalta and Piñol 2002, Lamy *et al*. 2011, Lamy *et al*. 2013, Hudson *et al*. in review), and indicates that hydraulic acclimation will probably not enable mature trees to acclimate to the effects of climate change. The single common adjustment response shared between control and experimentally droughted trees (reduction in leaf area and consequently increased $A_S$:$A_L$) only manifested in the year after the most severe drought intensity, and ultimately did not persist over the duration of the experiment (Fig. 3.3a). The apparent decrease in $A_S$:$A_L$ from pre-experiment conditions in 2011 may have resulted from the combination of minimal sapwood increment growth and the retention of older, more expanded, foliage from previous years. Drought-induced shedding of the older needle cohorts, combined with reduced needle expansion of 2011, would lead to elevated $A_S$:$A_L$ in 2012. Conditions

permitted more full needle expansion from 2012 onward, which in the absence of significant sapwood production, generally reduced $A_S$:$A_L$ to pre-experimental values.

Although we did not observe acclimation in hydraulic transport capacity in response to multiple years of experimentally enforced drought, differences in the relationship between $\Psi_{PD}$ and $\Delta\Psi$ (Fig. 3.5b), seasonal shifts in $g_S$ and $E$ (Fig. 3.6b & c), and respiration rate (Fig. 3.4d) indicate that some adjustments did occur. The instances of functional deviation we observed in the drought treatment trees conferred an improved ability to extract water from soil over a broader range of soil moisture content, increased sensitivity of leaf gas exchange to soil moisture availability, and reduced carbon consumption rate.

By increasing the range of $\Psi_{PD}$ over which positive $\Delta\Psi$ is maintained, drought treatment piñon demonstrated an ability to abandon strict isohydry (Fig. 3.1c & d, Fig. 3.5b). Shifts in stomatal regulation behavior have been documented in the literature, but specifically for angiosperms, which typically switched from anisohydry to isohydry with the onset of drought conditions (Rogiers *et al*. 2012, Domec and Johnson 2012), or became increasingly anisohydric with crop load (i.e. fruit production, Sadras and Trentacoste 2011). The decreased slope in the relationship between $\Psi_{PD}$ and $\Delta\Psi$ (Table 3.1, Fig. 3.4b) was driven by extreme values collected at the height of the naturally occurring drought in 2011 (Fig. 3.1c & d). Piñon in the original precipitation manipulation demonstrated similar excursions beyond the typical isohydric threshold at this same time, but generally did not maintain positive $\Delta\Psi$ (Hudson *et al*. in review). From October 2010 to July 2011, drought trees received ~ 48 mm total precipitation (Fig. 3.1a & b). Under these severe conditions, drought piñon permitted uncharacteristically

large negative water potentials and managed to generate a driving gradient for transpiration, but were predicted to lose ~30% shoot conductivity as a consequence (Fig. 3.7). The mechanism(s) by which piñon adjusted stomatal regulation thresholds remains unclear. Stomatal closure in another isohydric pine species depended on foliar concentrations of the phytohormone absisic acid (ABA) (Brodribb and McAdam 2013). Perhaps the degree and duration of water stress experienced by piñon in 2011 was sufficient to interfere with foliar ABA synthesis, or prevent transport of ABA from roots to leaves. Stomatal regulation by means of guard cell turgor collapse has been predicted to occur ~ -4 MPa (Brodribb and McAdam 2013), which would have been sufficient to prevent complete hydraulic failure (Fig. 3.7), but piñon $\Psi_W$ did not drop so low (Fig. 3.1 c & d). Atypical stomatal regulation was ultimately only temporary, as $\Psi_{MD}$ shifted back to ~ -2.5 MPa before the end of the 2012 drought, where it remained consistent for the remainder of the experiment (Fig. 3.1d), which suggests that excursions beyond isohydric limits require significant climate forcing.

Increasing transpiration rate following monsoon onset allows for more rapid carbon capture when water is available. Piñon photosynthesis followed a daily time course, with $A_n$ increasing from dawn to a midmorning maximum (~ 0800-0900h), before declining to zero by late morning (pre-monsoon) or early afternoon (mid-monsoon, data not shown, Limousin *et al*. 2013). Thus, increased $g_S$ and $E$ would enable droughted trees to maximize carbon capture within the limited window when water transport is feasible, on the daily and seasonal time scale. The increased slopes of relationships between $\Psi_{PD}$ and leaf gas exchange ($g_S$ and $E$) from pre- to post-monsoon suggest that chronic drought suppressed gas exchange when water was scarce, and enhanced gas exchange sensitivity

to water status when soil water was present (Table 3.1). It should be noted that droughted piñon $g_S$ and $E$ did not differ from control, but rather increased more dramatically with monsoon precipitation. The lack of treatment effect on gas exchange or carboxylation efficiency (Fig. 3.4, Fig. 3.6, Fig. 9) did not support our hypothesis that experimental drought would lead to reduced gas exchange via water restriction and strict stomatal limitation, but is consistent with other reports for piñon in the original experiment (Limousin *et al*. 2013)

Our observations of drought-induced reduction in carbon consumption (Fig. 3.4d) are consistent with findings of Sevanto et al. (2014), who also reported piñon subjected to (lethal) experimental drought responded by reducing respiration rate. Using an equation they developed to quantify the relationship between shoot total nonstructural carbohydrates (% shoot mass) to respiration rate, and acknowledging the caveat that this relationship was developed based on trees that were forced into a mortality sequence, we estimated that our droughted piñon had reduced total NSCs compared to control piñon, based on experiment mean $R_d$ (3.89% and 4.57%, respectively). This estimated decrease in NSC concentration is consistent with other reports of depleted NSC concentrations in response to non-lethal drought (Körner *et al*. 2003, Anderegg 2012). The reduction in $R_d$ should mitigate metabolic demand for NSCs, allowing for prolonged metabolic function under chronic stress, though the risk of carbon starvation is predicted to increase with sufficiently diminished NSC content (McDowell 2011). By reducing carbon allocated to maintenance of living tissues by cellular respiration, droughted piñon could also maintain carbon reserves necessary to reestablish hydraulic connections when soil moisture pools become available (Sayer and Haywood 2006, West *et al*. 2007).

### *3.4.3 Climate change impacts on bark beetles*

As small (~ 5 mm in length) ectotherms, bark beetles are tightly coupled to the ambient conditions of their environment, and temperature acts as a major constraint on beetle populations (Bentz *et al*. 2010, Raffa *et al*. 2015). The projected shifts to hotter and drier climates generally favor insect activity and outbreak potential because warmer temperatures accelerate insect reproductive physiology and development, and water stress renders trees more vulnerable to insect attack (Kurz *et al*. 2008, Dukes *et al*. 2009, Raffa *et al*. 2015). Eruptive species depend on overwhelming host defenses for successful infestation, which requires synchronous adult emergence and life-cycle phenologies that are determined by temperature-dependent physiological processes (Bentz *et al*. 2010). However, insect development typically follows a pattern of increase in developmental rate to a maximum, followed by a precipitous decline. Populations living near their thermal maximum are less likely to benefit from climate warming (Hicke *et al*. 2006, Raffa *et al*. 2015), and may be at risk of local extirpation. In addition to suppressing development, critically high temperatures increase dehydration risk, and reduce dispersal ability of bark beetles (Rouault *et al*. 2006).

Mortality from cold exposure is a primary constraint on bark beetle populations (Bentz *et al*. 2010). Climate change may increase frequency of extreme cold events, as shifts in jet-stream position driven by Arctic warming, lead to extreme cold events in mid-latitudes of North America (Overland *et al*. 2016). An increase in frequency of severe cold events that exceed lower thermal tolerance of bark beetles will reduce population sizes and outbreak risk, even in years of severe drought (Bentz *et al*. 2013). A severe cold snap in February 2011 that exceeded piñon ips cold tolerance (< -23ºC for 13

hours, Chansler 1966) may explain why bark beetle activity was nonexistent at our site in 2011 and minimal in 2012, even though this was the time period of highest regional drought severity (USDA 2015).

## 3.5 Conclusions

Our experiment demonstrates that piñon have a greater capacity to survive chronic drought than previously reported in the literature, with the caveat that they do not suffer bark beetle attack. Experimental drought limited water transport, but did not significantly impact hydraulic transport capacity. Isohydric stomatal regulation was correlated with a lack of acclimation in hydraulic architecture and photosynthetic capacity. During severe drought stress, experimentally droughted piñon demonstrated the ability to abandon strict isohydry, and permitted uncharacteristically low water potentials to generate a positive driving gradient for transpiration. This behavior was predicted to predispose piñon to increased embolism formation, and may not be sustainable under severe droughts of long duration, as it was only demonstrated at the peak of drought stress and significantly exacerbated the risk of hydraulic dysfunction. Our observations that $\Psi_{PD}$ of 0 gas exchange always exceeded $P_e$, coupled with reduced respiration rate and projected diminished shoot NSCs, lead to the conclusion that piñon suffering prolonged and severe drought stress demonstrate signs and symptoms of both hydraulic failure and carbon starvation. Most critically, if climate changes such as extreme cold events have negative consequences on bark beetle populations and outbreaks, our results suggest piñon pine survival may be substantially prolonged relative to model projections (McDowell *et al*. 2015).

# Chapter 4

# Linking spectral reflectance to hydraulic function demonstrates utility of remote sensing to infer water status and xylem transport capacity in a semi-arid conifer woodland

## 4.1 Introduction

Drought represents a major constraint on plant growth and productivity. Drought intensity is a function of critically low soil moisture content driven by limited precipitation, and may be exacerbated by high atmospheric demand for water vapor (Williams *et al*. 2013, Trenberth *et al*. 2014, Allen *et al*. 2015). Climate models predict increases in temperature and greater variability in precipitation, particularly in arid lands; both scenarios are likely to increase the frequency and severity of drought in these regions (Seager *et al*. 2007, Sheffield and Wood 2008, Williams *et al*. 2013). Observations of drought-related mortality have increased, and have revealed species-specific patterns of mortality (McDowell *et al*. 2008, Van Mantgem *et al.* 2009, Allen *et al*. 2010, Peng *et al*. 2011). Modeling efforts to predict how forests will respond to climate change depend on inputs of key plant traits and physiological function, including: predawn water potential, leaf mass per area, and hydraulic conductance (see McDowell *et al*. 2015 and references to models therein). Currently, dynamic global vegetation models (DVGMs) tend to group species into plant functional types (PFTs), but this approach

ignores trait variability within PFTs, which can be exacerbated when the number of plant functional types is small (Quillet *et al*. 2010, Reich *et al*. 2014, Reichstein *et al*. 2014, McDowell *et al*. 2015). Models that represent the functional diversity currently circumscribed by PFTs provide more accurate predictions of species contributions to ecological processes, particularly mortality (Scheiter *et al*. 2013, McDowell *et al*. 2015, Musavi *et al*. 2015). The parameters provide crucial details to characterize plant function but require time-intensive, resource-intensive, and/or semi-destructive protocols that may prohibit assessments of forests at large spatial and temporal scales (Stimson *et al*. 2005, Musavi *et al*. 2015).

The physiological processes that control plant water relations are key to characterize species-specific patterns of drought response. Measurements of pre-dawn water potential ($\Psi_{PD}$) are often used as a proxy for plant-level water availability, while midday water potential ($\Psi_{MD}$) provides a measure of water stress during gas exchange. The difference between $\Psi_{PD}$ and $\Psi_{MD}$ ($\Delta\Psi$) provides an index of daily water use determined by stomata, with values of zero reflecting stomatal closure during the day and large values reflecting high stomatal conductance. Drought stress tends to decrease $\Psi_{PD}$ and reduce $\Delta\Psi$ in a species-specific manner that is correlated with the drought limitations on xylem water transport (Pockman and Sperry 2000). Xylem hydraulic conductance decreases in a species-specific manner with decreasing water potential, as embolism formation and spread depends on species-specific structural attributes in the interconnections among xylem conduits. Critical loss of functional conduits leads to hydraulic failure (Tyree and Sperry 1991). Drought stress therefore limits xylem transport indirectly by forcing stomatal closure, or directly by severing the hydraulic connection

spanning the soil-plant-atmospheric continuum. The availability of large-scale estimates of plant water status would provide a key opportunity to evaluate and predict the impacts of drought at the ecosystem to regional spatial scale (Serrano *et al.* 2000, Stimson *et al.* 2005).

Remote sensing offers one avenue to obtain rapid, large-scale, synoptic data that can inform the physiological status of vegetation. A variety of indices that use ratios of foliar reflectance in specific wavelengths and/or wavebands have been developed to probe aspects of plant health including pigment composition and content (Gitelson and Merzylak 1997, Sims and Gamon 2003) and foliar tissue water content (Gao 1996, Peñuelas *et al.* 1997). Chlorophyll absorption of photosynthetically active radiation (PAR) dominates reflectance signals in the visible spectrum (350–700 nm). Spongy mesophyll structure and turgor influence reflectance signals in the near-infrared (NIR, 700-1100 nm). Reflectance signals in the shortwave infrared (SWIR, 1100-2500 nm) are directly sensitive to water content, thus leaf reflectance in these regions of the electromagnetic spectrum is a function of foliar hydration. Increased reflectance in the visible spectrum is a generic initial signal of foliar stress, derived from the sensitivity of chlorophyll content to deviations from optimal foliar health (Carter 1993, Carter and Knapp 2001). In particular, the position of the red edge of chlorophyll absorption in the VNIR has been shown to be highly sensitive to chlorophyll content (Gitelson and Merzylak 1997, Carter and Knapp 2001), and provides a reliable signal of detrimental water status. Water content is directly linked to foliar hydration, which is in turn maintained by xylem hydraulic supply (Tyree and Ewers 1991, Brodribb 2009). Thus there should be links between leaf spectral reflectance signals, and leaf water status and

subtending xylem hydraulic function, though the nature of those links will depend on species-specific structural and physiological characteristics (Brodribb 2009, Reich *et al*. 2014, Wullschleger *et al*. 2014, Musavi *et al*. 2015). Recent advances in remote sensing technologies have increased the spectral resolution at which forest canopies can be measured and the advent of hyperspectral remote sensing may provide opportunities for broad scale synoptic acquisition of species-specific measures of hydraulic function (Ustin and Gamon 2010).

The goal of this study was to evaluate the relationships between spectral reflectance patterns and direct measurements of plant water status and hydraulic function across a continuum of canopy stress for two species of conifer that dominate semi-arid woodlands in the southwestern US: piñon pine (*Pinus edulis* Englem.) and one seed juniper (*Juniperus monosperma* [Engelm.] Sarg.). Piñon-juniper woodlands have experienced severe drought multiple times within the past century, and each of these severe drought events has been punctuated by massive piñon mortality, and comparatively minor juniper mortality (Breshears *et al*. 2005, McDowell *et al*. 2008, Breshears *et al*. 2009 Floyd *et al*. 2009, Williams *et al*. 2013).

Researchers have previously demonstrated the utility of remote sensing to detect early onset canopy stress (Eitel *et al*. 2011), canopy structural changes following mortality events (Krofcheck *et al*. 2013), predict primary production (Krofcheck *et al*. 2016), and estimate leaf water potential and foliar water content (Stimson *et al.* 2005) in piñon and juniper woodlands. However, we currently lack the ability to gather detailed information concerning the hydraulic function of these species over broad spatial scales and within narrow timeframes. If we can determine relationships between time-intensive

measurements of tree physiological function and rapidly obtained leaf spectral signals, we will be better able to identify landscapes facing drought induced mortality risk, and quantify the magnitude of that mortality risk. Understanding the dynamics of mature tree responses to chronic stress, and developing the ability to recognize signals indicative of these responses will provide 1) critical information for DGVMs by increasing our ability to accurately predict forest responses to future drought disturbances, 2) novel data collection techniques that allow researchers to expand from plot-based direct measurements to larger landscape scales and less accessible sites, and 3) a means to rapidly identify forests with elevated mortality risk. In this study we assessed the utility of spectral reflectance signatures to predict direct measurements of plant hydraulic function. We hypothesized that multiple years of experimental precipitation reduction would provide a range of foliar health, such that 1) hydraulic transport capacity and leaf foliar water status will decline with increasing stress, and 2) changes in leaf spectral properties will correlate with aspects of plant physiological ecology sensitive to drought stress.

## 4.2 Materials and Methods

### *4.2.1 Study site*

The research was conducted in a piñon-juniper woodland in the Sevilleta National Wildlife Refuge, Socorro County, New Mexico (N 34°23′13″, W 106°31′29″), part of the US Long-Term Ecological Research network. The elevation at the site is approximately 1911 m, which is close to the lower elevation limit of piñon. Piñon and juniper are the dominant woody species. Soils were calcid aridisols characterized as Sedillo-Clovis

association of fan alluvium derived from conglomerate (Soil Survey Staff, Natural Resources Conservation Service, United States Department of Agriculture; http://websoilsurvey.nrcs.usda.gov/). Long-term mean monthly temperatures range from 2.6 °C in January to 23.1 °C in July; annual precipitation averages 362 mm at a meteorological station near the site (Cerro Montoso meteorological station, 2.2 km from and approximately 70 m higher than the study site, 1989–2009, http://sev.lternet.edu/). From 2007 to 2016, annual precipitation has varied from a minimum of 252 mm in 2011 to a maximum of 385.8 mm in 2013. The site is heavily influenced by the North American monsoon, as roughly half of the annual precipitation is produced by convective storms, typically during July through September.

We collected the data for this study from a subset of plots from a precipitation manipulation experiment (Pangle *et al*., 2012, Hudson *et al*. forthcoming). The four treatments applied were: (1) water addition; (2) water removal ('drought'); (3) cover control; and (4) ambient control. Water addition, which consisted of six monthly (April-October) 19 mm irrigation events, lasted from 2008-2013, and provided trees with at least 360 mm $yr^{-1}$. Water removal reduced ambient precipitation inputs by ~45%, restricting trees to less than 200 mm $yr^{-1}$ since at least 2011, and in some cases 2007 (see Hudson *et al*. forthcoming for details concerning the younger beetle exclusion experiment) These treatments furnished a continuum of canopy health, which we divided into three broad categories for the purposes of this study. We defined these branch health categories by visual assessment of foliar quality and quantity. Broad categories of water stress as determined by visual criteria should translate to statistically defined distinctions in spectral properties, as red edge-NIR capable spectral sensors have been shown to detect

shifts in reflectance before visual signs of stress (Eitel *et al.* 2011). Metrics of foliar quantity included needle size and number from current year growth. Visual deviation from fully expanded healthy current year foliage was used to delineate foliar quality. We verified our qualitative categories of canopy health by quantitative measurements of water ratio and chlorophyll content (see below). We defined three categories of canopy stress for live foliage as follows: negligible (bright green, fully expanded foliage), moderate (noticeable shift to darker green, less abundant foliage), and severe (markedly faded or yellowed green, sparse foliage, marked reduction in needle expansion) (Fig. 4.1). The range of water stress conditions generated by the precipitation manipulation experimental treatment plots allowed for identification of a sufficient number of trees of both species that satisfied these sample criteria. We selected five target trees of each species for sampling in each foliar health category, for a total of 30 individuals. All sampling was conducted on 27 September 2016.

*4.2.2 Plant water status*

Predawn and midday water potential samples (hereafter $\Psi_{PD}$ and $\Psi_{MD}$) were harvested between 0500-0530h and between 1200-1400h. Samples were sealed in humid plastic bags, and processed within 60 minutes of collection. We measured water potential ($\Psi_W$, MPa) using Scholander-type pressure chambers (PMS, Corvallis, OR).

*4.2.3 Spectral reflectance*

We used a spectroradiometer equipped with a leaf clip (FieldSpec 4, ASD Inc., Boulder, CO) to measure reflectance from attached foliage on south facing branches. Measurements were made between 1000h-1800h. The range of the spectroradiometer

Figure 4.1: Representatives of species and foliar stress category combinations. Piñon samples are in the top row, juniper samples are in the bottom row. Foliar stress intensifies from left to right as negligible, moderate, and severe. Coin envelopes are all 5.7 cm x 8.97 cm.

(350-2500 nm; 3 nm resolution at 700 nm, 10 nm at 1400/2100 nm; sampling bandwith of 1.4 nm at 350-1000 nm, 1.1 nm at 1001-2500 nm) allowed us to collect data from visible to shortwave infrared wavelengths. The spectral vegetation indices (SVIs) we calculated fell into two categories; those that assessed canopy water content (CWC) using near-infrared (NIR) and shortwave infrared (SWIR) wavelengths, and those that assessed foliar narrowband greenness (NBG) using visible light and NIR wavelengths. We selected four CWC and seven NBG vegetation indices (see Tables 4.1 & 4.2 for formulae) for the purposes of this study, based on their ubiquity in spectral vegetation analyses (Serrano *et al*. 2000, Sims and Gamon 2002).

*4.2.4 Chlorophyll content*

Leaf material used for spectral reflectance measurements was harvested and placed in a cooler with dry ice for transport to the lab. We kept leaf samples at -80ºC until prepared for chlorophyll extraction. Prior to extraction, we measured leaf area with a flat-bed scanner, so that the subset area could be included in the final leaf area total. To measure chlorophyll content ($Chl_{a+b}$), we crushed small quantities (< 0.5 g) of leaf material in liquid nitrogen using mortars and pestles. We extracted chlorophyll by soaking leaf tissue in 1 mL methanol for 24 hours in a refrigerator. We measured extract absorbance by spectrophotometer (Cary 50 UV-Vis, Varian Inc., Palo Alto, CA) at 652.0, 665.2 and 750 nm, and calculated $Chl_{a+b}$ content using coefficients determined by Pourra *et al*. (1983) in units $\mu g \bullet ml^{-1}$. We collected extracts until all $Chl_{a+b}$ was removed, as indicated by white visual appearance of the leaf tissue, and then we normalized $Chl_{a+b}$ concentrations to extraction tissue mass ($\mu g \bullet g^{-1}$).

Table 4.1: Canopy water content spectral vegetation indices used in this study. $\rho$ is reflectance at the specified wavelength (nm).

| SVI | Formula | Reference |
|---|---|---|
| Moisture Stress Index (MSI) | $\frac{\rho(1599\,nm)}{\rho(819\,nm)}$ | Hunt and Rock 1989 |
| Normalized Difference Infrared Index (NDII) | $\frac{(\rho(819\,nm)\,-\,\rho(1649\,nm))}{(\rho(819\,nm)\,+\,\rho(1649\,nm))}$ | Jackson *et al*. 2004 |
| Normalized Difference Water Index (NDWI) | $\frac{(\rho(860nm)\,-\,\rho(1240\,nm))}{(\rho(860nm)\,+\,\rho(1240\,nm))}$ | Stimson *et al*. 2005, modified from Gao 1996 |
| Water Band Index (WBI) | $\frac{\rho(970\,nm)}{\rho(900\,nm)}$ | Peñuelas et al. 1993 |

Table 4.2: Narrowband greenness spectral vegetation indices used in this study. $\rho$ is reflectance at the specified wavelength (nm).

| SVI | Formula | Reference |
|---|---|---|
| Normalized Difference Vegetation Index (NDVI) | $\frac{(\rho(860\ nm)\ -\ \rho(690\ nm))}{(\rho(860\ nm)+\ \rho(690\ nm))}$ | Stimson *et al*. 2005 |
| Red Edge Normalized Difference Vegetation Index (RENDVI) | $\frac{(\rho(750\ nm)\ -\ \rho(705\ nm))}{(\rho(750\ nm)+\ \rho(705\ nm))}$ | Sims and Gamon 2002 |
| Modified Red Edge Normalized Difference Vegetation Index (MRENDVI) | $\frac{(\rho(750\ nm)\ -\ \rho(705\ nm))}{(\rho(750\ nm)+\ \rho(705\ nm)-2\times p(445\ nm))}$ | Jackson *et al*. 2004 |
| Red Edge Position Index (REPI) | Maximum rate of change in the interval $\rho$(690 nm) to $\rho$(740 nm) | Carter and Knapp 2001 |
| Modified Red Edge Simple Ratio (MRESR) | $\frac{(\rho(750\ nm)\ -\ \rho(445\ nm))}{(\rho(705\ nm)\ -\ \rho(445\ nm))}$ | Sims and Gamon 2002 |
| Vogelmann Red Edge Index (VREI) | $\frac{\rho(740\ nm)}{\rho(720\ nm)}$ | Vogelmann *et al*. 1993 |
| Modified Chlorophyll Absorption Ratio Index (MCARI) | $[(\rho(700\ nm)-\rho(670\ nm))-0.2(\rho(700\ nm)-\rho(550\ nm))]\times\left(\frac{\rho(700\ nm)}{\rho(670nm)}\right)$ | Hunt and Rock 1989 |

*4.2.5 Hydraulic function and leaf water and carbon content*

We harvested branches that had been sampled for spectral reflectance, sealed each in a humid plastic bag, and transported them to the lab for hydraulic conductivity measurements. We measured hydraulic conductivity ($K_h$, kg•m•s$^{-1}$•MPa$^{-1}$) using a steady state flow meter (for full description of methods, see Hudson *et al*. 2010, Hudson *et al*. in review). $K_h$ samples were subsequently perfused with filtered safranin-O (0.01%) to stain functional sapwood. We normalized $K_h$ to xylem sapwood cross-section area (sapwood-specific conductivity, $K_S$, kg•m$^{-1}$•s$^{-1}$•MPa$^{-1}$) and distal leaf area (leaf-specific conductivity, $K_L$, g•m$^{-1}$•s$^{-1}$•MPa$^{-1}$). Xylem cross sections were photographed at 15x with a dissecting microscope (Carl Zeiss MicroImaging, Gottingen, Germany) and measured in ImageJ (National Institutes of Health, Bethesda, MD). The ratio of stained sapwood to total sapwood area was calculated to produce percent viable sapwood (PVS). Leaf area was calculated from haphazardly sampled subsets of foliage. Subsets were massed to get fresh weight, and scanned. For each sample, foliage subsets were placed in coin envelopes, while the remaining foliage was stripped and collected in a paper bag. All foliar tissue was dried in a 60ºC oven for 48 hours. Leaf mass per area (LMA, g•m$^{-2}$) was calculated by dividing subset dry mass by subset area; total leaf area was calculated by dividing remaining foliage dry mass by LMA, and adding the $Chl_{a+b}$ and LMA subset areas. Water ratio (WR) was calculated from the LMA foliage subset as: (fresh mass – dry mass)/(dry mass).

*4.2.6 Data analysis*

We conducted all data were analysis in R (R Core Team 2013). Two-way ANOVAs with post-hoc Tukey HSD tests detected significant differences (at $p \leq 0.05$) in

SVIs and physiological traits among species and foliar status and the interaction term species*status. To determine the suite of SVIs that best predicted measured physiological function, we used hierarchical model selection to identify the best set of predictor variables for each species/physiological trait combination. We used the R package pls (Mevik and Wehrens 2007) to perform principle component regressions (PCR) on each suite of SVIs identified by the model selection process. PCR scaled and orthogonalized SVI predictor variables to correct for issues of multicollinearity (Alchanatis and Cohen 2012). Multiple regressions and subsequent principle component regressions were also calculated for pooled data, to determine the SVI combinations that provided the most utility in predicting plant status or function at the landscape scale.

## 4.3 Results

### *4.3.1 Spectral reflectance*

The categories of foliar stress yielded distinct spectral signals (Fig. 4.2), though species-specific patterns differed. Reflectance across the visible-NIR-SWIR continuum diminished as foliar status declined in piñon, with the exception of a common minimum in the visible red wavelengths (660-680 nm). The most obvious differences were apparent in the NIR plateau, likely due to diminished mesophyll turgidity and leaf hydration as foliar health declined (Rock *et al*. 1986). Variation in reflectance was greater within foliar status categories in juniper. In the visible wavelengths, reflectance increased as foliar status declined, with distinct deviations most pronounced at the visible red wavelengths (660-680 nm) and red edge (690-715 nm), indicating that juniper chlorophyll content was sensitive to the variations in water stress captured by sampling

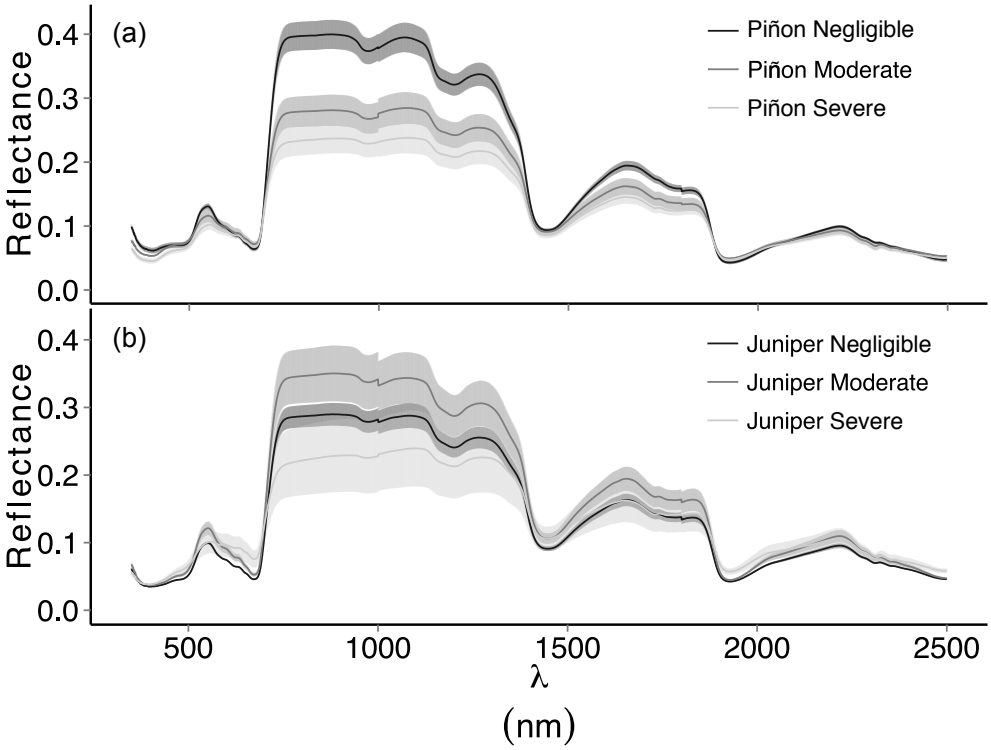


Figure 4.2: Reflectance spectra for piñon (a) and juniper (b) for each foliar stress category.

criteria. Greatest deviation in the NIR-SWIR was observed between the moderate and severe stress groups, due to decline in water content and relative increase in structural carbon as leaf tissue thinned. Between species, piñon demonstrated higher magnitude reflectance across the visible-NIR-SWIR continuum than juniper in the negligible stress group. In the moderate stress group, piñon demonstrated increased reflectance in visible wavelengths, particularly in the 660-680 nm interval, indicating lower chlorophyll content than juniper. The pattern flipped in NIR plateau and SWIR, which suggests that piñon have more mesophyll and greater water content per unit foliar mass. Severely stressed piñon and juniper converged on a common spectral signature, as prolonged water stress reduced chlorophyll and water content.

*4.3.2 Justification of foliar sampling categories*

With few exceptions, SVIs and direct measurements of plant physiological ecology differed significantly across the *a priori* defined foliar health categories (Fig. 4.3 & 4.4, Table 4.3, two-way ANOVA with *post hoc* Tukey HSD tests, $p < 0.05$). Thus, the sampling strategy we employed allowed us to survey a broad range of stress conditions in living trees for both species. The fact that piñon had universally higher water status than juniper indicates moderately dry soil conditions, as juniper $\Psi_{PD}$ more closely tracks soil water potential (Plaut *et al*. 2012, Pangle *et al*. 2015). Species-specific values for CWC SVIs in the negligible and severe stress groups $A_S$:$A_L$ reflect common homeostatic responses to drought stress, and corroborate the reduction observed in $K_S$ (Mencuccini and Grace 1996, McDowell *et al*. 2006, Martinéz-Vilalta *et al*. 2009, Martin-StPaul *et al*. 2013, Hudson *et al*. in review).

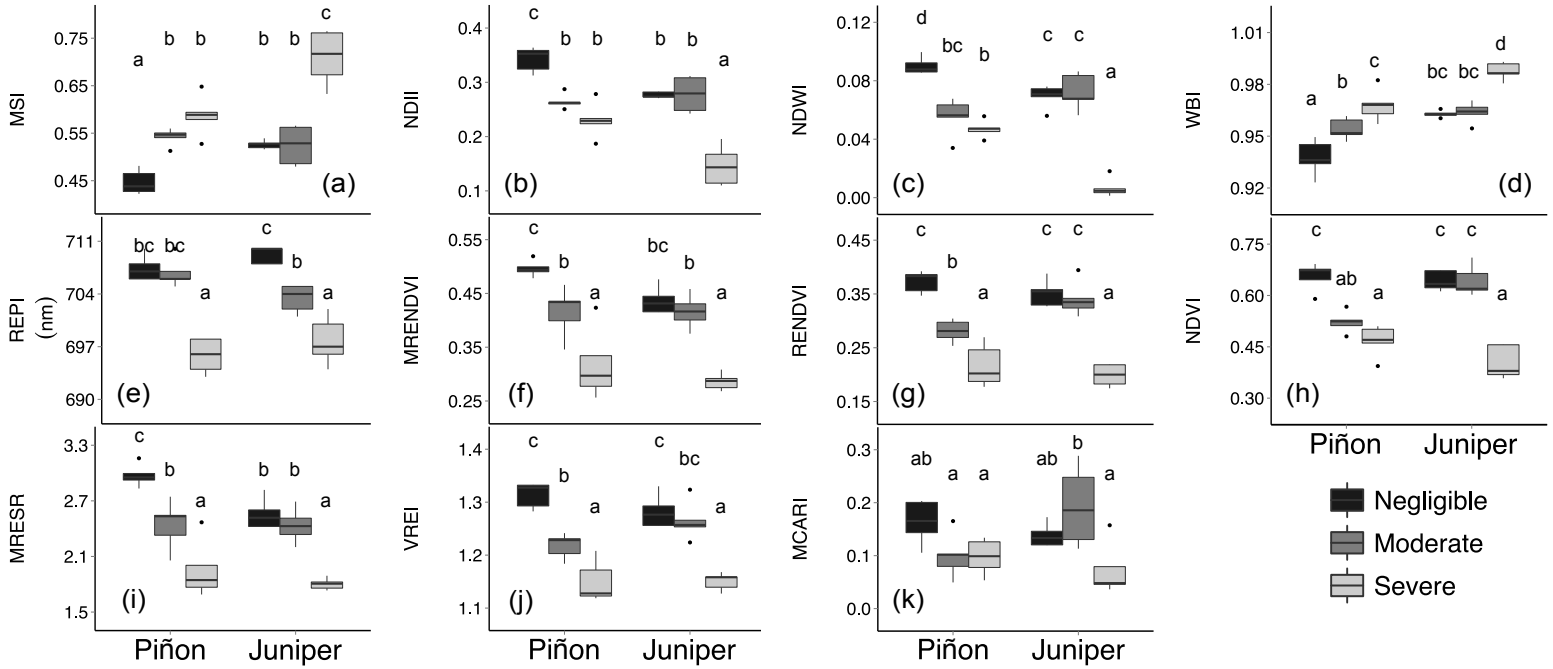


Figure 4.3. Boxplots of calculated canopy water content (a-d) and narrowband greenness (e-k) spectral vegetation indices. Letters denote significant differences across species/status combinations at $p \leq 0.05$.

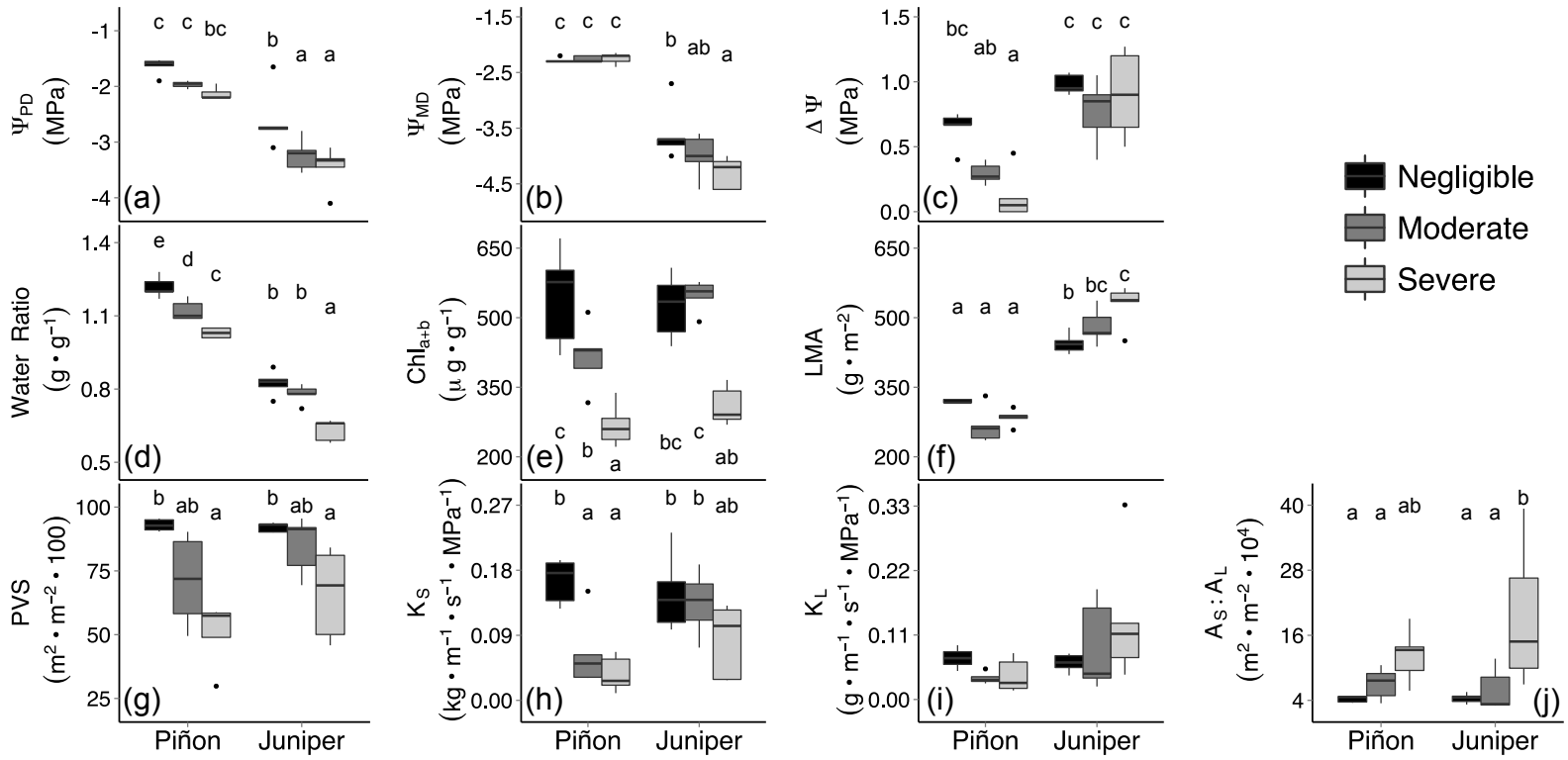


Figure 4.4: Boxplots of direct measurements of water potentials, ecomorphic traits and hydraulic function. Letters indicate significant differences across species/status combinations at $p \leq 0.05$.

Table 4.3: Results from two-way ANOVA tests and *post hoc* Tukey HSD comparisons of spectral vegetation indices, plant water status, ecomorphic traits and hydraulic function. Columns present the *p*-values of species, status and species-status interaction (Species:Status) in the tests, with significant results ($p \leq 0.05$) shown in bold.

| | Variable | Species | Status | Species:Status |
|---|---|---|---|---|
| Canopy Water Content | | | | |
| | MSI | **< 0.0001** | **< 0.0001** | **0.0007** |
| | NDII | **< 0.0001** | **< 0.0001** | **0.0008** |
| | NDWI | **0.0001** | **< 0.0001** | **< 0.0001** |
| | WBI | **< 0.0001** | **< 0.0001** | 0.06 |
| Narrowband Greenness | | | | |
| | REPI | 0.86 | **< 0.0001** | **0.01** |
| | MRENDVI | **0.04** | **< 0.0001** | 0.23 |
| | RENDVI | 0.5 | **< 0.0001** | **0.004** |
| | NDVI | 0.18 | **< 0.0001** | **< 0.0001** |
| | MRESR | **0.02** | **< 0.0001** | 0.09 |
| | VREI | 0.62 | **< 0.0001** | **0.02** |
| | MCARI | 0.4 | **0.007** | **0.01** |
| Water Status | | | | |
| | $\Psi_{PD}$ | **< 0.0001** | **0.0002** | 0.39 |
| | $\Psi_{MD}$ | **< 0.0001** | **0.04** | **0.03** |
| | $\Delta\Psi$ | **< 0.0001** | **0.004** | 0.06 |
| Ecomorphic Traits | | | | |
| | WR | **< 0.0001** | **< 0.0001** | 0.24 |
| | $Chl_{a+b}$ | **< 0.0001** | **< 0.0001** | **0.05** |
| | LMA | **< 0.0001** | 0.07 | **0.0008** |
| Hydraulic Function | | | | |
| | PVS | **0.05** | **< 0.0001** | 0.28 |
| | $K_S$ | **0.05** | **0.0002** | 0.1 |
| | $K_L$ | **0.04** | 0.55 | 0.15 |
| | $A_S$:$A_L$ | 0.37 | **0.0007** | 0.28 |

*4.3.3 Modeling plant function with SVIs*

Physiological response variables varied dramatically with respect to SVI suites that provided best-fit models; between species, no response variable was modeled by the same combination of SVIs (Table 4.4 for species-specific SVI suites, Table 4.5 for pooled data SVI suites). In general, piñon and juniper best fit multiple regressions required similar numbers of SVIs. Piñon models selected NDWI, REPI and WBI most frequently, while juniper models selected NDII, MRESR and NDVI most frequently. We used principal components loadings to investigate the degree to which components depended on CWCs and NBGs. When models selected from both categories of SVIs, principal components responsible for explaining the majority of variance (>75% in all cases) were loaded similarly by individual NBG and CWC indices. In other words, water content and greenness explained similar increments of variation in principal components, and thus shared equal relative importance for modeling plant water status and hydraulic function.

*4.3.4 Utility of SVIs to predict plant water status*

Species-specific combinations of SVIs had a strong ability to predict certain aspects of plant water status (Fig. 4.5a, c, & e). SVI models performed better for piñon than juniper. Piñon models captured > 90% of the variation in direct measurements of $\Psi_{PD}$, $\Psi_{MD}$ and $\Delta\Psi$, and the slopes of these relationships did not differ from one ($p < 0.3$). Water content and greenness contributed equally to predicting $\Psi_{PD}$, but $\Psi_{MD}$ and $\Delta\Psi$ depended more on NBG indices. In contrast to piñon models, juniper models relied entirely on NBG indices. SVIs continued to function as strong predictors of juniper water

Table 4.4: Species-specific SVI combinations generated by stepwise multiple regressions and used in principle components regression to model ecophysiological response variables. Asterisks associated with *adj* $R^2$ indicate significance as: * 0.05-0.01, **0.01-0.001, *** < 0.001.

| | | | Multiple Regression | | Principal Components Regression | | |
|---|---|---|---|---|---|---|---|
| Species | Response Variable | SVI suite | *adj.* AIC | *adj.* $R^2$ | *Components* | *RMSEP* | *adj.* $R^2$ |
| Piñon | | | | | | | |
| | $\Psi_{PD}$ | NDWI, WBI, RENDVI, VREI | -69.99 | 0.90*** | 4 | 0.09284 | 0.92*** |
| | $\Psi_{MD}$ | All* | -120.42 | 0.93* | 9 | 0.03744 | 0.98*** |
| | $\Delta\Psi$ | NDWI, WBI, MRESR, RENDVI, REPI, VREI | -64.04 | 0.89** | 6 | 0.1290 | 0.93*** |
| | WR | NDWI, WBI, MRESR, MRENDVI, RENDVI, REPI, VREI | -120.91 | 0.98*** | 7 | 0.02071 | 0.99*** |
| | $Chl_{a+b}$ | NDWI, WBI, MCARI, MRESR, REPI, NDVI | 129.05 | 0.85** | 6 | 80.26 | 0.91*** |
| | LMA | NDWI, MCARI | 258.23 | 0.4* | 2 | 27.10 | 0.45** |
| | PVS | NDWI, MSI, REPI | 71.87 | 0.82*** | 3 | 10.38 | 0.85*** |
| | $K_S$ | NDWI | -95.58 | 0.69*** | NA | NA | NA |
| | $\ln(A_S{:}A_L)$ | REPI, MCARI | -31.14 | 0.70*** | 2 | 0.3398 | 0.72*** |
| | $\ln(K_L)$ | MSI, MRENDVI, REPI | -21.87 | 0.49* | 2 | 0.4816 | 0.57*** |
| Juniper | | | | | | | |
| | $\Psi_{PD}$ | MRESR, REPI, NDVI | -43.27 | 0.86** | 3 | 0.3073 | 0.82*** |
| | $\Psi_{MD}$ | MRESR, NDVI | -41.22 | 0.78** | 2 | 0.2805 | 0.79*** |
| | $\Delta\Psi$ | NDII, NDWI, MCARI, MRENDVI, MRESR, REPI, NDVI | -40.17 | 0.42 | NA | NA | NA |
| | WR | NDII, WBI, MRENDVI, REPI | -105.32 | 0.94*** | 5 | 0.02565 | 0.96*** |
| | $Chl_{a+b}$ | NDII, NDWI | 116.11 | 0.88*** | 2 | 45.35 | 0.89*** |
| | LMA | NDII, NDWI, WBI, MCARI, MRESR, RENDVI, VREI, NDVI | 96.05 | 0.88*** | 8 | 26.02 | 0.94*** |
| | PVS | MCARI, MRENDVI, MRESR | 68.19 | 0.75*** | 3 | 9.202 | 0.79*** |
| | $K_S$ | MSI, NDII, NDWI, MCARI, MRENDVI, RENDVI, REPI, VREI, NDVI | -123.05 | 0.95*** | 7 | 0.017 | 0.95*** |
| | $\ln(A_S{:}A_L)$ | MSI, NDII, MCARI, RENDVI, REPI, VREI, NDVI | -11.33 | 0.63* | 7 | 0.7954 | 0.72*** |
| | $\ln(K_L)$ | NDII, NDWI, MRESR, RENDVI | -11.05 | 0.43* | 4 | 0.8285 | 0.56*** |

Table 4.5: Pooled data SVI combinations generated by stepwise multiple regressions and used in principle components regression to model ecophysiological response variables. Asterisks associated with *adj* $R^2$ indicate significance as: * 0.05-0.01, **0.01-0.001, *** < 0.001.

| | | | Multiple Regression | | Principal Components Regression | | |
|---|---|---|---|---|---|---|---|
| Species | Response Variable | SVI suite | *adj.* AIC | *adj.* $R^2$ | *Components* | *RMSEP* | *adj.* $R^2$ |
| Piñon | | | | | | | |
| | $\Psi_{PD}$ | WBI, MCARI | -42.87 | 0.64*** | 2 | 0.4529 | 0.66*** |
| | $\Psi_{MD}$ | NDVI, MSI, MCARI | -36.08 | 0.74*** | 3 | 0.5032 | 0.76*** |
| | $\Delta\Psi$ | REPI, VREI, MRENDVI, MSI | -77.13 | 0.61*** | 4 | 0.2574 | 0.66*** |
| | WR | WBI, NDVI, MSI, MCARI | -125.89 | 0.77*** | 4 | 0.1086 | 0.80*** |
| | $Chl_{a+b}$ | MSI, NDWI, MRENDVI, RENDVI, REPI | 259.2 | 0.79*** | 5 | 64.60 | 0.82*** |
| | LMA | MSI, NDII, WBI, MRENDVI, RENDVI | 256.81 | 0.71*** | 5 | 65.91 | 0.75** |
| | PVS | VREI, REPI | 162.69 | 0.51*** | 2 | 14.12 | 0.53*** |
| | $K_S$ | VREI | -180.75 | 0.46*** | NA | NA | NA |
| | $\ln(A_S{:}A_L)$ | MSI, NDWI, REPI | -37.17 | 0.53*** | 3 | 0.4987 | 0.57*** |
| | $\ln(K_L)$ | MSI, NDII, NDWI, WBI, RENDVI | -21.2 | 0.33* | 2 | 0.5649 | 0.43*** |

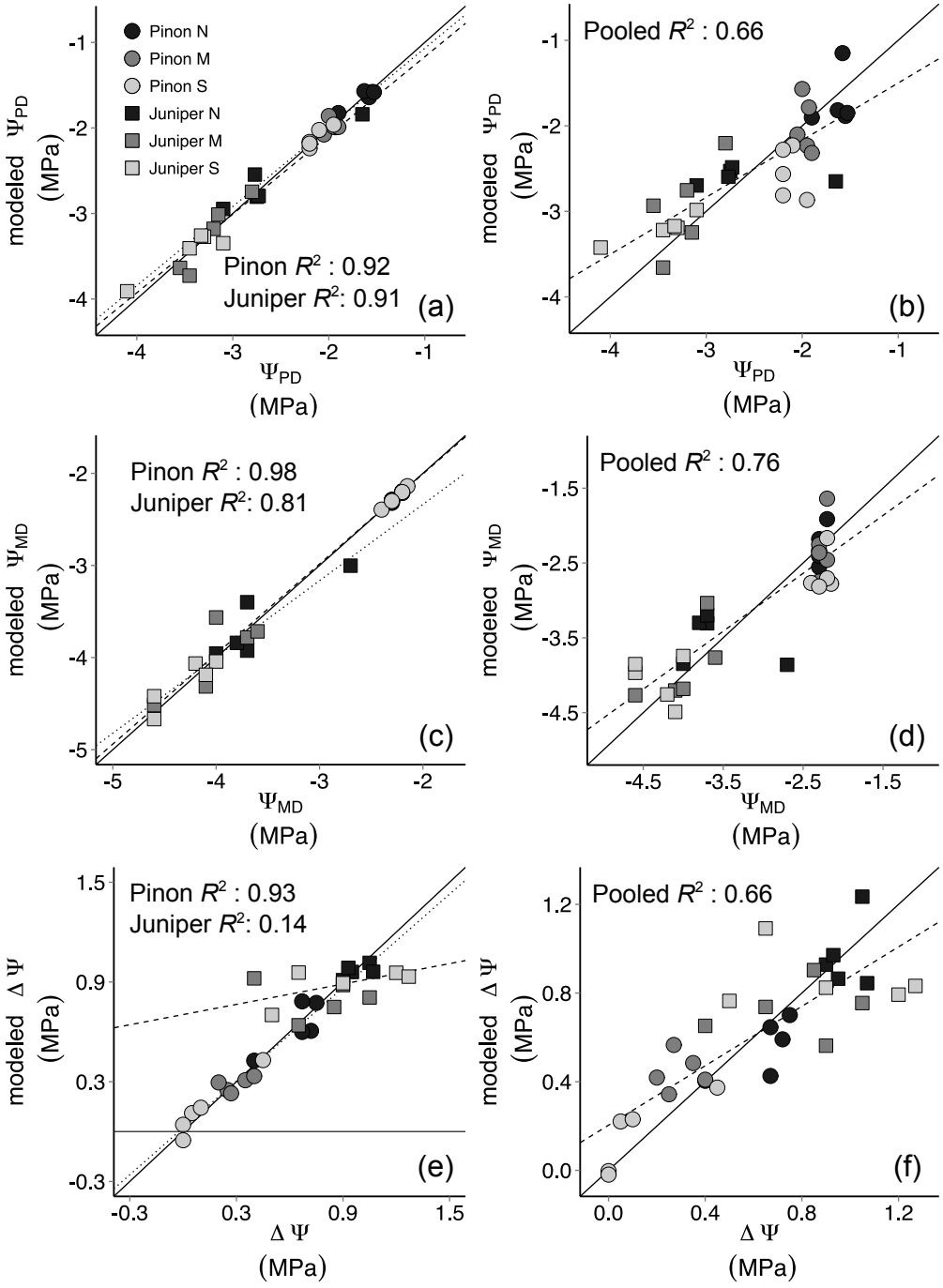


Figure 4.5: One to one plots of measured and SVI-predicted water potentials for species-specific (a, c, e) and pooled data (b, d, f) models. The 1:1 line in each plot is represented by the solid diagonal line. In (a, c, e), piñon fits are indicated by the dotted line, and juniper fits are indicated by the dashed line. In (b, d, f), pooled data model fits are indicated by the dashed line.

status, explaining > 80% of the variation in direct measurements of $\Psi_{PD}$ and $\Psi_{MD}$, and with slopes not different to one ($p \leq 0.1$) However, no model could successfully predict juniper $\Delta\Psi$ (best fit multiple regression $p = 0.09$).

The less successful modeling attempts to predict piñon $\Psi_{MD}$ (most SVIs needed) and juniper $\Delta\Psi$ (no successful model) arise as a consequence of specific stomatal regulation strategies. Isohydric piñon typically exhibit $\Psi_{MD}$ ~ -2.2 to -2.5 MPa, regardless of plant water status (Breshears *et al*. 2005, Plaut *et al*. 2012, Limousin *et al*. 2013, Pangle *et al*. 2015, Hudson *et al*. in review, Hudson *et al*. forthcoming). In contrast, anisohydric juniper permits leaf $\Psi_W$ to track soil $\Psi_W$, maintaining a positive $\Delta\Psi$ of ~ 1 MPa to drive transpiration, across a broad spectrum of soil moisture conditions (Hudson *et al*. in review.) Hence, a highly parameterized model (10 SVIs rendered into 9 components) for piñon, and no successful model for juniper, resulted from attempting to model physiological traits that do not have significant variability with spectral signals that contained significant variability.

Differences in stomatal regulation strategy confounded model success when species data were pooled (Fig. 4.5b, d, & f). Pooled data models required new SVI combinations (Table 4.5), and reduced the ability of models to successfully predict water status. All models captured significant variation in direct measurements of plant water status (66-75%). However, all regression slopes between measured and modeled values were less than one ($p \leq 0.008$). Thus predicted values were correlated with, but did not accurately predict, direct measurements. In particular, $\Psi_W$ tended to be overestimated (i.e., predicted to be more severe) for piñon, and underestimated for juniper, probably

because piñon exhibited a more narrow range in $\Psi_W$ than juniper, but both species shared broad overlap in values of NBGs selected by the modeling process.

*4.3.5 Utility of SVIs to predict ecomorphic traits*

As with plant water status, species-specific SVI models captured most of the variance in direct measurements of foliar water content, chlorophyll content and leaf structural carbon investment (Fig. 4.6a, c, & e). Models of ecomorphic traits were among the most complex produced, but as a group, returned the highest coefficients of determination (i.e., $R^2 > 0.89$). None of the slopes of the relationships between measured and modeled ecomorphic traits deviated significantly from one ($p > 0.25$). Foliar water content models performed quite well for both species, with > 95% variation captured by modeled WR. Piñon and juniper WR models required both CWC and NBG SVIs, though piñon relied more on NBGs than did juniper. Foliar chlorophyll content models captured ~90% of variation in measured $Chl_{a+b}$. Though the piñon model slightly outperformed the juniper model, the juniper model required fewer SVIs. Interestingly, juniper chlorophyll content was best predicted by water indices, and did not use any measure of greenness. Models of leaf mass per area performed similarly for each species, with modeled LMA capturing 94% of the variation in measured LMA.

Pooling the data resulted in reductions in both model complexity and performance (Table 4.4, Fig. 4.6b, d, & f). Models of ecomorphic traits still performed well (modeled vs. measured $R^2_{adj.} \geq 0.75$), but slopes of relationships between modeled and measured traits were all less than one ($p \leq 0.014$). SVI-based trait estimates from pooled data models were not accurate predictions of ecomorphic traits, possibly because piñon and juniper had similar NBG signatures, but fundamental differences in foliar structure and

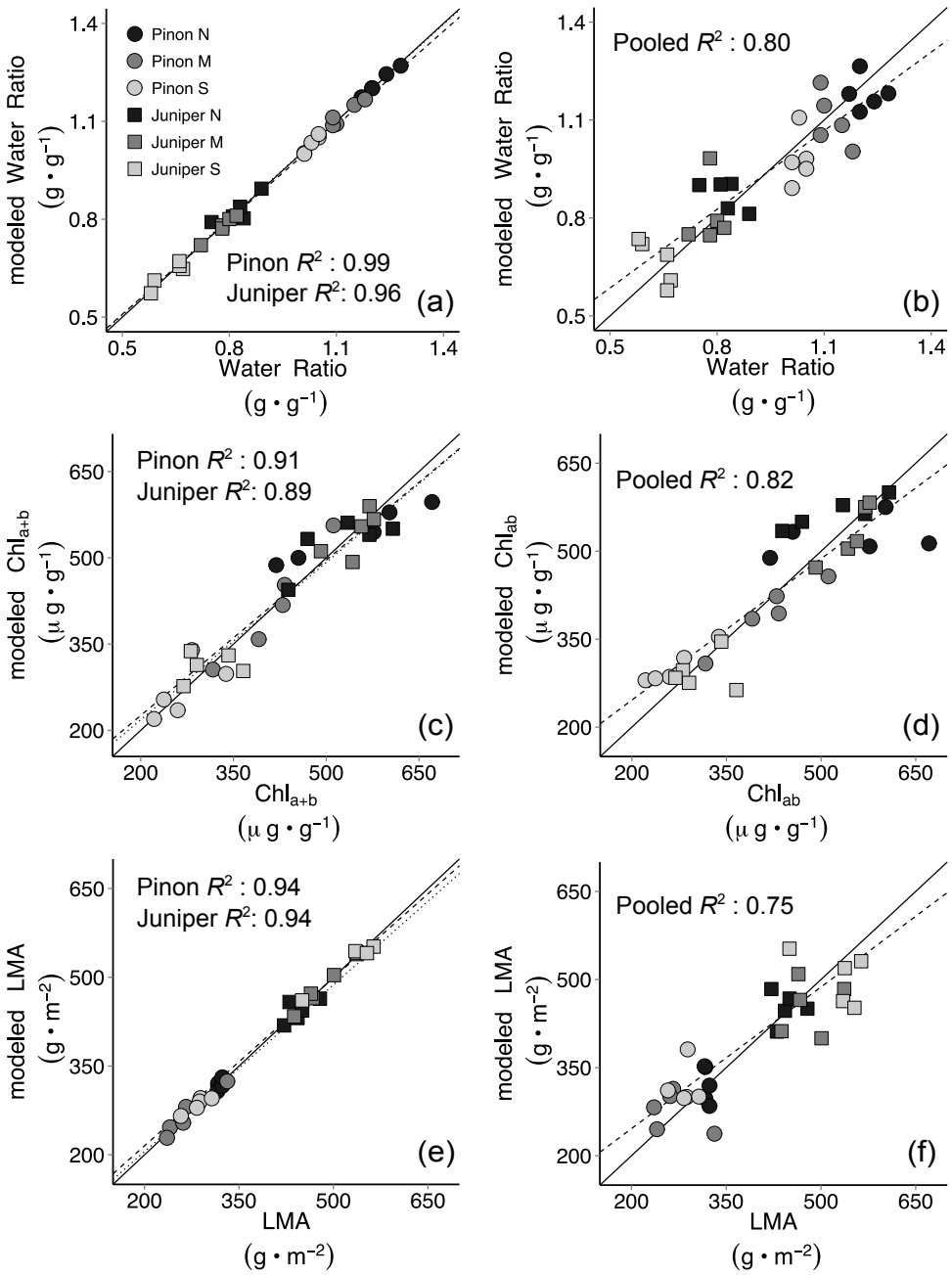


Figure 4.6: One to one plots of measured and SVI-predicted water ratio, chlorophyll content, and leaf mass per area for species-specific (a, c, e) and pooled data (b, d, f) models. The 1:1 line in each plot is represented by the solid diagonal line. In (a, c, e), piñon fits are indicated by the dotted line, and juniper fits are indicated by the dashed line. In (b, d, f), pooled data model fits are indicated by the dashed line.

arrangement. This is illustrated by the reversal of species over/underestimation patterns in the pooled WR and LMA models, while the $Chl_{a+b}$ model showed no species bias.

*4.3.6 Utility of SVIs to predict shoot hydraulic function*

SVIs were not as robust predictors of hydraulic function, when compared to foliar water status and ecomorphic traits (Fig. 4.7 a, b, c, & d). Yet SVI models accurately predicted PVS for both piñon and juniper, with high fidelity to measured values (slopes of modeled vs. measured PVS did not deviate from 1, $p \geq 0.1$). Best-fit PVS models were similarly complex; each required three SVIs and three PCR components. The piñon model depended more on CWC than NBG indices, and the juniper model relied solely on NBG indices. Piñon $K_S$ correlated with NDWI ($R^2_{adj.} = 0.69$, $p < 0.0001$); no combination of SVIs explained more variance in $K_S$. Juniper $K_S$ required greater model complexity, and depended upon a majority of spectral indices (9 of 11 SVIs). PCR reduced the nine SVIs into seven components, which produced modeled $K_S$ values that captured 95% of the variation in measured $K_S$. Natural log transformations rendered $A_S$:$A_L$ and $K_L$ more tractable for species-specific modeling. SVI models successfully replicated measured ln($A_S$:$A_L$) for both species. The juniper model required more indices than piñon (seven compared to two), but predicted ln($A_S$:$A_L$) more accurately. While juniper used NBGs and CWCs, piñon used only NBGs. Shoot hydraulic supply was the only physiological response variable not accurately reproduced for at least one species by SVI-based models. Similarity in measured $K_L$ between species and across foliar status categories may explain the similarity in species-specific model function. Piñon ln($K_L$) approximation relied more on spectral signals of greenness, while juniper ln($K_L$) depended equally upon greenness and water content.

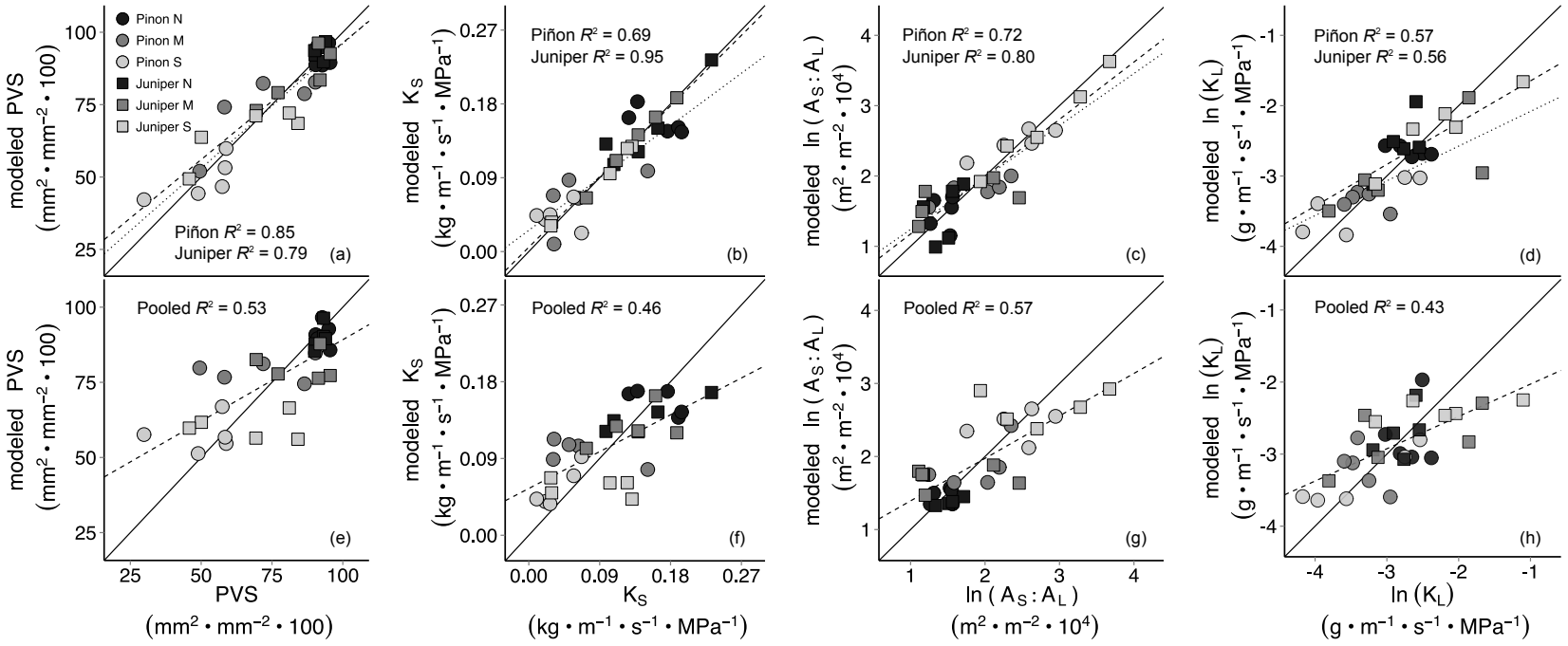


Figure 4.7: One to one plots of measured and SVI-predicted percent viable sapwood, sapwood-specific conductivity, sapwood area to leaf area ratio, and leaf-specific conductivity for species-specific (a, b, c, d) and pooled data (e, f, g, h) models. The 1:1 line in each plot is represented by the solid diagonal line. In (a, b, c, d), piñon fits are indicated by the dotted line, and juniper fits are indicated by the dashed line. In (e, f, g, h), pooled data models fit are indicated by the dashed line.

Pooled species models performed less well compared to species-specific model counterparts for all hydraulic traits (Fig. 4.7 e, f, g, & h). Slopes of regressions between modeled and measured traits were all less than one ($p < 0.0001$ in all cases). $K_S$ was the only instance of a pooled data response variable that was best predicted by a single SVI, in this case, VREI ($R^2_{adj.} = 0.46$, $p < 0.0001$). Predictions of hydraulic transport ($K_S$ and $K_L$) were the least successful in capturing the variation in direct measurements ($\leq 46\%$).

## 4.4 Discussion

At the time of writing, this study is the first to demonstrate the utility of spectral data to estimate shoot hydraulic function in conifers, and support our hypothesis that the intimate relationship between xylem hydraulic supply and leaf water status should be quantifiable by spectral signals. Even though *a priori* foliar stress categories were not universally supported by either spectral or ecophysiological metrics (Fig. 4.3 & 4.4), we were able to investigate plant function over a broad continuum of foliar health and xylem integrity (Fig. 4.1, Fig. 4.8). We found strong correlations between spectral signals and direct measurements of plant water status (Fig. 5), foliar hydration and structure (Fig. 4.6), and stem hydraulic transport and xylem functional status (Fig. 4.7, Fig. 4.8).

Our research extends upon previous work that relied on simple linear regressions to estimate aspects of plant water content or water potential in conifers using SVIs (Hunt and Rock 1989, Stimson *et al*. 2005). The attraction of this method lies in the ease of application, as standard SVIs were used with simple linear equations to predict plant status (Clevers *et al*. 2008). However, differences in foliar structure were cited as impediments to the predictive ability of single SVIs (Stimson *et al.* 2005, Ustin and

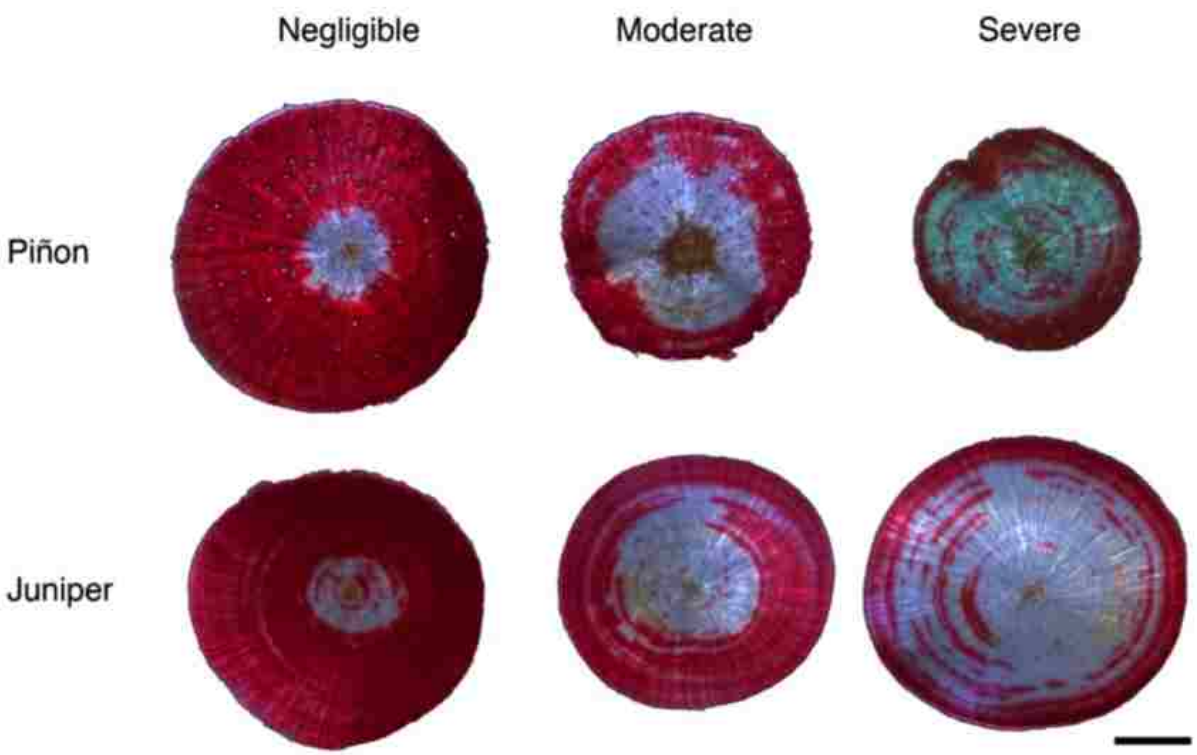


Figure 4.8: Representative xylem cross sections from each species/status combination. Red staining indicates functional sapwood. All sections were imaged at 15x, scale bar is 1 mm.

Gamon 2010, Musavi *et al*. 2015). Our observation that pooled data models always preformed less well than species-specific models support this conclusion. Species-specific models generated in this study required higher dimensionality, but resulted in an enhanced ability to accurately predict critical aspects of plant water status and hydraulic function (Fig. 4.5, Fig. 4.6, Fig. 4.7). This approach also allowed the development of models suitable to move beyond predictions of leaf water content to predictions of xylem hydraulic transport efficiency and integrity (Fig. 4.7, Fig. 4.8).

PJ represents an ecosystem wherein the dominant species are reduced to a single PFT (needleleaf evergreen trees) in DVGMs, but the differences in stomatal behavior, foliar structure, and hydraulic function between piñon and juniper lead to a variety of predicted regional vegetation outcomes for different climate scenarios (McDowell *et al*. 2015). The regional models used to predict PJ mortality in McDowell *et al*. (2015) depended on $\Psi_{PD}$ as a driver of survival or mortality, which our study indicates can be accurately estimated using remote sensing data for both piñon and juniper. Our results suggest that hyperspectral sampling coupled with sub-canopy resolution may be leveraged to assess plant water status on broad spatial scales that are currently impractical to measure by tradition means (i.e., pressure chamber or psychrometer).

Differences in stomatal regulation behavior determine the degree of connectivity with soil moisture pools; species-specific signals should therefore provide nuanced information to contextualize drought stress. Juniper permits gas exchange through stomata over a broad span of soil water potential (Limousin *et al*. 2013), and juniper spectral signals provided insight to soil moisture availability and drought severity (Fig. 4.4a, Fig. 4.5a). Anisohydric behavior may also explain why juniper chlorophyll content

was best predicted by CWC indices, because chlorophyll content has been shown to be tightly coupled with foliar hydration (Filella and Peñuelas 1994, Carter and Knapp 2001). Piñon hydraulically isolates from dry soils and prevents water loss by strict stomatal closure (Pangle *et al*. 2015), so shifts in piñon spectral indices indicative of drought stress may provide context for drought duration, though more work needs to be done to quantify this relationship. The fact that CWC indices consistently distinguished piñon and juniper at the extremes of our foliar health continuum suggests that these two species may function as different 'optical types' in periods of low and high drought intensity, and can be potentially separated at coarser sampling scales (Fig. 4.3a, b, c & d; Ustin and Gamon 2010). Future work needs to focus on how spectral responses change with respect to seasonality and phenology, to determine the consistency of spectral signals to accurately predict water status and hydraulic function over time in PJ.

Perhaps more immediately relevant to concerns of future forest mortality, this study has identified spectral indices that best recognize piñon exhibiting physiological function and foliar status indicative of trees with high insect-related mortality risk. By design, our sampling effort included piñon that are part of an ongoing experiment investigating physiological responses to chronic drought stress (annual precipitation reduced by ~45%) combined with exclusion of lethal biotic agents (bark beetles, *Ips confusus* (Leconte)) (Hudson *et al*. forthcoming). These trees, which comprised the majority of the piñon severe stress group, have demonstrated physiological function similar to piñon in a related drought experiment than were attacked and killed by bark beetles (chronically low $\Psi_{PD}$ and near zero stem sap-flow for more than seven months, Plaut *et al*. 2012). NBG indices related to red edge position (REPI, MRESR, MRENDVI,

RENDVI and VREI) successfully identified and isolated severe stress group piñon (Fig. 4.3). Though shifts in red edge dependent SVIs have been shown to be of use in the initial detection of stress (Eitel *et al*. 2011, Krofcheck *et al*. 2016), other studies have found red edge position to be indicative of foliar water content only after significant loss in foliar water content (Filella and Peñuelas 1994). Our findings are consistent with the latter observation, as red edge dependent SVIs functioned well in delineating differences in foliar stress that developed over years of experimental drought. Our findings indicate that these particular indices have the best ability to diagnose piñon canopies facing high risk of bark beetle attack. The stochastic nature of bark beetle population dynamics limits our ability to predict the location of future outbreaks (Raffa *et al*. 2008). For example, most New Mexico piñon mortality in the 1999-2003 drought occurred in the northern portion of the state (Clifford *et al.* 2008), while southern populations experienced greater mortality in the 2010-2013 drought, even though drought conditions were pervasive statewide over these two time periods (USDA 2015). Our results suggest that it is possible to identify the location and extent of piñon populations with significantly exacerbated risk of beetle attack on the basis of spectral signals of water stress, particularly those related to red edge position. We also note that red edge dependent SVIs isolated severe stress juniper as well, and should serve equally well in to identify juniper canopies experiencing significant water stress (Carter 1993, Filella and Peñuelas 1994, Gitelson and Merzlyak 1997). Our findings suggest it will be possible for future research to monitor plant hydraulic function under drought progression, and associated mortality, with respect to site-specific microclimate, aspect, and edaphic contexts.

We recognize that our method of hyperspectral high-resolution sampling of foliar

tissue by leaf clip represents the optimal scenario for collecting plant spectral data to relate to hydraulic function, as this method avoided influence from background soil, sub-canopy vegetation, woody material, and canopy complexity. However, we have shown that spectral signals contain information that allows accurate predictions of plant water potential and hydraulic transport. Efforts to correlate reflectance data from aerial platforms with ground-based measurements of plant hydraulics are now necessary to demonstrate the feasibility of scaling our method to airborne sampling of plant water status and hydraulic function.

## 4.5 Conclusions

Our study is the first to demonstrate the utility of spectral data to accurately predict hydraulic function in trees. This work builds on efforts that demonstrated correlations between individual spectral indices and plant water status by taking advantage of 1) more information contained in spectral signals and 2) increased model dimensions available through PCR. We have shown that species-specific SVI combinations can be leveraged to estimate several key plant physiological traits necessary for assessing forest health, and valuable for dynamic vegetation modeling efforts. In addition, we have identified SVIs suitable for assessing insect-related mortality risk for piñon. Remote sensing has advantages over direct measurements in terms of rapidity of data collection and increased spatial scale, and our results indicate the potential for rapid and large-scale collection of data capable of characterizing multiple aspects of plant hydraulic function, as well as assessing forests for mortality risk.

We acknowledge that our study has limitations. First, we derived our SVIs from high-resolution hyperspectral data that required expensive tools to collect, and that are not available from all satellite platforms. Second, we collected data is such a way as to eliminate the influence of background reflectance from soil and understory vegetation-though several of the indices used were designed to ameliorate such unwanted signal interference. In addition, we note that fundamental differences in foliar structure limited the ability of our SVI-based models to accurately predict plant water status and hydraulic function when species data were pooled. Thus, we caution that sub-canopy imaging resolution and accurate species classifications are necessary for optimal model success. However, we remain optimistic that this study will inspire further research into the use of remote sensing data for broad-scale investigations of plant water status and hydraulics.

# Chapter 5

## Summary

The predicted shift to increased drought severity and frequency (Seager *et al*. 2007, Williams *et al*. 2010), combined with high sensitivity to drought stress (Breshears *et al*. 2005) presents a grim future for piñon-juniper woodlands in their current extent (Williams *et al*. 2013, McDowell *et al.* 2015). To better understand mature tree responses to climate change, I engaged in multiple-year measurements of plant hydraulic function and structure in piñon and juniper subjected to prolonged precipitation manipulation. My dissertation investigated the variation in piñon and juniper responses to chronic abiotic forcing with respect to acclimative potential of xylem hydraulic structure and function (Chapter 1), piñon-specific drought responses in the absence of lethal biotic agents (Chapter 2), and the utility of remote sensing to infer plant hydraulic performance, and collect data relevant to species-specific modeling efforts (Chapter 3).

In Chapter 1, we assessed the potential of piñon and juniper to acclimate aspects of hydraulic architecture in response to altered precipitation regimes. We repeatedly measured plant water status ($\Psi_W$) in conjunction with hydraulic transport efficiency at the tissue ($K_S$) and shoot ($K_L$) level on target trees in a long-term precipitation manipulation experiment over a period of five years. We also investigated vulnerability to embolism and earlywood tracheid anatomy, to characterize transport safety and capacity. Supplemental watering elevated plant water status ($\Psi_{PD}$), xylem transport efficiency ($K_S$), and shoot level hydraulic supply ($K_L$) relative to experimental drought. However, the key findings of this work were that neither piñon, nor juniper, demonstrated acclimation by

altering xylem transport efficiency ($K_S$), safety ($P_e$, $P_{50}$, $P_{max}$), or anatomy ($D_H$, $T_W$, $(T_W/D)^2$), and thus acclimation of xylem transport efficiency and safety in mature trees will likely not contribute to the responses of widespread coniferous biomes, such as pinon-juniper woodland, to climate change.

In Chapter 2, we used repeated measures of plant water status, sap-flow, hydraulic transport efficiency and leaf-level gas exchange to monitor the hydraulic responses of piñon to drought onset and persistence over 6 years, in the absence of lethal insect activity. Our experimental target trees demonstrated water statuses and hydraulic functions identical to piñon that died in the original precipitation manipulation experiment (i.e., $\Psi_{PD} < -2.2$ MPa, $J_S < 5$ g•m$^{-2}$•s$^{-1}$, Plaut et al. 2012). Pesticide treatment prevented bark beetle activity in our experimental plots, even when bark beetle populations erupted in 2013, and local piñon mortality spiked. As in Chapter 1, experimental drought did not stimulate acclimation in hydraulic transport capacity or safety. Our findings show that piñon does not succumb to carbon starvation or hydraulic failure after 6+ years of severely restricted precipitation. Extremely low $\Psi_{PD}$ and $\Psi_{MD}$ observed during the height of the overarching natural drought in 2011 predicted an increased risk of hydraulic failure, and reduced respiration under experimental drought may indicate declines in non-structural carbohydrate stores that signal the initial stages of a mortality sequence, but to date, all pesticide-treated piñon have survived severe and chronic drought stress. Our results also highlight the importance of insects as mortality agents, and the need for climate models to incorporate insect/host dynamics to improve mortality forecasting accuracy.

In Chapter 3 we investigated the utility of hyperspectral remote sensing to estimate foliar water content, shoot water potential, and subtending branch xylem hydraulic function. Previous work had shown simple linear correlations between commonly used spectral indices (NDVI, NDWI) and foliar water content and water potential in piñon and juniper (Stimson et al. 2005). We demonstrated that species-specific models based on SVI combinations determined by hierarchical model selection and principal components regressions significantly increased the predictive ability of remote sensing data to estimate direct measurements of plant water status, foliar hydration and structural carbon investment, and stem hydraulic transport and xylem functional status. This study represents the first attempt to leverage remotely sensed data to investigate xylem hydraulic transport efficiency and functional status. In addition, we found that spectral indices based on red edge position (MRENDVI, RENDVI, MRESR, REPI and VREI) consistently identified piñon canopies at elevated risk of bark beetle attack. This work enhances our ability to detect 1) the spatial extent of water stress and correlated xylem function and status, and 2) the location and extent of piñon populations with significantly exacerbated risk of beetle attack.

The body of work that comprises this dissertation contributes to our understanding of how mature trees in piñon-juniper woodland respond to abiotic forcing, and how these responses can be assessed quickly, at large scale, and with non-destructive techniques. The combination of multiple years of in-situ measurements of plant hydraulic function, and validation of models of plant hydraulic function based on remote sensing data, provides detailed species-specific data necessary for improving vegetation modeling efforts, as well as a novel approach for using remote sensing to expand the scale over

which such data can be feasibly collected.

## References

Adams, H. D., Germino, M. J., Breshears, D. D., Barron-Gafford, G. A., Guardiola-Claramonte, M., Zou, C. B., & Huxman, T. E. (2013). Nonstructural leaf carbohydrate dynamics of Pinus edulisduring drought-induced tree mortality reveal role for carbon metabolism in mortality mechanism. *New Phytologist*, *197*(4), 1142–1151.

Alchanatis, V., & Cohen, Y. (2012). Spectral and spatial methods of hyperspectral image analysis for estimation of biophysical and biochemical properties of agricultural crops. In P.S. Thenkabail, J.G. Lyon, & A. Huete (Eds.) *Hyperspectral Remote Sensing of Vegetation* (289-308). Boca Raton, FL: CRC Press.

Alder, N. N., Sperry, J. S., & Pockman, W. T. (1996). Root and stem xylem embolism, stomatal conductance, and leaf turgor in *Acer grandidentatum* populations along a soil moisture gradient. *Oecologia*, *105*(3), 293–301.

Allen, C., Macalady, A., Chenchouni, H., Bachelet, D., McDowell, N. G., Vennetier, M., et al. (2010). A global overview of drought and heat-induced tree mortality reveals emerging climate change risks for forests. *Forest Ecology and Management*, *259*, 660–684.

Allen, C. D., Breshears, D. D., & McDowell, N. G. (2015). On underestimation of global vulnerability to tree mortality and forest die-off from hotter drought in the Anthropocene. *Ecosphere*, *6*(8), 1–55.

Anderegg, W. R. L. (2012). Complex aspen forest carbon and root dynamics during drought. *Climatic Change*, *111*(3-4), 983–991.

Anderegg, W. R. L., Flint, A., Huang, C.-Y., Flint, L., Berry, J. A., Davis, F. W., et al. (2015). Tree mortality predicted from drought-induced vascular damage. *Nature Geoscience*, *8*(5), 367–371.

Anderson-Teixeira, K. J., Delong, J. P., Fox, A. M., Brese, D. A., & Litvak, M. E. (2011). Differential responses of production and respiration to temperature and moisture drive the carbon balance across a climatic gradient in New Mexico. *Global Change Biology*, *17*, 410–424.

Awad, H., Barigah, T., Badel, E., Cochard, H., & Herbette, S. (2010). Poplar vulnerability to xylem cavitation acclimates to drier soil conditions. *Physiologia Plantarum*, *139*, 280–288. http://doi.org/10.1111/j.1399-3054.2010.01367.x

Barnard, D. M., Meinzer, F. C., Lachenbruch, B., McCulloh, K. A., Johnson, D. M., & Woodruff, D. R. (2011). Climate-related trends in sapwood biophysical properties in two conifers: avoidance of hydraulic dysfunction through coordinated adjustments in xylem efficiency, safety and capacitance. *Plant, Cell & Environment*, *34*(4), 643–654.

Bates, D., & Maechler, M. (2010) Package ‘lme4.’ hhttp://lme4. r-forge.r-project.org/i

Bauch, J., Liese, W., & Schultze, R. (1972). The morphological variability of the bordered pit membranes in gymnosperms. *Wood Science and Technology*, *6*(3), 165–184.

Beikircher, B., & Mayr, S. (2009). Intraspecific differences in drought tolerance and acclimation in hydraulics of *Ligustrum vulgare* and *Viburnum lantana*. *Tree Physiology*, *29*(6), 765–775. http://doi.org/10.1093/treephys/tpp018

Bentz, B. J., Regnière, J., Fettig, C. J., Hansen, E. M., Hayes, J. L., Hicke, J. A., et al. (2010). Climate Change and Bark Beetles of the Western United States and Canada: Direct and Indirect Effects. *Bioscience*, *60*(8), 602–613.

Bentz, B., Logan, J., MacMahon, J., Allen, C. D., Ayres, M., Berg, E., et al. (2013). Bark Beetle Outbreaks in Western North America:, 1–46.

Biederman, J. A., Scott, R. L., Goulden, M. L., Vargas, R., Litvak, M. E., Kolb, T. E., et al. (2016). Terrestrial carbon balance in a drier world: the effects of water availability in southwestern North America. *Global Change Biology*, *22*(5), 1867–1879.

Bonan, G. B. (2008). Forests and climate change: forcings, feedbacks, and the climate benefits of forests. *Science*, *320*(5882), 1444–1449.

Borchert, R., & Pockman, W. T. (2005). Water storage capacitance and xylem tension in isolated branches of temperate and tropical trees. *Tree Physiology*.

Bouche, P. S., Larter, M., Domec, J. C., Burlett, R., Gasson, P., Jansen, S., & Delzon, S. (2014). A broad survey of hydraulic and mechanical safety in the xylem of conifers. *Journal of Experimental Botany*, *65*(15), 4419–4431.

Breshears, D. D., Cobb, N. S., Rich, P. M., Price, K. P., Allen, C. D., Balice, R. G., et al. (2005). Regional vegetation die-off in response to global-change-type drought. *Proceedings of the National Academy of Sciences of the United States of America*, *102*(42), 15144–15148.

Breshears, D. D., Myers, O. B., Meyer, C. W., Barnes, F. J., Zou, C. B., Allen, C. D., et al. (2009). Tree die-off in response to global change-type drought: mortality insights from a decade of plant water potential measurements. *Frontiers in Ecology and the Environment*, *7*(4), 185–189.

Brodribb, T., & Feild, T. S. (2000). Stem hydraulic supply is linked to leaf photosynthetic capacity: evidence from New Caledonian and Tasmanian rainforests. *Plant, Cell & Environment*, *23*, 1381–1388.

Brodribb, T. J. (2009). Xylem hydraulic physiology: The functional backbone of terrestrial plant productivity. *Plant Science*, *177*(4), 245–251.

Brodribb, T. J., & McAdam, S. A. M. (2013). Abscisic Acid Mediates a Divergence in the Drought Response of Two Conifers. *Plant Physiology*, *162*, 1370–1377.

Bryukhanova, M., & Fonti, P. (2012). Xylem plasticity allows rapid hydraulic adjustment to annual climatic variability. *Trees*, *27*(3), 485–496.

Bucci, S. J., Goldstein, G., Meinzer, F. C., Scholz, F. G., Franco, A. C., & Bustamante, M. (2004). Functional convergence in hydraulic architecture and water relations of tropical savanna trees: from leaf to whole plant. *Tree Physiology*, *24*(8), 891–899.

Carter, G. A. (1993). Responses of Lea Spectral Reflectance to Plant Stress. *American Journal of Botany*, *80*, 239–243.

Carter, G. A., & Knapp, A. K. (2001). Leaf optical properties in higher plants: linking spectral characteristics to stress and chlorophyll concentration. *American Journal of Botany*, *88*(4), 677–684.

Clevers, J. G. P. W., Kooistra, L., & Schaepman, M. E. (2008). Using spectral information from the NIR water absorption features for the retrieval of canopy water content. *International Journal of Applied Earth Observation and Geoinformation*, *10*(3), 388–397.

Chansler, J. F. (1966). Cold Hardiness of Two Species of Ips Beetles. *Journal of Forestry*, *64*(9), 622–624.

Choat, B., Jansen, S., Brodribb, T. J., Cochard, H., Delzon, S., Bhaskar, R., et al. (2012). Global convergence in the vulnerability of forests to drought. *Nature*, *491*, 752–756.

Clifford, M. J., Rocca, M. E., Delph, R., Ford, P. L., & Cobb, N. S. (2008). Drought induced tree mortality and ensuing bark beetle outbreaks in southwestern pinyon-juniper woodlands. *Proceeding RMRS*, 1–13.

Clifford, M. J., Royer, P. D., Cobb, N. S., Breshears, D. D., & Ford, P. L. (2013). Precipitation thresholds and drought-induced tree die-off: insights from patterns of *Pinus edulis* mortality along an environmental stress gradient. *New Phytologist*, 413–421.

Cochard, H., Hölttä, T., Herbette, S., Delzon, S., & Mencuccini, M. (2009). New insights into the mechanisms of water-stress-induced cavitation in conifers. *Plant Physiology*, *151*(2), 949–954.

Cochard, H., & Delzon, S. (2013). Hydraulic failure and repair are not routine in trees. *Annals of Forest Science*, *70*, 659–661.

Corcuera, L., Cochard, H., Gil-Pelegrin, E., & Notivol, E. (2011). Phenotypic plasticity in mesic populations of *Pinus pinaster* improves resistance to xylem embolism (P50) under

severe drought. *Trees*, *25*(6), 1033–1042.

Dickman, L. T., McDowell, N. G., Sevanto, S., Pangle, R. E., & Pockman, W. T. (2015) Carbohydrate dynamics and mortality in a piñon-juniper woodland under three future precipitation scenarios. *Plant, Cell & Environment*, *38*(4), 729-739.

Dixon, M.A., Grace, J., & Tyree M.T. (1984) Concurrent measurements of stem density, leaf water potential and cavitation on a shoot of *Thuja occidentalis* L. *Plant, Cell and Environment* 7,615–618.

Domec, J. C., & Gartner, B. L. (2001). Cavitation and water storage capacity in bole xylem segments of mature and young Douglas-fir trees. *Trees*, *15*(4), 204–214.

Domec, J. C., & Gartner, B. L. (2002). How do water transport and water storage differ in coniferous earlywood and latewood? *Journal of Experimental Botany*, *53*(379), 2369–2379.

Domec, J. C., & Johnson, D. M. (2012). Does homeostasis or disturbance of homeostasis in minimum leaf water potential explain the isohydric versus anisohydric behavior of Vitis vinifera L. cultivars? *Tree Physiology*, *32*(3), 245–248.

Dukes, J. S., Pontius, J., Orwig, D., Garnas, J. R., Rodgers, V. L., Brazee, N., et al. (2009). Responses of insect pests, pathogens, and invasive plant species to climate change in the forests of northeastern North America: What can we predict? This article is one of a selection of papers from NE Forests 2100: A Synthesis of Climate Change Impacts on Forests of the Northeastern US and Eastern Canada. *Canadian Journal of Forest Research*, *39*(2), 231–248.

Duursma, R. A. (2015). Plantecophys - An R Package for Analysing and Modelling Leaf Gas Exchange Data. *PLoS ONE*, *10*(11), e0143346. http://doi.org/10.1371/journal.pone.0143346.t001

Eilmann, B., Zweifel, R., Buchmann, N., Fonti, P., & Rigling, A. (2009). Drought-induced adaptation of the xylem in Scots pine and pubescent oak. *Tree Physiology*, *29*(8), 1011–1020.

Eitel, J. U. H., Vierling, L. A., Litvak, M. E., Long, D. S., Schulthess, U., Ager, A. A., et al. (2011). Remote Sensing of Environment. *Remote Sensing of Environment*, *115*(12), 3640–3646.

Feild, T. S., Hudson, P. J., Balun, L., Chatelet, D. S., Patino, A. A., Sharma, C. A., & McLaren, K. (2011). The ecophysiology of xylem hydraulic constraints by “basal” vessels in Canella winterana (Canellaceae). *International Journal of Plant Sciences*, *172*(7), 879–888.

Filella, I., & Peñuelas, J. (1994). The red edge position and shape as indicators of plant chlorophyll content, biomass and hydric status. *International Journal of Remote Sensing*, *15*(7), 1459–1470.

Fisher, R., McDowell, N. G., Purves, D., Moorcroft, P., Sitch, S., Cox, P., et al. (2010). Assessing uncertainties in a second-generation dynamic vegetation model caused by ecological scale limitations. *New Phytologist*, *187*(3), 666–681.

Floyd, M. L., Clifford, M., Cobb, N. S., & Hanna, D. (2009). Relationship of stand characteristics to drought-induced mortality in three Southwestern piñon–juniper woodlands. *Ecological Applications*, *19*(5), 1223–1230.

Franks, P. J., Drake, P. L., & Froend, R. H. (2007). Anisohydric but isohydrodynamic: seasonally constant plant water potential gradient explained by a stomatal control mechanism incorporating variable plant hydraulic conductance. *Plant, Cell & Environment*, *30*(1), 19–30.

Fonti, P., Heller, O., Cherubini, P., Rigling, A., & Arend, M. (2012). Wood anatomical responses of oak saplings exposed to air warming and soil drought. *Plant Biology*, *15*, 210–219.

Gao, B. C. (1996). NDWI A Normalized Difference Water Index for Remote Sensing of Vegetation Liquid Water From Space. *Remote Sensing of Environment*, *58*, 257–266.

Garcia-Forner, N., Adams, H. D., Sevanto, S., Collins, A. D., Dickman, L. T., Hudson, P. J., et al. (2016). Responses of two semiarid conifer tree species to reduced precipitation and warming reveal new perspectives for stomatal regulation. *Plant, Cell & Environment*, *39*(1), 38–49.

Gaylord, M. L., Kolb, T. E., Pockman, W. T., Plaut, J. A., Yepez, E. A., Macalady, A. K., et al. (2013). Drought predisposes piñon-juniper woodlands to insect attacks and mortality. *New Phytologist*, *198*(2), 567–578.

Gaylord, M. L., Kolb, T. E., & McDowell, N. G. (2015). Mechanisms of piñon pine mortality after severe drought: a retrospective study of mature trees. *Tree Physiology*, *35*(8), 806–816.

Gitelson, A. A., & Merzlyak, M. N. (1997). Remote estimation of chlorophyll content in higher plant leaves. *International Journal of Remote Sensing*, *18*(12), 2691–2697.

Gleason, S. M., Westoby, M., Jansen, S., Choat, B., Hacke, U. G., Pratt, R. B., et al. (2015). Weak tradeoff between xylem safety and xylem-specific hydraulic efficiency across the world's woody plant species. *New Phytologist*, *209*(1), 123–136.

Goulden, M. L., & Field, C. B. (1994). Three methods for monitoring the gas exchange of individual tree canopies: ventilated-chamber, sap-flow and Penman-Monteith

measurements on evergreen oaks. *Functional Ecology*, *8*, 125–135.

Granier, A. (1987). Evaluation of transpiration in a Douglas-fir stand by means of sap flow measurements. *Tree Physiology*, *3*, 309–320.

Grier, C. C., & Running, S. W. (2011). Leaf area of mature northwestern coniferous forests: Relation to site water balance. *Ecology*, *58*, 893–899.

Hacke, U. G., Sperry, J. S., Pockman, W. T., Davis, S. D., & McCulloh, K. A. (2001). Trends in wood density and structure are linked to prevention of xylem implosion by negative pressure. *Oecologia*, *126*(4), 457–461.

Hacke, U. G., Sperry, J. S., & Pittermann, J. (2004). Analysis of circular bordered pit function II. Gymnosperm tracheids with torus-margo pit membranes. *American Journal of Botany*, *91*(3), 386–400.

Hacke, U. G., & Jansen, S. (2009). Embolism resistance of three boreal conifer species varies with pit structure. *New Phytologist*, *182*(3), 675–686.

Herbette, S., Wortemann, R., Awad, H., Huc, R., Cochard, H., & Barigah, T. S. (2010). Insights into xylem vulnerability to cavitation in *Fagus sylvatica* L.: phenotypic and environmental sources of variability. *Tree Physiology*, *30*(11), 1448–1455.

Hicke, J. A., Logan, J. A., Powell, J., & Ojima, D. S. (2006). Changing temperatures influence suitability for modeled mountain pine beetle ( Dendroctonus ponderosae) outbreaks in the western United States. *Journal of Geophysical Research*, *111*(G2). http://doi.org/10.1029/2005JG000101

Hicke, J. A., Meddens, A. J. H., & Kolden, C. A. (2016). Recent Tree Mortality in the Western United States from Bark Beetles and Forest Fires. *Forest Science*, *62*(2), 141–153.

Hsiao, T. C., & Acevedo, E. (1974). Plant responses to water deficits, water-use efficiency, and drought resistance. *Agricultural Meteorology*, *14*, 59–84.

Hubbard, R., Ryan, M., & Stiller, V. (2001). Stomatal conductance and photosynthesis vary linearly with plant hydraulic conductance in ponderosa pine. *Plant, Cell & Environment*, *24*, 113–121.

Hudson, P. J., Razanatsoa, J., & Feild, T. S. (2009). Early vessel evolution and the diverisification of wood function: Insights from Malagasy Canellales. *American Journal of Botany*, *97*(1), 80–93.

Hudson, P. J., Limousin, J. -M., Krofcheck, D. J., Boutz, A. L., , Pangle, R. E., Gehres, N., McDowell, N. G., & Pockman, W. T. (in review). Impacts of long-term precipitation

manipulation on hydraulic architecture and xylem anatomy of piñon and juniper in Southwest USA.

Hudson, P. J., Boutz, A. L., Limousin, J. -M., Pangle, R. E., Gehres, N., McDowell, N. G., & Pockman, W. T. (in preparation). Drought responses of piñon pine protected from bark beetle attack: quantifying hydraulic adjustments driven by chronic abiotic stress.

Hunt, E. R., & Rock, B. N. (1989). Detection of changes in leaf water content using Near- and Middle-Infrared reflectances. *Remote Sensing of Environment*, *30*(1), 43–54.

Jackson, T. J., Chen, D., Cosh, M., Li, F., Anderson, M., Walthall, C., et al. (2004). Vegetation water content mapping using Landsat data derived normalized difference water index for corn and soybeans. *Remote Sensing of Environment*, *92*(4), 475–482.

Klein, T. (2014). The variability of stomatal sensitivity to leaf water potential across tree species indicates a continuum between isohydric and anisohydric behaviours. *Functional Ecology*, *28*(6), 1313–1320.

Klein, T., Di Matteo, G., Rotenberg, E., Cohen, S., & Yakir, D. (2013). Differential ecophysiological response of a major Mediterranean pine species across a climatic gradient. *Tree Physiology*, *33*(1), 26–36. http://doi.org/10.1093/treephys/tps116

Körner, C. (2015). ScienceDirectParadigm shift in plant growth control. *Current Opinion in Plant Biology*, *25*, 107–114.

Krofcheck, D. J., Eitel, J. U. H., Vierling, L. A., Schulthess, U., Hilton, T. M., Dettweiler-Robinson, E., et al. (2013). Detecting mortality induced structural and functional changes in a piñon-juniper woodland using Landsat and RapidEye time series. *Remote Sensing of Environment*, 1–12. http://doi.org/10.1016/j.rse.2013.11.009

Krofcheck, D., Eitel, J., Lippitt, C., Vierling, L., Schulthess, U., & Litvak, M. (2016). Remote sensing based simple models of GPP in both disturbed and undisturbed piñon-juniper woodlands in the Southwestern U.S. *Remote Sensing*, *8*(1), 20.

Ladjal, M., Huc, R., & Ducrey, M. (2005). Drought effects on hydraulic conductivity and xylem vulnerability to embolism in diverse species and provenances of Mediterranean cedars. *Tree Physiology*, *25*, 1109–1117.

Lajtha, K., & Barnes, F. J. (1991). Carbon gain and water use in pinyon pine-juniper woodlands of northern New Mexico: field versus phytotron chamber measurements. *Tree Physiology*, *9*, 59–67.

Lamy, J.-B., Bouffier, L., Burlett, R., Plomion, C., Cochard, H., & Delzon, S. (2011). Uniform selection as a primary force reducing population genetic differentiation of cavitation resistance across a species range. *PLoS ONE*, *6*(8), e23476.

http://doi.org/10.1371/journal.pone.0023476.s003

Lamy, J.-B., Delzon, S., Bouche, P. S., Alia, R., Vendramin, G. G., Cochard, H., & Plomion, C. (2013). Limited genetic variability and phenotypic plasticity detected for cavitation resistance in a Mediterranean pine. *New Phytologist*, *201*(3), 874–886.

Limousin, J. M., Bickford, C. P., Dickman, L. T., Pangle, R. E., Hudson, P. J., Boutz, A. L., et al. (2013). Regulation and acclimation of leaf gas exchange in a piñon–juniper woodland exposed to three different precipitation regimes. *Plant, Cell & Environment*, *36*(10), 1812–1825.

Linton, M. J., Sperry, J. S., & Williams, D. G. (1998). Limits to water transport in *Juniperus osteosperma* and *Pinus edulis*: implications for drought tolerance and regulation of transpiration. *Functional Ecology*, *12*(6), 906–911.

Maherali, H., & DeLucia, E. H. (2000). Xylem conductivity and vulnerability to cavitation of ponderosa pine growing in contrasting climates. *Tree Physiology*, *20*(13), 859–867.

Maherali, H., Pockman, W. T., & Jackson, R. B. (2004). Adaptive variation in the vulnerability of woody plants to xylem cavitation. *Ecology*, *85*(8), 2184–2199.

Manzoni, S., Vico, G., Katul, G., Palmroth, S., Jackson, R. B., & Porporato, A. (2013). Hydraulic limits on maximum plant transpiration and the emergence of the safety-efficiency trade-off. *New Phytologist*, *198*(1), 169–178.

Martin-StPaul, N. K., Limousin, J.-M., Vogt-Schilb, H., Rodríguez-Calcerrada, J., Rambal, S., Longepierre, D., & Misson, L. (2013). The temporal response to drought in a Mediterranean evergreen tree: comparing a regional precipitation gradient and a throughfall exclusion experiment. *Global Change Biology*, *19*(8), 2413–2426.

Martínez-Vilalta, J., & Piñol, J. (2002). Drought-induced mortality and hydraulic architecture in pine populations of the NE Iberian Peninsula. *Forest Ecology and Management*, *161*, 247–256.

Martínez-Vilalta, J., Cochard, H., Mencuccini, M., Sterck, F., Herrero, A., Korhonen, J. F. J., et al. (2009). Hydraulic adjustment of Scots pine across Europe. *New Phytologist*, *184*(2), 353–364.

Martínez-Vilalta, J., Poyatos, R., Aguadé, D., Retana, J., & Mencuccini, M. (2014). A new look at water transport regulation in plants. *New Phytologist*, *204*(1), 105–115.

McCulloh, K. A., Johnson, D. M., Meinzer, F. C., & Woodruff, D. R. (2014). The dynamic pipeline: hydraulic capacitance and xylem hydraulic safety in four tall conifer species. *Plant, Cell & Environment*, *37*(5), 1171–1183.

McDowell, N. G., Adams, H. D., Bailey, J. D., Hess, M., & Kolb, T. E. (2006). Homeostatic maintenance of ponderosa pine gas exchange in response to stand density changes. *Ecological Appliactions*, *16*(3), 1164–1182.

McDowell, N. G., Pockman, W. T., Allen, C. D., Breshears, D. D., Cobb, N., Kolb, T., et al. (2008). Mechanisms of plant survival and mortality during drought: why do some plants survive while others succumb to drought? *New Phytologist*, *178*(4), 719–739.

McDowell, N. G. (2011). Mechanisms linking drought, hydraulics, carbon metabolism, and vegetation mortality. *Plant Physiology*, *155*(3), 1051–1059.

McDowell, N. G., Beerling, D. J., Breshears, D. D., Fisher, R. A., Raffa, K. F., & Stitt, M. (2011). The interdependence of mechanisms underlying climate-driven vegetation mortality. *Trends in Ecology & Evolution*, *26*(10), 523–532.

McDowell, N. G., Fisher, R. A., Xu, C., Domec, J. C., Hölttä, T., Mackay, D. S., et al. (2013). Evaluating theories of drought-induced vegetation mortality using a multimodel-experiment framework. *New Phytologist*, *200*(2), 304–321.

McDowell, N. G., Williams, A. P., Xu, C., Pockman, W. T., Dickman, L. T., Sevanto, S., et al. (2015). Multi-scale predictions of massive conifer mortality due to chronic temperature rise. *Nature Climate Change*, *6*(3), 295–300.

McMahon, S. M., Harrison, S. P., Armbruster, W. S., Bartlein, P. J., Beale, C. M., Edwards, M. E., et al. (2011). Improving assessment and modelling of climate change impacts on global terrestrial biodiversity. *Trends in Ecology & Evolution*, *26*(5), 249–259.

Medeiros, J. S., & Pockman, W. T. (2010). Drought increases freezing tolerance of both leaves and xylem of *Larrea tridentata*. *Plant, Cell & Environment*, *34*(1), 43–51.

Meinzer, F. C., Woodruff, D. R., Domec, J.-C., Goldstein, G., Campanello, P. I., Gatti, M. G., & Villalobos-Vega, R. (2008). Coordination of leaf and stem water transport properties in tropical forest trees. *Oecologia*, *156*(1), 31–41.

Meinzer, F. C., Johnson, D. M., Lachenbruch, B., McCulloh, K. A., & Woodruff, D. R. (2009). Xylem hydraulic safety margins in woody plants: coordination of stomatal control of xylem tension with hydraulic capacitance. *Functional Ecology*, *23*(5), 922–930.

Mencuccini, M., & Grace, J. (1996). Climate influences the leaf area/sapwood area ratio in Scots pine. *Tree Physiology*, *15*, 1–10.

Mencuccini, M. (2003). The ecological significance of long-distance water transport: short-term regulation, long-term acclimation and the hydraulic costs of stature across

plant life forms. *Plant, Cell & Environment*, *26*(1), 163–182.

Mevik, B.-H., & Wehrens, R. (2007). The pls package: principal component and partial least squares regression in R. *Journal of Statistical Software*, *18*(2), 1–23.

Moore D.I. (2014) Meteorology Data at the Sevilleta National Wildlife Refuge, New Mexico, (1987–2014).

Musavi, T., Mahecha, M. D., Migliavacca, M., Reichstein, M., van de Weg, M. J., van Bodegom, P. M., et al. (2015). The imprint of plants on ecosystem functioning: A data-driven approach. *International Journal of Applied Earth Observation and Geoinformation*, *43*, 119–131.

Neufeld, H. S., Grantz, D. A., Meinzer, F. C., Goldstein, G., Crisosto, G. M., & Crisosto, C. (1992). Genotypic variability in vulnerability of leaf xylem to cavitation in water-stressed and well-irrigated sugarcane. *Plant Physiology*, *100*(2), 1020–1028.

Oren, R., Sperry, J. S., Katul, G. G., Pataki, D. E., Ewers, B. E., Phillips, N., & Schäfer, K. V. R. (2002). Survey and synthesis of intra- and interspecific variation in stomatal sensitivity to vapour pressure deficit. *Plant, Cell & Environment*, *22*(12), 1515–1526.

Overland, J. E., Dethloff, K., Francis, J. A., Hall, R. J., Hanna, E., Kim, S.-J., et al. (2016). Nonlinear response of mid-latitude weather to the changing Arctic, *6*(11), 992–999. http://doi.org/10.1038/nclimate3121

Pangle, R. E., Hill, J. P., Plaut, J. A., Yepez, E. A., & Elliot, J. R. (2012). Methodology and performance of a rainfall manipulation experiment in a piñon-juniper woodland. *Ecosphere*, *3*(4), 1–20.

Pangle, R. E., Limousin, J.-M., Plaut, J. A., Yepez, E. A., Hudson, P. J., Boutz, A. L., et al. (2015). Prolonged experimental drought reduces plant hydraulic conductance and transpiration and increases mortality in a piñon-juniper woodland. *Ecology and Evolution*, *5*(8), 1618–1638.

Peng, C., Ma, Z., Lei, X., Zhu, Q., Chen, H., Wang, W., et al. (2011). A drought-induced pervasive increase in tree mortality across Canada's boreal forests. *Nature Climate Change*, *1*(12), 467–471.

Peñuelas, J., Filella, I., Biel, C., Serrano, L., & Savé, R. (1993). The reflectance at the 950-970 nm region as an indicator of plant water status. *International Journal of Remote Sensing*, *14*(10), 1887–1905.

Peñuelas, J., Piñol, J., Ogaya, R., & Filella, I. (1997). Estimation of plant water content by the reflectance Water Index WI (R900/R970). *International Journal of Remote Sensing*, *18*(13), 2869–2875.

Pinheiro L., Bates D., Sarkar D., DebRoy S., & R-core team. (2013) Package 'nlme'. Retreived from http://cran.r-project.org/web/packages/nlme/nlme.pdf

Pittermann, J. (2005). Torus-margo pits help conifers compete with angiosperms. *Science*, *310*(5756), 1924–1924.

Pittermann, J., Sperry, J. S., Hacke, U. G., Wheeler, J. K., & Sikkema, E. H. (2006a). Inter-tracheid pitting and the hydraulic efficiency of conifer wood: the role of tracheid allometry and cavitation protection. *American Journal of Botany*, *93*(9), 1265–1273.

Pittermann, J., Sperry, J. S., Wheeler, J. K., Hacke, U. G., & Sikkema, E. H. (2006b). Mechanical reinforcement of tracheids compromises the hydraulic efficiency of conifer xylem. *Plant, Cell & Environment*, *29*(8), 1618–1628.
Plaut, J. A., Yepez, E. A., Hill, J., Pangle, R., Sperry, J. S., Pockman, W. T., & McDowell, N. G. (2012). Hydraulic limits preceding mortality in a piñon-juniper woodland under experimental drought. *Plant, Cell & Environment*, *35*, 1601–1617.

Plaut, J. A., Wadsworth, W. D., Pangle, R., Yepez, E. A., McDowell, N. G., & Pockman, W. T. (2013). Reduced transpiration response to precipitation pulses precedes mortality in a piñon-juniper woodland subject to prolonged drought. *New Phytologist*, *200*(2), 375–387.

Plavcova, L., & Hacke, U. G. (2014). Phenotypic and developmental plasticity of xylem in hybrid poplar saplings subjected to experimental drought, nitrogen fertilization, and shading. *Journal of Experimental Botany, 63*(18), 6481–6491.

Pockman, W. T., & Sperry, J. S. (2000). Vulnerability to xylem cavitation and the distribution of Sonoran Desert vegetation. *American Journal of Botany*, *87*(9), 1287–1299.

Pockman W.T. & McDowell N.G. (2015) Ecosystem-scale rainfall manipulation in a Piñon-Juniper woodland: Tree Sapwood and Leaf Area Data (2011). Long Term Ecological Research Network.
http://dx.doi.org/10.6073/pasta/f4fbe653cd0a2b7bf645675fdc2294fa

Porra, R. J., Thomson, W. A., & Kriedemann, P. E. (1989). Determination of accurate extinction coefficients and simultaneous equations for assaying chlorophylls a and b extracted with four different solvents: verification of the concentration of chlorophyll standards by atomic absorption spectroscopy. *Biochimica Et Biophysica Acta*, *975*, 384–394.

Poulter, B., Frank, D., Ciais, P., Myneni, R. B., Andela, N., Bi, J., et al. (2015). Contribution of semi-arid ecosystems to interannual variability of the global carbon cycle. *Nature*, *509*(7502), 600–603.

Quillet, A., Peng, C., & Garneau, M. (2010). Toward dynamic global vegetation models for simulating vegetation–climate interactions and feedbacks: recent developments, limitations, and future challenges. *Environmental Reviews*, *18*(NA), 333–353.

R Development Core Team (2013) R: A Language and Environment for Statistical Computing, R Foundation for Statistical Computing, Vienna, Austria.

Raffa, K. F., Aukema, B. H., Bentz, B. J., Carroll, A. L., Hicke, J. A., Turner, M. G., & Romme, W. H. (2008). Cross-scale Drivers of Natural Disturbances Prone to Anthropogenic Amplification: The Dynamics of Bark Beetle Eruptions. *Bioscience*, *58*(6), 501.

Raffa, K.F., Grégoire, J. –C., & Lindgren, B.S. (2015). Natural history and ecology of bark beetles. In F. E. Vega & R. W. Hofstetter (Eds.) *Bark Beetles: Biology and Ecology of Native and Invasive Species* (1-40). London, UK: Academic Press.

Reich, P. B., Rich, R. L., Lu, X., Wang, Y. P., & Oleksyn, J. (2014). Biogeographic variation in evergreen conifer needle longevity and impacts on boreal forest carbon cycle projections. *Proceedings of the National Academy of Sciences*, *111*(38), 13703–13708.

Reichstein, M., Bahn, M., Ciais, P., Frank, D., Mahecha, M. D., Seneviratne, S. I., et al. (2014). Climate extremes and the carbon cycle. *Nature*, *500*(7462), 287–295.

Rogiers, S. Y., Greer, D. H., Hatfield, J. M., Hutton, R. J., Clarke, S. J., Hutchinson, P. A., & Somers, A. (2012). Stomatal response of an anisohydric grapevine cultivar to evaporative demand, available soil moisture and abscisic acid. *Tree Physiology*, *32*(3), 249–261.

Romme, W. H., Allen, C. D., Bailey, J. D., Baker, W. L., Bestelmeyer, B. T., Brown, P. M., et al. (2009). Historical and modern disturbance regimes, stand structures, and landscape dynamics in pinon-juniper vegetation of the western United States. *Rangeland Ecology & Management*, *62*(3), 203–222.

Rouault, G., Candau, J.-N., Lieutier, F., Nageleisen, L.-M., Martin, J.-C., & Warzée, N. (2006). Effects of drought and heat on forest insect populations in relation to the 2003 drought in Western Europe. *Annals of Forest Science*, *63*(6), 613–624.

Sadras, V. O., & Trentacoste, E. R. (2011). Phenotypic plasticity of stem water potential correlates with crop load in horticultural trees. *Tree Physiology*, *31*(5), 494–499.

Sayer, M. A. S., & Haywood, J. D. (2006). Fine root production and carbohydrate concentrations of mature longleaf pine (*Pinus palustris* P. Mill.) as affected by season of prescribed fire and drought. *Trees*, *20*(2), 165–175.

Scheiter, S., Langan, L., & Higgins, S. I. (2013). Next-generation dynamic global vegetation models: learning from community ecology. *New Phytologist*, *198*(3), 957–969.

Schiller, G., & Cohen, Y. (1995). Water regime of a pine forest under a Mediterranean climate. *Agricultural and Forest Meteorology*, *74*(3-4), 181–193.

Seager, R., Ting, M., Held, I., Kushnir, Y., Lu, J., Vecchi, G., et al. (2007). Model projections of an imminent transition to a more arid climate in Southwestern North America. *Science*, *316*, 1181–1184.

Seager, R., Vecchi, G. A., & MacDonald, G. M. (2010). Greenhouse warming and the 21st century hydroclimate of southwestern North America. *Proceedings of the National Academy of Sciences of the United States of America*, *107*(50), 21277–21282.

Serrano, L. (2000). Deriving Water Content of Chaparral Vegetation from AVIRIS Data. *Remote Sensing of Environment*, *74*(3), 570–581.

Sevanto, S., McDowell, N. G., Dickman, L. T., Pangle, R., & Pockman, W. T. (2013). How do trees die? A test of the hydraulic failure and carbon starvation hypotheses. *Plant, Cell & Environment*, *37*(1), 153–161.

Sevanto, S. (2014). Phloem transport and drought. *Journal of Experimental Botany*, *65*(7), 1751–1759. http://doi.org/10.1093/jxb/ert467

Shaw, D, J., Steed, E, B., DeBlander, & T, L. (2005). Forest Inventory and Analysis (FIA) Annual Inventory Answers the Question: What Is Happening to Pinyon-Juniper Woodlands? *Journal of Forestry*, *103*(6), 280–285.

Sheffield, J., & Wood, E. F. (2008). Projected changes in drought occurrence under future global warming from multi-model, multi-scenario, IPCC AR4 simulations. *Climate Dynamics*, *31*(1), 79–105.

Sheriff, D. D., & Whitehead, D. (1984). Photosynthesis and wood structure in *Pinus radiata* during dehydration and immediately after rewatering. *Plant, Cell & Environment*, *7*, 53–62.

Sims, D. A., & Gamon, J. A. (2002). Relationships between leaf pigment content and spectral reflectance across a wide range of species, leaf structures and developmental stages. *Remote Sensing of Environment*, *81*, 337–354.

Sims, D. A., & Gamon, J. A. (2003). Estimation of vegetation water content and photosynthetic tissue area from spectral reflectance: a comparison of indices based on liquid water and chlorophyll absorption features. *Remote Sensing of Environment*, *84*(4), 526–537.

Skelton, R. P., West, A. G., & Dawson, T. E. (2015). Predicting plant vulnerability to drought in biodiverse regions using functional traits. *Proceedings of the National Academy of Sciences of the United States of America*, *112*(18), 5744–5749.

Sperry, J. S. & Tyree, M. T. (1990) Water-stress-induced xylem embolism in three species of conifers. *Plant, Cell & Environment* 13*,* 427–436.

Sperry, J. S., & Saliendra, N. Z. (1994). Intra-and inter-plant variation in xylem cavitation in *Betula occidentalis*. *Plant, Cell & Environment*, *17*, 1233–1241.

Sperry, J. S. (2000). Hydraulic constraints on plant gas exchange. *Agricultural and Forest Meteorology*, *104*(1), 13–23.

Sperry, J. S., Hacke, U. G., Oren, R., & Comstock, J. P. (2002). Water deficits and hydraulic limits to leaf water supply. *Plant, Cell & Environment*, *25*(2), 251–263.

Sperry, J. S., & Hacke, U. G. (2004). Analysis of circular bordered pit function I. Angiosperm vessels with homogenous pit membranes. *American Journal of Botany*, *91*(3), 369–385.

Sperry, J. S., Hacke, U. G., & Pittermann, J. (2006). Size and function in conifer tracheids and angiosperm vessels. *American Journal of Botany*, *93*(10), 1490–1500.

Sterck, F. J., Zweifel, R., Sass-Klaassen, U., & Chowdhury, Q. (2008). Persisting soil drought reduces leaf-specific conductivity in Scots pine (*Pinus sylvestris*) and pubescent oak (*Quercus pubescens*). *Tree Physiology*, *28*, 529–536.

Stiller, V. (2009). Soil salinity and drought alter wood density and vulnerability to xylem cavitation of baldcypress (*Taxodium distichum* (L.) Rich.) seedlings. *Environmental and Experimental Botany*, *67*(1), 164–171.

Stimson, H. C., Breshears, D. D., Ustin, S. L., & Kefauver, S. C. (2005). Spectral sensing of foliar water conditions in two co-occurring conifer species: Pinus edulis and Juniperus monosperma. *Remote Sensing of Environment*, *96*(1), 108–118.

Trenberth, K. E., Dai, A., van der Schrier, G., Jones, P. D., Barichivich, J., Briffa, K. R., & Sheffield, J. (2013). Global warming and changes in drought. *Nature Climate Change*, *4*(1), 17–22.

Tyree, M., & Sperry, J. S. (1989). Vulnerability of xylem to cavitation and embolism. *Annual Review of Plant Physiology and Plant Molecular Biology*, *40*, 19–38.

Tyree, M. T., & Ewers, F. W. (1991). The hydraulic architecture of trees and other woody plants. *New Phytologist*, *119*(3), 345–360.

U.S.D.A. Forest Service (2004). Forest Insect and Disease Conditions in the

Southwestern Region, 2003. Southwestern Region Forestry and Forest Health Pub. No. R3-16-13. http://www.fs.fed.us/r3/resources/health/fid_surveys. shtml

U.S.D.A. Forest Service (2015). Forest Insect and Disease Conditions in the Southwestern Region, 2014. Southwestern Region Forestry and Forest Health Pub. No. R3-04-02. http://www.fs.fed.us/r3/resources/health/fid_surveys. shtml

Ustin, S. L., & Gamon, J. A. (2010). Remote sensing of plant functional types. *New Phytologist*, *186*(4), 795–816.

van Mantgem, P. J., Stephenson, N. L., Byrne, J. C., Daniels, L. D., Franklin, J. F., Fule, P. Z., et al. (2009). Widespread Increase of Tree Mortality Rates in the Western United States. *Science*, *323*(5913), 521–524.

Vogelmann, J. E., Rock, B. N., & Moss, D. M. (1993). Red edge spectral measurements from sugar maple leaves. *International Journal of Remote Sensing*, *14*(8), 1563–1575.

Weed, A. S., Ayres, M. P., & Hicke, J. A. (2013). Consequences of climate change for biotic disturbances in North American forests. *Ecological Monographs*, *83*(4), 441–470.

West, A. G., Hultine, K. R., Jackson, T. L., & Ehleringer, J. R. (2007). Differential summer water use by *Pinus edulis* and *Juniperus osteosperma* reflects contrasting hydraulic characteristics. *Tree Physiology*, *27*(12), 1711–1720.

Williams, A. P., Allen, C. D., Macalady, A. K., Griffin, D., Woodhouse, C. A., Meko, D. M., et al. (2013). Temperature as a potent driver of regional forest drought stress and tree mortality. *Nature Climate Change*, *3*(3), 292–297.

Williams, A. P., Allen, C. D., Millar, C. I., Swetnam, T. W., Michaelsen, J., Still, C. J., et al. (2010). Forest responses to increasing aridity and warmth in the southwestern United States. *Proceedings of the National Academy of Sciences of the United States of America*, *107*(50), 21289–21294.

Winter, B. (2013). Linear models and linear mixed effects models in R with linguistic applications. arXiv:1308.5499. [http://arxiv.org/pdf/1308.5499.pdf]

Wortemann, R., Herbette, S., Barigah, T. S., Fumanal, B., Alia, R., Ducousso, A., et al. (2011). Genotypic variability and phenotypic plasticity of cavitation resistance in *Fagus sylvatica* L. across Europe. *Tree Physiology*, *31*(11), 1175–1182.

Wullschleger, S. D., Meinzer, F. C., & Vertessy, R. A. (1998). A review of whole-plant water use studies in trees. *Tree Physiology*, *18*, 499–512.

Wullschleger, S. D., Epstein, H. E., Box, E. O., Euskirchen, E. S., Goswami, S., Iversen, C. M., et al. (2014). Plant functional types in Earth system models: past experiences and future directions for application of dynamic vegetation models in high-latitude ecosystems. *Annals of Botany*, *114*(1), 1–16.

Zelinka, S. L., Bourne, K. J., Hermanson, J. C., Glass, S. V., Costa, A., & Wiedenhoeft, A. C. (2015). Force-displacement measurements of earlywood bordered pits using a mesomechanical tester. *Plant, Cell & Environment*, *38*(10), 2088–2097.

Zimmerman M.H. (1983) *Xylem Structure and the Ascent of Sap*. Springer-Verlag, New York, NY, USA.

Zwieniecki, M. A., Melcher, P. J., & Holbrook, N. (2001). Hydrogel control of xylem hydraulic resistance in plants. *Science*, *291*(5506), 1059–1062. http://doi.org/10.1126/science.1057175